

**ELECTROMAGNETIC FIELD ASSISTED
POLISHING (EMFP) OF ADVANCED
CERAMICS**

By

MURAT CETIN

Bachelor of Science

Yildiz Technical University

Istanbul, Turkey

1993

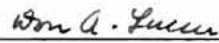
Submitted to the Faculty of the
Graduate College of the
Oklahoma State University
in partial fulfillment of
the requirements for
the Degree of
MASTER OF SCIENCE
July, 1997

**ELECTROMAGNETIC FIELD ASSISTED
POLISHING (EMFP) OF ADVANCED
CERAMICS**

Thesis Approved:



Thesis Adviser



Dean of the Graduate College

PREFACE

Ceramic bearing balls offer significant advantages when compared to other bearing materials. Their superior performance is due to special material properties such as their higher compressive strength, hardness, lower density, higher stiffness, higher operating temperatures, and self lubricating properties. When these exceptional properties are combined, they provide longer service life and a reliable product. However, their high hardness together with brittleness is a big disadvantage in terms of manufacturing.

Merely extending the conventional manufacturing technique, namely V-Groove Lapping, for ceramics is a time consuming and not a cost effective process because of the higher hardness of these ceramic materials. Use of high polishing loads also produces surface defects which can reduce the strength and service life of the ceramic bearing balls. Expensive diamond abrasives and long processing times increase the manufacturing cost significantly.

Magnetic float polishing (MFP) was introduced and employed to address and overcome some of the problems faced with conventional polishing. This technique was initially developed in Japan [Kato and Umehara]. It is a simple technique that utilizes magnetic fluid, commercially available sub-micron size abrasives, and a driving spindle. This technique requires magnetic field which can be generated either by permanent magnets or an electromagnet, in order to utilize a magnetic buoyancy force of a non-

magnetic body in a magnetic fluid. Magnetic float polishing technique involves little capital costs and can be incorporated with existing machine tools.

The magnetic field required for the magnetic float polishing has been typically generated by using permanent magnets. It has also been reported and proven in the literature that bearing balls can be finished to a desired manufacturing quality by using the permanent magnet polishing apparatus [Raghunandan and Komanduri, 1997 and Jiang and Komanduri, 1997].

As an alternative to the permanent magnet polishing apparatus, electromagnetic field assisted polishing apparatus was also designed and fabricated at Oklahoma State University. Initial design was developed by Dr. Shinmura of Japan at Oklahoma State University, and later altered to form a ring pole electromagnetic field assisted polishing apparatus. Eventhough, this new design showed promising results, it did not meet with the required finish requirements.

In order to address this problem, a modified ring pole design was proposed and built as an alternative to the ring pole design. During the evaluation of this new design, FEM analysis was employed to compare and simulate the results with the ring pole design.

Experimental studies were carried out using the modified ring pole design as well as the original ring pole design. The experimental studies serve to create the necessary data base for establishing optimum polishing conditions. Approximately 4.5 $\mu\text{m}/\text{min}$ material removal rate was accomplished when polishing silicon nitride workpiece material as compared to 2 $\mu\text{m}/\text{min}$ with the permanent magnet apparatus. Surface

roughness (R_a) of 13 nm was also observed. The average sphericity with the ring pole design was 0.45 μm and with the modified ring pole design was 0.9 μm .

ACKNOWLEDGEMENTS

I would like to express my gratitude and thanks to Dr. Ranga Komanduri at Oklahoma State University for invaluable guidance and assistance during this research project. Working with him and the others in the group, has been a great pleasure and honor for me for a lifetime.

This research was funded by grants from the Ceramic Bearing Technology Program of the Advanced Research Projects Agency (ARPA) of the Department of Defense (DoD) and by the National Science Foundation. I would like to thank Dr. W. Coblenz with the Air Force, Dr. K. Mecklenburg of the Wright Patterson AFB, Dr. L. Fehrenbacher of T.A. & T. Inc, Drs. Larsen Basse, J. Lee, Ming Lev, and B.M. Kramer of N.S.F. for their interest and support. I would also like to thank Dr. D.A. Lucca and Dr. R. L. Dougherty for agreeing to serve in my committee.

I would also like to express my thanks to Dr. Makaram Raghunandan for his valuable discussions and helps throughout the research. Also special thanks to Dr. Ali Noori-Khajavi for his help during the ANSYS analysis. Without these two, this task would have been impossible

Special thanks to my colleagues in the MAERL; Ming Jiang, Brian Perry, Vinoo Thomas, Johniee Hixson, and Mallika Kamarajugadda for their help and valuable discussions. Thanks also due to Margaret Mitchell and Jerry Dale.

On a personal note, the author acknowledges the invaluable support and encouragement of his family and Mr. Ayhan Sahenk.

TABLE OF CONTENTS

Chapter		Page
1	Introduction.....	1
	1.1 Ceramic Bearing Balls and Their Advantages.....	1
	1.2 Magnetic Field Assisted Polishing Techniques	3
2	Literature Review.....	10
	2.1 Magnetic Field Assisted Polishing	10
	2.2 Magnetic Fluid Assisted Polishing	11
	2.3 Magnetic Float Polishing	13
	2.3.1 Effect of the Float and the Total Grinding Load.....	14
	2.3.2 Effect of Abrasive Size and Concentration.....	17
	2.3.3 Effect of Rotational Speed	19
	2.3.4 Effect of the field Supporting Stiffness	19
	2.4 Magnetic Float Assisted Polishing Mechanics	20
	2.5 Tribology and Material Removal Mechanism of Ceramics.....	23
	2.6 Electromagnetic Float Polishing	25
3	Problem Statement	28
	3.1 Magnetic Float Polishing	28
	3.2 Electromagnetic Float Polishing	29
4	Analysis of the Electromagnetic Field Assisted Polishing (EMFP) Apparatus... 31	
	4.1 Initial Design of the Electromagnetic Field Assisted Polishing Apparatus	31
	4.2 Elements of the Electromagnet Polishing Apparatus (Initial Design).....	34
	4.3 Finite Elements Analysis of the Straight Field Polishing Apparatus.....	36
	4.4 Finite Elements Analysis for Ring Pole Electromagnetic Polishing Apparatus and Modification in the Analysis	41
	4.5 Modified Ring Pole Electromagnetic Polishing Apparatus	50
	4.6 Modifications in Force Measurement for Electromagnetic Polishing Apparatus	58
5	Experimental Studies	62
	5.1 Experimental Details and Procedure.....	63
	5.2 Effect on Material Removal Rate.....	65

	5.2.1 Material Removal Rate in the Ring Pole Design.....	66
	5.2.2 Material Removal Rate in the Modified Ring Pole Design.....	71
5.3	Effect on Surface Finish.....	74
	5.3.1 Optimum Surface Finish Sequence.....	83
5.4	Sphericity	97
6	Discussion.....	110
7	Conclusions.....	115
	7.1 Future Work.....	116
	Bibliography	118
	Appendix A.....	120

LIST OF TABLES

Table		Page
1.1	Comparison of properties between silicon nitride, aluminum oxide and SUJ2 bearing steel.....	2
1.2	Hardness and density values of the abrasive and workpiece materials being used in magnetic float polishing process	8
5.1	Variables involved in magnetic float polishing	63
5.2	Polishing process sequence for optimum surface finish in the electromagnetic field assisted polishing apparatus	83
5.3	Comparison of the optimum surface polishing sequence with another set of polishing test	86

LIST OF FIGURES

Figure

1.1	Schematic of magnetic abrasive finishing of cylindrical surface (External)	4
1.2	Schematic of permanent magnet apparatus with concentric shaft	5
1.3	Schematic of permanent magnet apparatus with eccentric shaft	5
1.4	Schematic of electromagnet apparatus with concentric shaft	6
2.1	Buoyant force acting on non-magnetic body in magnetic fluid under magnetic field	11
2.2	Apparatus of internal polishing of tube with magnetic fluid grinding.....	12
2.3	Effect of float on magnetic grinding load, using permanent magnet design	14
2.4	Effect of float on material removal rate at various speeds with and without a float	15
2.5	Effect of load on material removal rate with and without a float	15
2.6	Effect of float on sphericity	16
2.7	Effect of abrasive concentration on material removal rate	18
2.8	Effect of abrasive grain size on material removal rate.....	18
2.9	Effect of magnetic field supporting stiffness on material removal rate	20
2.10	Magnetic float polishing model notations for (a) cell geometry and motions and (b) float forces and torques.....	21
2.11	Stress field classification in terms of working units	24
2.12	Straight field electromagnetic polishing apparatus designed by Shinmura and Komanduri	26

2.13	Ring pole electromagnetic field assisted polishing apparatus	27
4.1	Magnetic field orientation through the straight field pole design of Shinmura and Komanduri	32
4.2	(a) Initial design of the lower intensifier, (b) Magnetic field gradients generated by the initial lower intensifier, (c) Modified lower intensifier with the water cooling system.....	33
4.3	Schematic of the power system for electromagnetic field assisted polishing apparatus	35
4.4	ANSYS model for straight field electromagnetic field assisted polishing apparatus	37
4.5	Theoretical solution with ANSYS for magnetic flux density in straight field electromagnetic float polishing apparatus	39
4.6	Theoretical solution with ANSYS for magnetic field strength in straight field electromagnetic float polishing apparatus	39
4.7	Magnetic flux density, B, versus height inside the polishing chamber for straight field electromagnetic polishing apparatus.....	38
4.8	Variation in calculated theoretical buoyancy forces with height in straight field electromagnetic polishing apparatus	40
4.9	ANSYS geometric model for the ring pole electromagnetic float polishing apparatus.....	42
4.10	Modified magnetic flux density results with ANSYS analysis for the ring pole electromagnetic polishing apparatus.....	43
4.11	Modified magnetic field strength results with ANSYS analysis for the ring pole electromagnetic polishing apparatus.....	44
4.12	Magnetic flux density for the straight and the ring pole designs.....	45
4.13	Variation in buoyancy forces with height for the straight field and ring pole designs	46
4.14	The situation of the polishing chamber filled with the magnetic fluid	47
4.15	Magnetic flux density, B, of the ring pole with a thickness of 12.7 mm	48

4.16	Magnetic flux density, B, of the ring pole with a thickness of 25.4 mm	48
4.17	Magnetic flux density, B, of the ring pole with a thickness of 38.1 mm	49
4.18	Magnetic flux density, B, of the ring pole with a thickness of 50.8 mm	49
4.19	Area plot for electromagnetic polishing apparatus in axi-symmetric analysis option in ANSYS	51
4.20	B-H Curve for low carbon steel	52
4.21	Magnetic flux lines inside the modified electromagnetic polishing apparatus	53
4.22	Vector form of magnetic flux density in the modified electromagnetic polishing apparatus	54
4.23	Vector form of magnetic field strength in the modified electromagnetic polishing apparatus	54
4.24	Total magnetic flux density in the modified electromagnetic polishing apparatus	55
4.25	Total magnetic field strength in the modified electromagnetic polishing apparatus	55
4.26	Modified ring pole electromagnetic polishing apparatus	57
4.27	Dimensions of the Uniforce sensor that was used to monitor the force applied to silicon nitride balls in the electromagnetic field assisted polishing apparatus	59
4.28	Uniforce sensor used in the electromagnetic float polishing apparatus	59
4.29	Experimental and theoretical buoyancy forces for the ring pole electromagnetic float polishing apparatus	60
4.30	Experimental buoyancy forces for the modified ring pole design	61
5.1	Experimental setup for electromagnetic field assisted polishing	62
5.2	Orientation of the magnetic fluid and the abrasives under the applied magnetic field in electromagnetic field assisted polishing apparatus	66

5.3	Effect of the rotational speed on material removal rate in the ring pole electromagnetic field assisted polishing apparatus	67
5.4	Effect of the abrasive concentration on material removal rate in the ring pole electromagnetic field assisted polishing apparatus	68
5.5	Material removal rate with different rotational speeds by using SiC 400 grid size as the polishing abrasive in the ring pole electromagnetic field assisted polishing apparatus.....	69
5.6	(a) Pits dominant SEM micrograph of a ball polished by using 4000 rpm and 30% volume abrasive concentration of B ₄ C 500 (17 µm).....	70
5.6	(b) Scratches dominant SEM micrograph of a ball polished ball by using 4000 rpm and 30% volume abrasive concentration of B ₄ C 500 (17 µm)	71
5.7	Effect of the rotational speed on material removal rate in the modified ring pole electromagnetic field assisted polishing apparatus.....	72
5.8	Effect of the abrasive concentration on material removal rate in the modified ring pole electromagnetic field assisted polishing apparatus	73
5.9	The effect of abrasive grain size on material removal rate in the modified ring pole electromagnetic field assisted polishing apparatus.....	74
5.10	The effect of the rotational speed on surface roughness in the ring pole electromagnetic field assisted polishing apparatus	75
5.11	Surface traces obtained from Rank Taylor Hobson 120L Talysurf instrument of the silicon nitride balls with varying rotational speed of the driving shaft in the ring pole design	77
5.12	Effect of the rotational speed on material removal rate in the modified ring pole electromagnetic field assisted polishing apparatus	78
5.13	Surface traces obtained from Rank Taylor Hobson 120L Talysurf instrument of the silicon nitride balls with varying rotational speed of the driving shaft in the modified ring pole design.....	80
5.14	Effect of the abrasive grain size on surface finish in the modified ring pole electromagnetic field assisted polishing apparatus.....	81
5.15	Surface traces obtained Rank Taylor Hobson 120L Talysurf instrument of the silicon nitride balls with varying grid sizes in the modified ring pole electromagnetic field assisted polishing apparatus	82

5.16	Surface roughness traces from Rank Taylor Habson 120L Talysurf in optimum surface finish sequence in the electromagnetic field assisted polishing apparatus.....	85
5.17	ZYGO plots at a lower magnification (20X Fizeau) of a ball polished with SiC (1-5 μm) with the electromagnetic field assisted polishing apparatus.....	87
5.18	ZYGO plots at a higher magnification (100X Fizeau) of a ball polished with SiC (1-5 μm) with the electromagnetic field assisted polishing apparatus.....	88
5.19	ZYGO plots at a lower magnification (20X Fizeau) of a ball polished with Cr_2O_3 (1-5 μm) with the electromagnetic field assisted polishing apparatus	89
5.20	ZYGO plots at a higher magnification (100X Fizeau) of a ball polished with Cr_2O_3 (1-5 μm) with the electromagnetic field assisted polishing apparatus	90
5.21(a)	SEM micrograph at 2000X magnification polished with conventional polishing techniques.....	91
5.21(b)	SEM micrograph at 5000X magnification polished with conventional polishing techniques.....	92
5.22(a)	SEM micrograph at 2000X magnification polished with 1-5 μm Cr_2O_3 in the electromagnetic float polishing apparatus.....	92
5.22(b)	SEM micrograph at 5000X magnification polished with 1-5 μm Cr_2O_3 in the electromagnetic float polishing apparatus.....	93
5.23(a)	SEM micrograph at 1000X magnification polished with 3 μm CeO_2 in the electromagnetic float polishing apparatus.....	94
5.23(b)	SEM micrograph at 5000X magnification polished with 3 μm CeO_2 in the electromagnetic float polishing apparatus.....	94
5.24(a)	ZYGO plots at low magnification (20X Fizeau) of a ball polished with CeO_2 (3 μm) with the electromagnetic float polishing apparatus	95
5.24(b)	ZYGO plots at high magnification (100X Fizeau) of a ball polished with CeO_2 (3 μm) with the electromagnetic float polishing apparatus	96
5.25	Talysurf trace of a silicon nitride bearing ball polished with CeO_2 (3 μm) in the electromagnetic field assisted polishing apparatus	97
5.26	Factors effecting the ball sphericity in magnetic float polishing	98

5.27	Effect of the rotational speed on the ball sphericity in the modified ring pole electromagnetic field assisted polishing apparatus.....	99
5.28	Effect of abrasive concentration on sphericity in the ring pole electromagnetic field assisted polishing apparatus	100
5.29	Talyround traces of a ball with different abrasive concentration in the ring pole design.....	102
5.30	Effect of abrasive concentration on sphericity in the modified ring pole electromagnetic field assisted polishing apparatus	103
5.31	Talyround traces of a ball with different abrasive concentration in the modified ring pole design	105
5.32	Effect of the polishing load on sphericity in the modified ring pole electromagnetic polishing apparatus.....	106
5.33	Change in sphericity with time in the ring pole design	107
5.34	Change in sphericity with time in the modified ring pole design.....	107
5.35	Talyround traces for the ring pole design	108
5.36	Talyround traces for the modified ring pole design.....	109
6.1	Situation of the magnetic fluid and the abrasives under the magnetic field in the electromagnetic float polishing apparatus.....	112
6.2	Situation of the magnetic fluid and the abrasives under the magnetic field in the permanent magnet float polishing apparatus	112

CHAPTER 1

INTRODUCTION

1.1 Ceramic Bearing Balls and Their Advantages

Advanced ceramics, such as silicon nitride exhibit several unique properties compared to conventional steels for bearing applications. Their superior performance is attributed to their higher compressive strength, high hardness, high stiffness, and lower density, higher speeds, and higher operating temperatures. Consequently, high precision ceramic bearings can provide longer and more reliable performance in service.

However, ceramic ball bearings manufactured by several weeks polishing techniques are more expensive and takes considerable time for finishing. Conventional grinding and polishing techniques require the use of diamond abrasives, thus increasing the component cost significantly. Also, because of the use of hard diamond abrasives to finish brittle silicon nitride by conventional techniques, subsurface damage occurs on the silicone nitride balls in the form of pits, cracks, etc. as material removal is predominantly by brittle fracture.

Table 1.1 shows a comparison of various properties of two ceramics and conventional steel used in bearing applications. It can be seen that silicon nitride has many superior properties compared to alumina or steel [Kato et al, 1986]. For example, silicone nitride has approximately 60% lower density than SUJ2 bearing steel and the

Young's Modulus is nearly 50% higher. Another leading characteristic of silicone nitride is that it can be operated at higher temperatures and higher speeds. Bearing balls made of silicone nitride can be used with little or no lubrication, as they are self lubricating. For these reasons, they have approximately ten times longer service life than steel bearing balls.

Table 1.1 Comparison of properties among
silicon nitride, aluminum oxide, and SUJ2 bearing steel

Properties	Silicon Nitride	Aluminum Oxide	Steel
Vickers Hardness, kgf/mm^2	1532	1783	848
Elastic Modulus, GPa	294	343	190
Poisson's Ratio	0.27	0.25	0.28
Density, g/cm^3	3.2	3.8	7.8
Fracture Toughness, $\text{MPa m}^{1/2}$	5.2	4.0	45.0
Thermal Expansion, Coeff. $10^{-6}/^\circ\text{C}$	3.7	7.1	12.3
Thermal Conductivity, $\text{cal.cm/cm}^2.\text{sec.}^\circ\text{C}$	0.03	0.06	0.13

Even though silicon nitride bearing balls have such distinguished advantages mentioned above, compared to conventional bearing balls of steel, they also have some disadvantages. One of the biggest problems is low fracture toughness which for silicon nitride is approximately $5.2 \text{ MPa m}^{1/2}$ and for steel bearing materials approximately $45 \text{ MPa m}^{1/2}$. In order for ceramic balls to perform well, the fracture toughness should be as high as possible. Also, fracture toughness depends on manufacturing quality of these

ceramic components. This has been one of the biggest challenges for the manufacturers. At the same time, large forces employed in conventional polishing methods tend to induce sub-surface damage and this damage may lead to unwanted reliability and shorter service life.

1.2 Magnetic Field Assisted Polishing Techniques

In the early 1940's, the U.S. saw the development of magnetic field assisted polishing. The new technique was contrived in order to polish gun barrels [Coats, 1940]. Later this method of polishing was practiced in the former U.S.S.R and used in a variety of polishing applications in which the workpieces were relatively large and difficult to machine [Baron, 1975].

Magnetic field assisted polishing is a process in which a magnetic field is generated either by permanent magnets, or an electromagnet and abrasives which are oriented along the generated magnetic field. Polishing processes are utilized by rotating the workpiece inside the generated magnetic field and oriented toward the abrasive medium. Magnetic field assisted polishing can be grouped into two principal methods, the first of which is magnetic float polishing (MFP) and the other is the magnetic abrasive finishing (MAF). The major difference between these methods is the type of medium being used.

Magnetic abrasive finishing can be used to polish either flat surfaces or cylindrical surfaces which can be internal or external. This method can finish both magnetic and non-magnetic materials [Shinmura 1990, Shinmura 1993 and Fox 1994] (Figure 1.1). In

this method, material removal may be either by mechanical or chemical action which can be accomplished by the forces due to the generated magnetic field gradients. Material removal occurs when the workpiece is rotated inside the magnetic field and the oriented abrasives along the magnetic field scratch the surface of the workpiece. As mentioned previously, magnetic abrasive finishing is better suited for flat and cylindrical surfaces, whereas the magnetic float polishing technique has been developed for spherical surfaces.

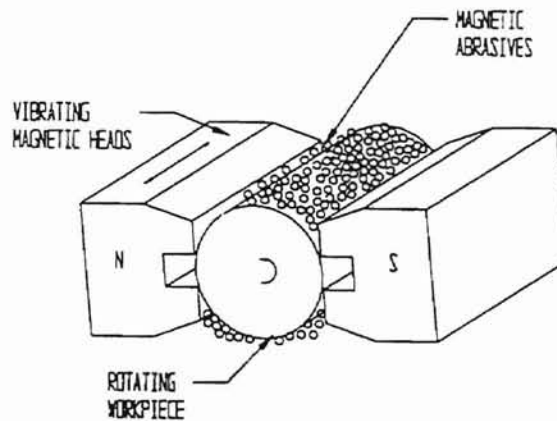


Figure 1.1 Schematic of magnetic abrasive finishing of cylindrical surface (External)

Magnetic float polishing (MFP) is another type of magnetic field assisted polishing. In this technique, it is desirable to have non-magnetic workpiece materials, although magnetic materials can also be finished by this technique. Rollers, flats, internal surfaces and spherical surfaces can be polished by magnetic float polishing. Since, the objective of this research is to investigate the possibility of polishing of silicon nitride bearing balls, primary emphasis will be placed on spherical surfaces.

Even though the concept behind magnetic abrasive finishing (MAF) and magnetic float polishing (MFP) is similar, there are notable differences. Basically, in magnetic abrasive finishing (MAF), the abrasive particles are pushed against the workpiece surface

due to magnetic field orientation; whereas in magnetic float polishing (MFP), abrasive particles are pressed to the workpiece surface by the generated buoyancy forces. In order to polish bearing balls, there are three different types of magnetic float polishing apparatus designed. They are permanent magnets with a concentric shaft, permanent magnets with an eccentric shaft and an electromagnet with a concentric shaft. Schematics of these three different magnetic float polishing apparatus are shown in Figures 1.2, 1.3, and 1.4

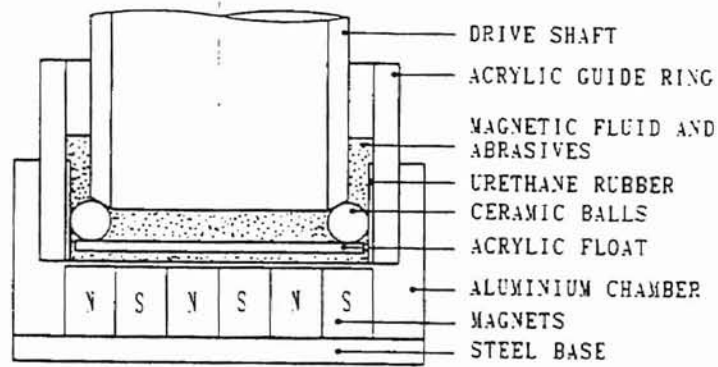


Figure 1.2 Schematic of permanent magnet apparatus with concentric shaft

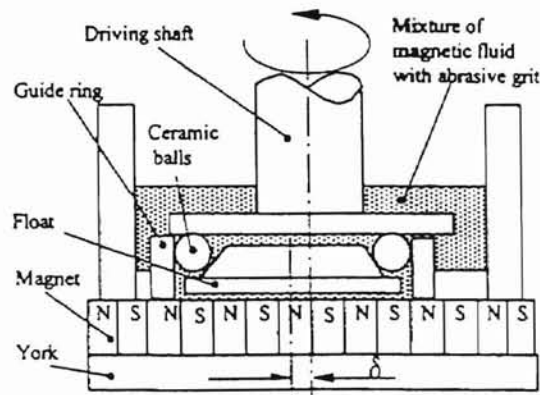


Figure 1.3 Schematic of permanent magnet apparatus with eccentric shaft

underneath the balls. Hence, material removal can be achieved due to rotating motion between the workpiece surface and the abrasives.

Magnetic field assisted polishing offers several advantages due to its unique features. These features are lower forces (~ 1 N/ball), higher speeds (up to 6000 rpm), use of conventional abrasives, use of chemo-mechanical polishing and a simple apparatus which can be incorporated into a conventional machine tool. These features enable increased removal rates, extremely smooth and microcrack-free surfaces, lower capital costs, smaller inventory and an economical product.

The main features of the magnetic float polishing technique are magnetic fluid, abrasives, and the work material being polished. Magnetic fluid is a colloidal suspension of angstrom size magnetic particles (~ 100 Å) which consists mainly of magnetite and the liquid carrier. This liquid carrier may be either water or hydrocarbon. Generally, magnetic fluid is characterized by its field strength or magnetization values. When magnetic fluid is placed under a magnetic field, magnetic particles respond to that field and orient the carrier fluid. Saturation magnetization of the magnetic fluid is approximately 10^5 A/m which corresponds to 600 Gauss. It is also noteworthy that the magnetic field strength (in other words magnetization) depends upon the concentration of magnetic particles inside the carrier medium. In magnetic float polishing, due to the magnetic field gradient, magnetic particles respond to a force which is called the buoyancy force. Buoyancy forces depend on the gradient and strength of the magnetic field, and the saturation magnetization of the carrier magnetic fluid.

As mentioned previously, another important feature of the magnetic float polishing is the abrasives. These commercially available abrasives are added to the

magnetic fluid during the polishing process and the amount of abrasives is less than 10% of the volume. In this research, the abrasives used include:

- Boron carbide (B_4C)
- Silicon carbide (SiC)
- Chromium oxide (Cr_2O_3)

Density and hardness of these abrasives is presented in Table 1.2 along with the workpiece material being used, silicon nitride.

Table 1.2 Hardness and Density values of the abrasive and workpiece materials being used in magnetic float polishing process [Raghunandan 1996].

Material	Hardness MPa	Density g/cc
Silicon Nitride Si_3N_4	1600-2200	3.2
Boron Carbide B_4C	3400	2.5
Silicon Carbide SiC	2500	3.2
Chromium Oxide Cr_2O_3	2000-2200	5.2
Aluminum Oxide Al_2O_3	2100	4.0

Considering the hardness values of these abrasives and the workpiece materials, it should be noted that boron carbide and silicon carbide abrasives are generally used for roughing processes and chromium oxide for the final polishing process.

Yet another important feature of the magnetic float polishing process is the workpiece material, silicon nitride. Properties of silicon nitride work material are

presented in Table 1.1. Basically, silicon nitride is a synthetic raw material and can be manufactured by means of chemical reactions at high temperatures ranging approximately from 1000 to 1600 °C [Ault et. al. 1993]. There are essentially three methods to produce silicon nitride powder, namely:

- Reacting silicon metal powder with nitrogen
- Reacting SiO₂, carbon, and nitrogen
- Reacting chlorosilanes with a gas containing nitrogen or a nitrogen compound.

Powder metallurgy techniques can be used to fabricate silicon nitride products as well. These products are then fired in nitrogen to produce a porous silicon nitride raw material which is called reaction-bonded or reaction-sintered silicon nitride. This type of manufacturing technique produces lower strength, lower toughness and less oxidation resistant silicon nitride, also called α -phase silicon nitride. When oxygen and aluminum are substituted for nitrogen, the product manufactured is β -phase silicon nitride which is tougher and more dense than α -phase silicon nitride. In this investigation, the silicon nitride work material used is fabricated with the technique known as hot isostatically pressing (HIP). In this technique, silicon nitride powder is heated up to 1700 °C and subjected to a pressure higher than 300 MPa in a nitrogen atmosphere. This technique results in greater uniformity and a more dense silicon nitride product.

CHAPTER 2

LITERATURE REVIEW

2.1 Magnetic Field Assisted Polishing

The magnetic field assisted polishing technique was first introduced by Coats [1940]. This technique was applied to finish gun barrels as was mentioned previously. In this process, magnets were placed near the barrels and abrasive particles were placed inside these barrels. By rotating the barrels, polishing was accomplished. Later, the magnetic field assisted polishing technique found applications in the finishing of large nonmagnetic work materials in the former U.S.S.R. and Bulgaria. [Baron of the U.S.S.R., 1975 and Makedonski of Bulgaria, 1974].

Magnetic field assisted polishing techniques were initially used to polish internal surfaces. For example, Shinmura [1989] used this technique to finish non-magnetic tubes. This technique was also utilized to polish external surfaces as well. Shinmura [1985] developed new methods to polish cylinders and flat surfaces where the main concept behind the process was not much different than that which was initially developed. Use of the magnetic abrasives in a strong field was the main idea of these methods. In these processes, polishing was in a completely dry abrasive environment. The abrasives used in these methods were either mixed with iron particles or sintered to the magnetic particles.

2.2 Magnetic Fluid Assisted Polishing

Use of magnetic fluid as a medium for the polishing process was first introduced by Tani of Japan [1984]. He used magnetite iron oxide particles inside the magnetic fluid to polish acrylic resin. In his experiments, Tani used the concept of buoyant forces acting upon a non-magnetic body in a magnetic fluid under a magnetic field. (see Figure 2.1). This idea was initially introduced by Rosenweig [1966]. He states in his paper that non-magnetic particles can be oriented in a certain direction in a magnetic fluid under a specifically designed magnetic field. These non-magnetic particles can be maintained due to Brownian motion, which also needs the assistance of a surfactant. This surfactant prevents the magnetic particles from agglomerating under van der Waal forces.

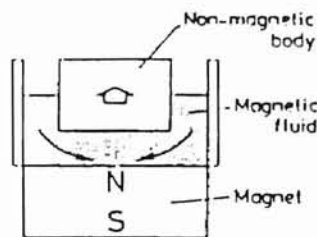


Figure 2.1 Buoyant force acting on non-magnetic body in magnetic fluid under magnetic field.

Magnetic fluid assisted polishing techniques can be utilized to polish a variety of shapes. Umehara of Japan has also introduced a method for polishing internal surfaces with a magnetic fluid [1995]. In this method, the internal surface of a long tube of which

the diameter is less than 20 mm can be polished by means of magnetic fluid polishing. A schematic of this apparatus is shown in Figure 2.2

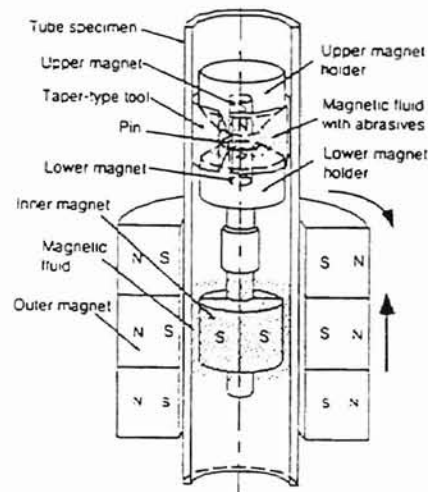


Figure 2.2 Apparatus of internal polishing of tube with magnetic fluid grinding [Umehara et.al.1995]

In this method, there are two different type of forces applied to the workpiece: one a normal force which provides the relative motion between the tool and the internal surface of the tube, and the other a tangential force which provides the finishing action. With this method, Umehara et al obtained 0.28 $\mu\text{m}/\text{min}$ removal rate with a 55 μm of SiC abrasive and stainless steel taper type tool, and a surface roughness of 0.04 μm R_a with a 1 μm SiC abrasive and PVA taper type tool.

2.3 Magnetic Float Polishing

The magnetic float polishing (MFP) technique was first introduced by Umehara and Kato [1987] to polish spherical surfaces. In their experiments, they polished cold pressed and sintered silicon nitride balls of 9 mm diameter using a silicon carbide abrasive. Water based magnetic fluid with 400 Gauss magnetization and a spindle speed of 20,000 RPM were used. The required magnetic field was generated using 4 mm square permanent magnets which were assembled with alternate N and S poles. This magnetic field design with permanent magnets provided them with a magnetic field strength of 9.2×10^5 A/m. The main difference when compared to Tani's work was the use of a float. This float which is generally fabricated from acrylic resin was used to provide the required support to the balls. Umehara and Kato conducted experiments to determine the effect of variables on the surface finish, sphericity and material removal rate in magnetic float polishing. They identified the following variables as the most influential parameters.

- Effect of the float and the total grinding load
- Effect of abrasive size and concentration
- Effect of the rotational speed
- Effect of the field supporting stiffness

In the following, the effects of these parameters will be briefly reviewed.

2.3.1 Effect of the float and the total grinding load

The introduction of the float was a major contribution of Kato and Umehara [1990] in magnetic fluid polishing of bearing balls. The total grinding load was increased from 2 N without the float to 6 N with a float. Umehara and Kato carried out experiments to find the effect of the float and grinding load. The results of these experiments are presented in Figures 2.3, 2.4, 2.5, and 2.6. In Figure 2.3, it can be seen that if the gap decreases, the magnetic grinding load increases no matter if a float is used or not. However, it is also obvious that use of a float increases the grinding load (magnetic buoyancy force) drastically. It can also be seen that the use of a float increases the area where the magnetic buoyancy forces act and therefore the increase in the magnetic buoyancy force provides higher grinding loads.

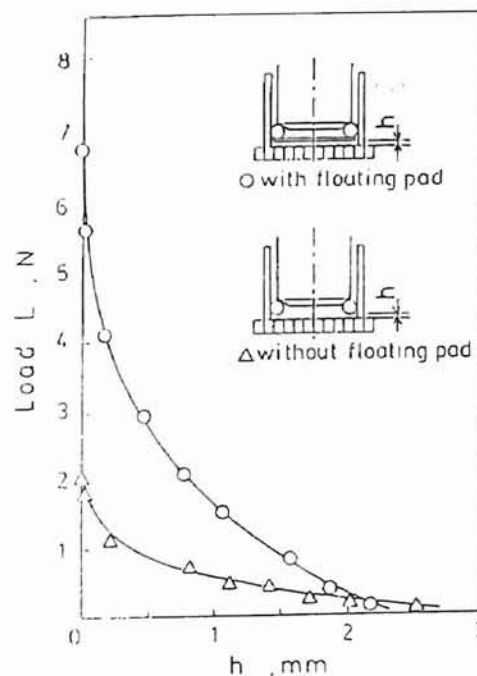


Figure 2.3 Effect of a float on magnetic grinding load, using permanent magnet design.
[Umehara and Kato, 1990]

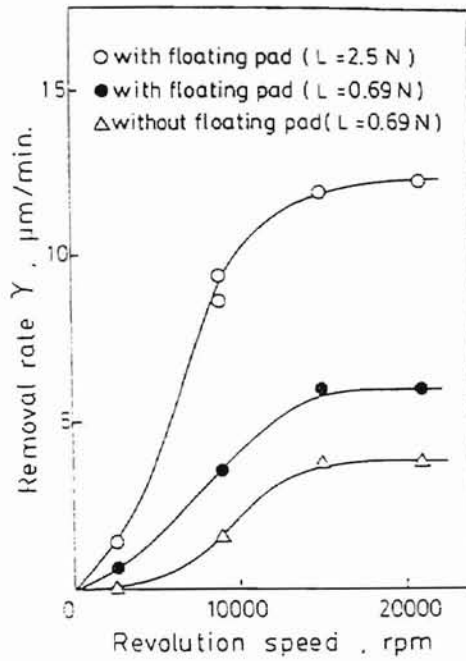


Figure 2.4 Effect of a float on material removal rate at various speeds with and without a float [Umehara and Kato, 1990]

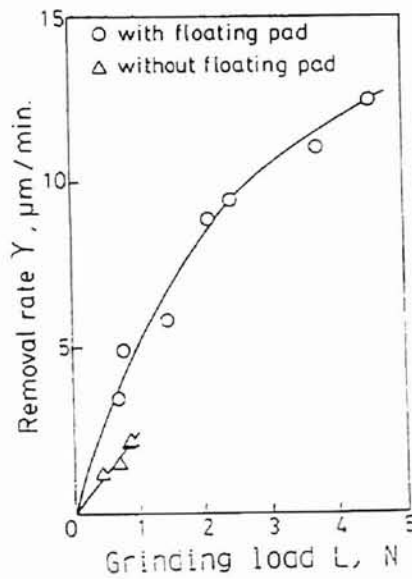


Figure 2.5 Effect of grinding load on material removal rate with and without a float [Umehara and Kato, 1990]

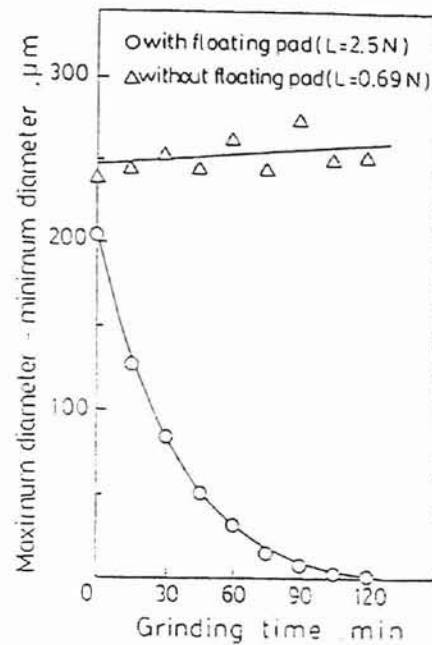


Figure 2.6 Effect of float on sphericity. [Umehara and Kato, 1990]

In Figure 2.4, the effect of a float on material removal at various rotational speeds is illustrated. Since the benefit of the float is increased force, increased force leads to an increase in material removal rates. It should be also noted that an increase in speed also increases the removal rate. In Figure 2.5, the effect of grinding load on material removal rate is presented. In this case, an increase in the load augments the material removal rate. In their experiments, Umehara and Kato used 0.4 N/ball and they polished 11 balls altogether. Use of a float also provides improvement in the shape accuracy of silicon nitride balls. Figure 2.6 shows that the use of a float decreases sphericity drastically and helps to achieve the requirements for a bearing ball. It can be concluded that use of a float leads to an increase in grinding loads, an increase in the material removal rate, and a

decrease in the sphericity. It was also found that the use of a float improves surface finish. All of these parameters for the polishing of silicon nitride bearing balls are very important and all these improvements can be achieved because use of a float leads to a 3-point contact which provides a more uniform material removal process.

2.3.2 Effect of Abrasive Size and Concentration

When comparing the use of diamond abrasives in conventional polishing techniques with the use of commercially available abrasives in the magnetic float polishing method, the advantages of the later technique are two-fold. First, with magnetic float polishing, it is possible to obtain fracture-free surfaces and secondly the overall cost can be reduced significantly. Umehara and Kato [1990] also investigated the effects of abrasive concentration and abrasive size. The results of this investigation are presented in Figure 2.7 and Figure 2.8. In Figure 2.7, it can be seen that material removal rate reaches a saturation point when the abrasive concentration is 10% by volume. Therefore, it can be concluded that 10% by volume abrasive concentration is the optimum condition for magnetic float polishing. In Figure 2.8, the effect of abrasive grain size on material removal rate is presented. After approximately 50 μm grain size, material removal rate nearly follows a constant trend. When the abrasive grain size is less than 50 μm , material removal rate is directly proportional to abrasive grain size; and as the abrasive grain size decreases, material removal rate also decreases.

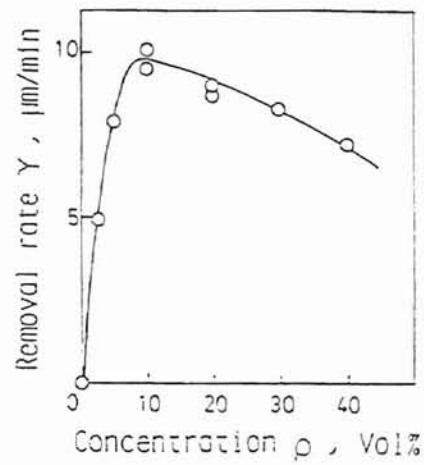


Figure 2.7 Effect of abrasive concentration on material removal rate.
[Umehara and Kato, 1990]

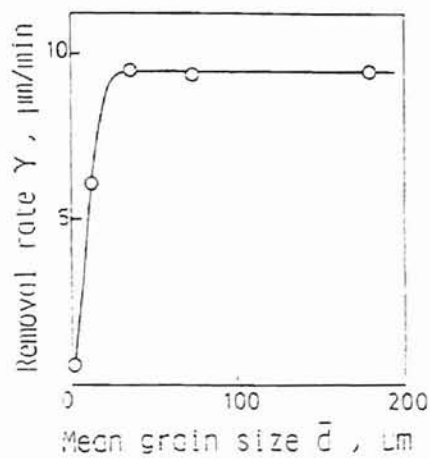


Figure 2.8 Effect of abrasive grain size on material removal rate.
[Umehara and Kato, 1990]

2.3.3 Effect of Rotational Speed

The effect of rotational speed on material removal rate was also investigated by Umehara and Kato [1990]. They found the material removal rate to increase with increasing speed approximately 15,000 rpm, after which it reaches a saturation point (Figure 2.4). Of course, it should be kept in mind that these experimental values are obtained by just considering the rotational speed of the driving shaft.

2.3.4 Effect of Field Support Stiffness

In order to find the effect of the field support stiffness, Umehara et al [1994] carried out several experiments. These experiments were conducted by keeping the grinding load constant and varying the width of the magnets. The effect of the field supporting stiffness on material removal rate is presented in Figure 2.9. It shows that lower stiffness values can be obtained by using smaller size magnets, but use of these smaller magnets yields lower material removal rates. They also found that an even greater improvement in material removal rate can be achieved by using higher field support stiffness. From this, it appears that a lower field support stiffness can result in lower surface finish.

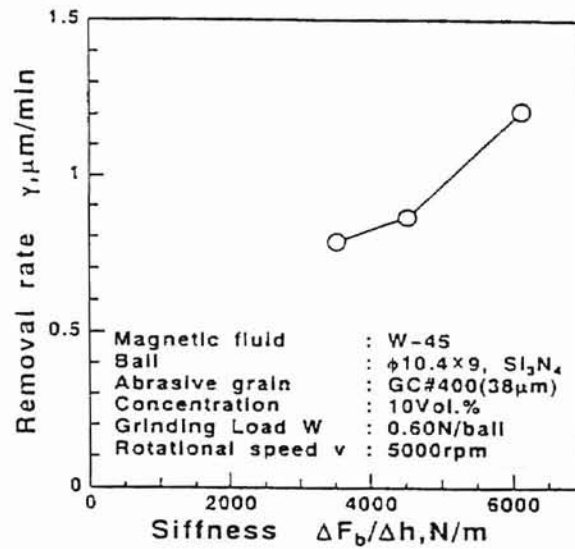


Figure 2.9 Effect of the magnetic field support stiffness on material removal rate
[Umehara et al, 1994]

2.4 Magnetic Float Assisted Polishing Mechanics

In order to formulate the mechanics of the magnetic float assisted polishing process, several studies have been carried out mainly by Childs et al. [1994b]. The main purpose is to predict the motion of the ball as well as the float during the magnetic float polishing process.

$$V = (K/H) W_s v_s$$

Childs et al. found that the model developed and the calculations fit Archard's wear law where V is material removal rate, K is the wear coefficient, H is the hardness of the silicon nitride ball, v_s is the sliding velocity and W_s is the load between the shaft and a ball.

The motion of the ball is defined by the ball circulation rate around the chamber, the spin, and spin direction of a ball about its own axis. The motion of the float is defined using its rotation rate. In order to establish the kinematics of the ball motion, the grinding cell geometry and the variables of this motion were defined in Figure 2.10.

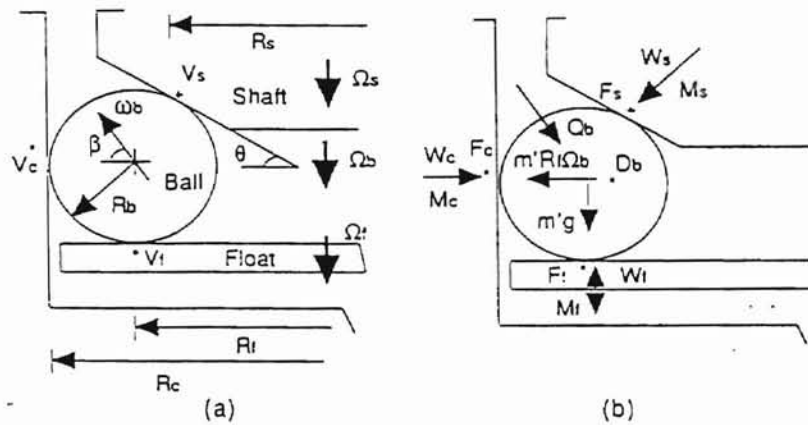


Figure 2.10 Magnetic float polishing model notation for (a) cell geometry and motion and (b) float forces and torques [Childs et al 1994b]

After generating this model, the sliding speed of a ball with respect to the chamber, shaft, and float, and the volume material removal can be developed and expressed as follows:

Sliding speed of a ball with respect to the chamber, $V_c = R_f \Omega_b - R_b \omega_b \sin \beta$

Sliding speed of a ball with respect to the driving shaft, $V_s = R_s \Omega_s - R_f \Omega_b - R_b \omega_b \cos(\beta - \theta)$

Sliding speed of a ball with respect to the float, $V_f = R_f \Omega_b - R_b \omega_b \cos \beta - R_f \Omega_f$

Volume material removed = $0.54(K/H)(\omega_b \sin \beta + \Omega_f) W_m^{4/3} (R_b)^{1/3} / E$

where:

K is the wear coefficient

H is the hardness of a silicon nitride workpiece

W_m is the contact load

E is Young's modulus of silicon nitride

R_c is the inner radius of chamber

R_b is the radius of ball

$R_f = R_c - R_b$ is the radius where the ball contacts the float

$R_s = R_f - R_b \sin \theta$ is the radius of the shaft

Ω_s is the shaft angular speed

Ω_f is the float angular speed

Ω_b is the ball circulation speed

θ is the conical slope of the chamber

ω_b is the ball spin angular speed

β is the angle of ball spin axis.

The model developed has good reliability as the calculated values agree closely with the experimental results. Higher contact loads reduce sliding velocity and the motion of a ball can easily be affected by the changes in the sliding friction coefficient and the fluid viscosity. It can also be observed that higher sliding speeds yield higher removal rates thereby improving the efficiency of the polishing process.

2.5 Tribology and Material Removal Mechanism of Ceramics

As mentioned earlier, high hardness, brittleness, low thermal conductivity and chemical inertness are the main tribological properties of ceramics; which is quite different when compared with metals. Tribological properties of ceramics such as the friction, wear, and tribo-chemical wear of ceramics were investigated by Kato [1990]. Friction coefficients of ceramics in air varies from 0.44 to 0.90 which is not very different from oxidized metals in the air. However, in a vacuum environment, the coefficient of friction of all ceramics is less than unity which is quite different when compared to metals. The reason for that being is the brittleness of ceramics in a vacuum environment. The cause for that brittleness is that ceramics do not allow junction growth by plastic deformation. In his paper, Kato states that oxide film reduces friction because of this lack of junction growth in ceramics. It is also concluded that friction of ceramics is originally sensitive to contamination. In the same paper, it has been mentioned that wear mechanisms in ceramics can occur by cracks around the contact zone and these cracks can be hertzian, lateral, median and radial. It was also found that in dry rolling friction, the wear process of ceramics is dominated by brittle fracture.

Brittle fracture and ductile regime removal theories in ceramics was initially investigated by Yoshikawa [1967]. Yoshikawa described by expressing the size of the stress field using working units which are grouped under four main domains. These domains are characterized by the defect structure as shown in Figure 2.11. In this analysis, the workpiece material was considered to be a defect free material. It is suggested that in domain 1, material removal could not be due to mechanical action

because material removal takes place only on the order of an atom or a molecule. Therefore in this domain, chemical action should be dominant. Since the workpiece is considered as a defect free material, the material removal takes place like an ideal crystal in domain 2. In domain 2, it is considered that applied loads help to generate dislocations which are the dominant material removal factors in domain 3. It is stated that in this domain initially, plastic deformation occurs, followed by the generation of the cracks.

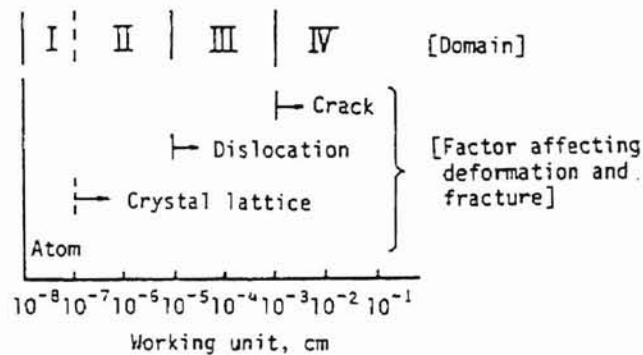


Figure 2.11 Stress field classification in terms of working units (Yoshikawa, 1967)

In the magnetic float polishing process, Childs et al. [1994a] showed that this fracture formation occurs due to 2-body abrasion. Umehara and Komanduri [1994] also reported that the material removal in magnetic float polishing takes place due to 2-body abrasion. Komanduri et al. [1996] state that the material removal mechanism by this

fracture formation depends on the nature of bonding, which is either ionic or covalent bonding in the case of ceramics. Akazawa and Kato [1988] also show that material removal is observed due to tribo-chemical action in ceramics. Bhagavatula and Komanduri [1996] also provided some evidence of chemo-mechanical material removal in magnetic float polishing. They show that, by using a chromium oxide abrasive, a surface finish (R_a) of less than 10 nm can be obtained which is believed to be due to a chemo-mechanical material removal. Eventhough, aluminum oxide and chromium oxide have almost the same material hardness, material removal rates on silicon nitride balls with chromium oxide abrasive are found to be higher than aluminum oxide abrasive, which also indicates that chemo-mechanical might be dominant with chromium oxide.

2.6 Electromagnetic Float Polishing

In order to polish ceramic bearing balls, Umehara's design [1990] was presented earlier. In his design, the magnetic field is generated by using permanent magnets. As an alternative to the permanent magnet polishing apparatus, an electromagnetic float polishing apparatus design was proposed by Shinmura and Komanduri [1992]. By using similar features of a permanent magnet polishing apparatus, an electromagnet polishing apparatus design was carried out (Figure 2.12). Umehara's permanent magnet design has a magnetic field strength of 0.6T, and this magnetic field strength value is incorporated in the design of an electromagnetic field assisted polishing apparatus (EMFP). This new design is called the straight field electromagnetic polishing apparatus. This equipment was built and used by Dock [1994]. During the evaluation of straight field

electromagnetic polishing equipment by using the finite element method, it was found that this new design does not provide a uniform magnetic field orientation; and the balls polished with this equipment do not meet the surface finish and sphericity requirements.

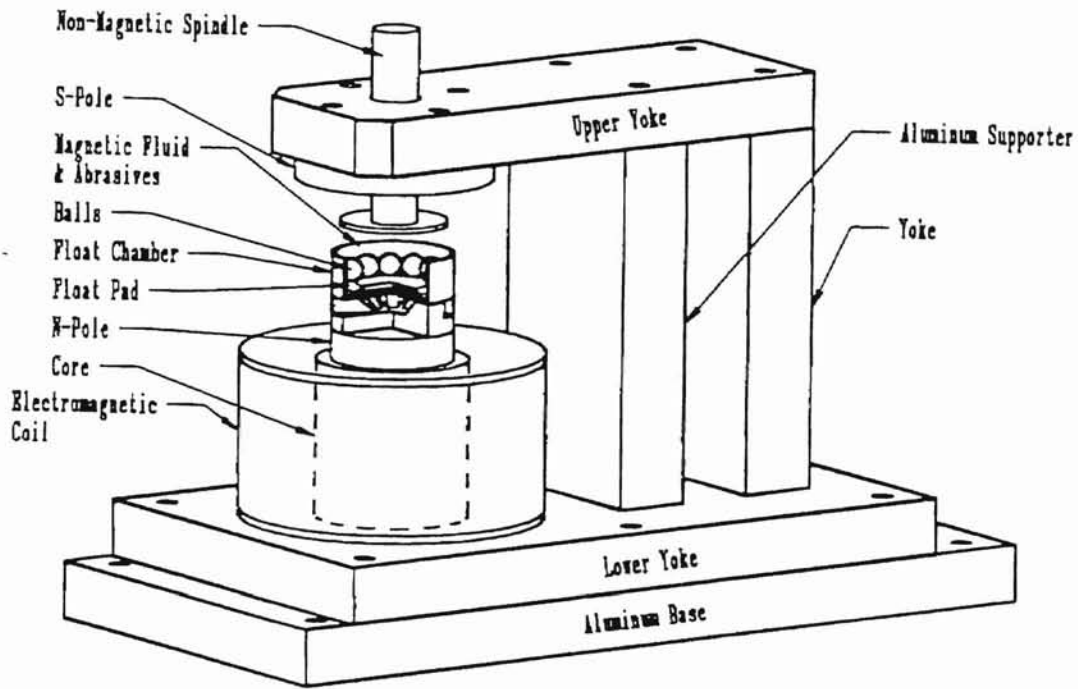


Figure 2.12 Straight field electromagnetic polishing apparatus designed by Shinmura and Komanduri[1992]

Because the results achieved with the straight field design were not satisfying, the parameters were reevaluated and a ring pole electromagnetic polishing apparatus design proposed and built (Figure 2.13) by Dock [1994]. Although, with this new design, promising results (surface finish of $0.171\text{ }\mu\text{m}$ with Cr_2O_3 1200 grit and sphericity of $2.9\text{ }\mu\text{m}$) were obtained, it is yet to meet with the requirements that are essential for a ceramic bearing ball.

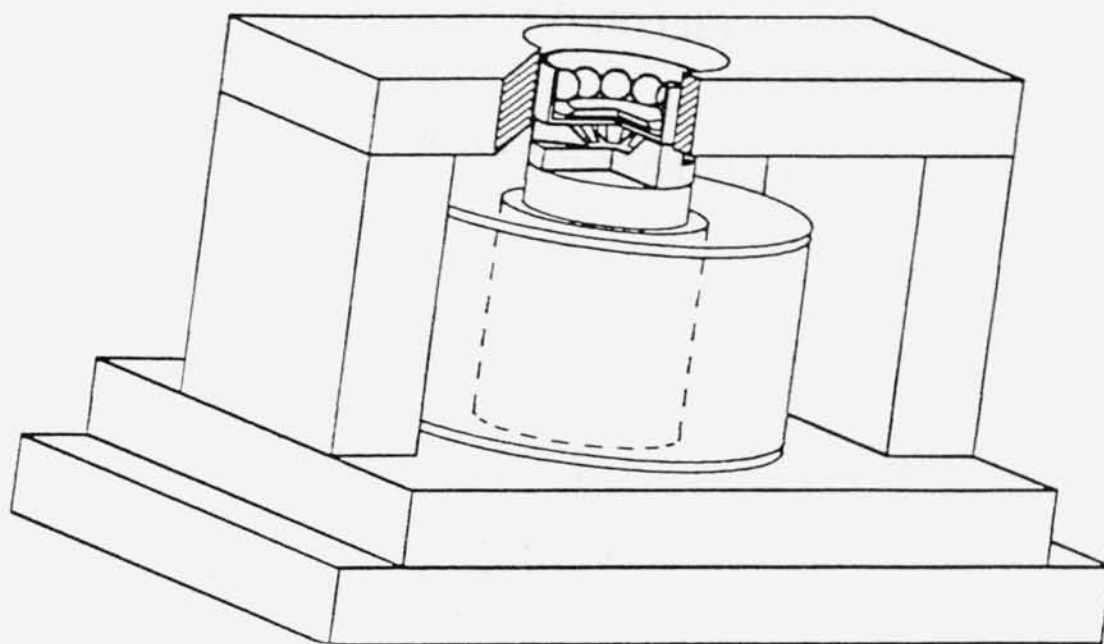


Figure 2.13 Ring pole electromagnetic field assisted polishing apparatus proposed by Dock [1994]

CHAPTER 3

PROBLEM STATEMENT

3.1 Magnetic Float Polishing

The magnetic float polishing technique has been showing promising results for finishing silicon nitride bearing balls. Longer manufacturing time, high cost, and creation subsurface damage are the main disadvantages of the conventional polishing techniques. In order to eliminate these problems, the magnetic float polishing technique was proposed as an alternative process to finish advanced ceramics.

In the early stages of the magnetic float polishing investigation, researchers generated the necessary magnetic field by using permanent magnets. In order to provide the desired magnetic field orientation, these permanent magnets are arranged with alternating N and S poles. With this permanent magnet design, it is possible to generate buoyancy forces up to 7 N, depending on the size and residual magnetization of the magnets. Since the size of the magnet and the magnetic field strength are fixed in a certain design, buoyancy forces cannot be altered for that particular design. This is the biggest limitation of the permanent magnet polishing apparatus; however satisfactory results can be obtained.

3.2 Electromagnetic Float Polishing

The electromagnetic field assisted polishing apparatus designed by Shinmura and Komanduri and built by Dock [1994] was another important step in finishing ceramic bearing balls. The process is very similar to the permanent magnet design. The biggest difference is the way the magnetic field orients. The theoretical considerations of the electromagnetic field design were based on the field strength values that a permanent magnet provides. Magnetic field is generated by using a 1018 low carbon steel core and a copper coil around this core. It is possible to provide a magnetic field strength of 1.8 T which is approximately three times larger than the field strength obtained from permanent magnets. The theoretical advantage of this higher magnetic field strength is the possibility of higher material removal rates and improvement in the form errors.

Dock [1994] obtained promising results from the electromagnetic field assisted polishing apparatus (a surface finish of $0.171\text{ }\mu\text{m}$ with Cr_2O_3 (1200 grit) abrasive and a sphericity of $2.9\text{ }\mu\text{m}$). These values, however do not meet the requirements for a bearing ball for high precision applications. Also, the database created for the effect of various polishing parameters on the process (namely, surface finish, sphericity, material removal rate) should be completed. Modifications should also be made to provide as much uniformity in magnetic field generation as possible to improve sphericity and surface finish using the electromagnetic float polishing process. The finite element analysis package of ANSYS was employed to determine the most influential parameters in the polishing process. An effective force measurement method should also be developed to

have a better control of the process. Also numerous characterization tests were conducted to discover the potential and performance of the electromagnetic float polishing apparatus by considering material removal rate, surface finish and sphericity.

CHAPTER 4

ANALYSIS OF THE ELECTROMAGNETIC FIELD ASSISTED POLISHING (EMFP) APPARATUS

4.1 Initial Design of the Electromagnetic Field Assisted Polishing Apparatus

Electromagnetic field assisted polishing was first proposed by Tani [1984]. Although, the proposed electromagnet was not for balls, it showed a great deal of reliability in terms of use of electromagnets for the polishing process. In order to polish the balls, the first electromagnetic design was developed by Shinmura and Komanduri [1992]. In the initial step of designing equipment for polishing balls, Shinmura and Komanduri used the design parameters of Umehara's permanent magnet design which had a magnetic field strength of 0.6 T. In order to reach the specific magnetic field strength, the required current and the number of wire turns were calculated. A schematic of this initial design was presented in Figure 2.12 in Chapter 2. In this design most of the elements were fabricated out of AISI 1018 low carbon steel, except for the aluminum base and side supporter and the copper coil. It should also be mentioned that the chamber and the drive shaft are made of a nonmagnetic material, namely type 304 seamless stainless steel.

Anticipated magnetic field orientation from Shinmura's design is presented in Figure 4.1. As can be seen from this figure, the magnetic field passes through all of the low carbon steel parts of the design and eventually through the polishing chamber. The lower intensifier was found to be the most important element in the generation of the magnetic field inside the polishing chamber; while the gap between the lower and upper intensifier also played an essential role in terms of the magnetic field strength. It was also found that the shape of the lower intensifier determines the field gradients.

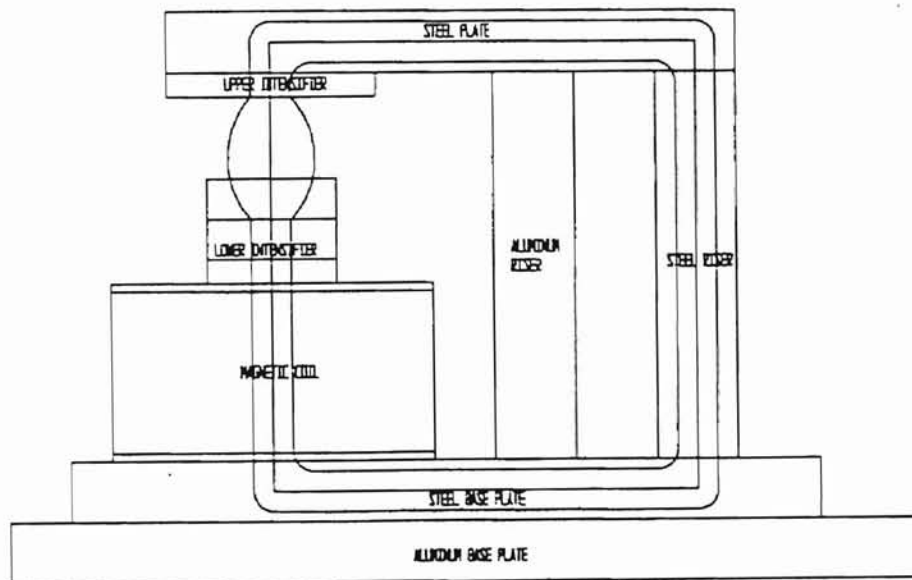


Figure 4.1 Magnetic field orientation through the straight pole design of Shinmura and Komanduri [Dock, 1994]

This initial shape of the lower intensifier was proposed to generate similar magnetic field gradients, but the design produced strong and weak areas in the orientation of the magnetic field, see Figure 4.2 (a). This variation in the magnetic field strength was found to have a negative effect on the shape of the balls, and therefore to bad sphericity. The alternating distance from the top portion of the magnetic field intensifier leads to a negative stiffness and the lower parts of the intensifier pull the balls from the driving shaft instead of pushing, see Figure 4.2(b). Another problem with the lower intensifier was the heat generated by the magnetic coil. This heat was found to be transferred to the polishing chamber by the lower intensifier causing the evaporation of the magnetic fluid, which leads to a higher viscosity of the magnetic fluid and irregular sliding speeds of the balls. Therefore, a modified lower intensifier with a water cooling system (see Figure 4.2 (c)) was proposed and fabricated by Dock [1994].

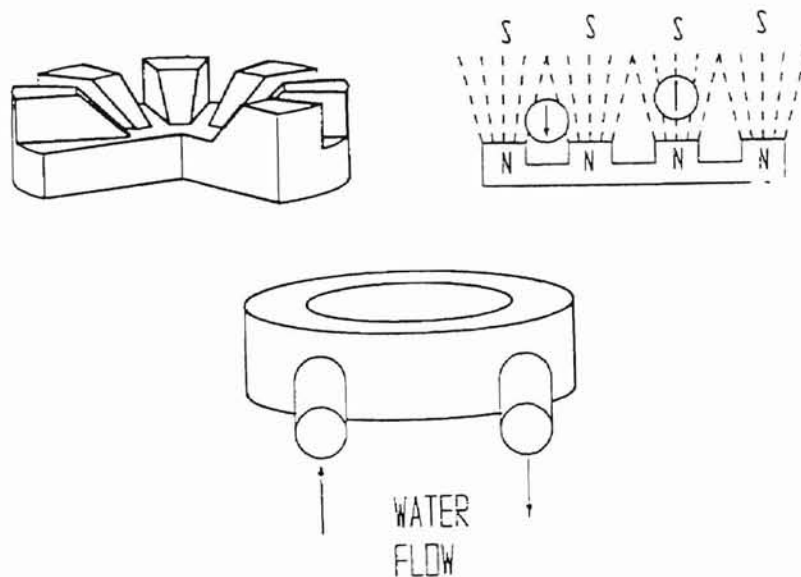


Figure 4.2 (a) Initial design of the lower intensifier, (b) Magnetic field gradients generated by the initial lower intensifier design, (c) Modified lower intensifier design with the water cooling system. [Dock, 1994]

4.2 Elements of the Electromagnet Polishing Apparatus (Initial Design).

As mentioned previously, the electromagnetic field assisted polishing apparatus was designed by incorporating the magnetic field strength used in the permanent magnet polishing apparatus. In order to provide the same magnetic field strength of 0.6 T as in the permanent magnet, the required current and number of turns in the coil was calculated by Shinmura and Komanduri [1992]. The electromagnetic coil was constructed of three separate coils each of which had 1800 turns of 10 AWG insulated copper wire, (see Figure 4.3) and 3 Ω of resistance. Each coil was excited with a power supply which generates 24 V, 6 A continuous current. There were also 3 separate Apex PA12 power amplifiers that were used per coil to regulate the voltage sent to these coils. The output power from these power amplifiers was controlled with a potentiometer which adjusted the current that goes into the coils. Also, three ampere meters were used to monitor the current. After the current passed through these power amplifiers and the potentiometer, the current then went to three separate full wave bridges per coil. These full wave bridges prevented the direction change in the current and therefore provided a fixed polarity for the coils. And also these full wave bridges protected the power amplifiers from the voltage backlash which occurred when the power is removed from the magnetic coils.

As already pointed out the main parts of the electromagnetic field assisted polishing apparatus, were manufactured from 1018 low carbon steel (Figure 2.12) with the base plate and one of the risers was made from 6061 aluminum. This aluminum base plate served to prevent linkage of the field to a machine table where the aluminum riser

was used to reduce the cantilever effect of the top plate. The chamber and the drive shaft were made of type 304 seamless stainless steel so that the magnetic field did not leak through the chamber and link the drive shaft to the Bridgeport machine tool.

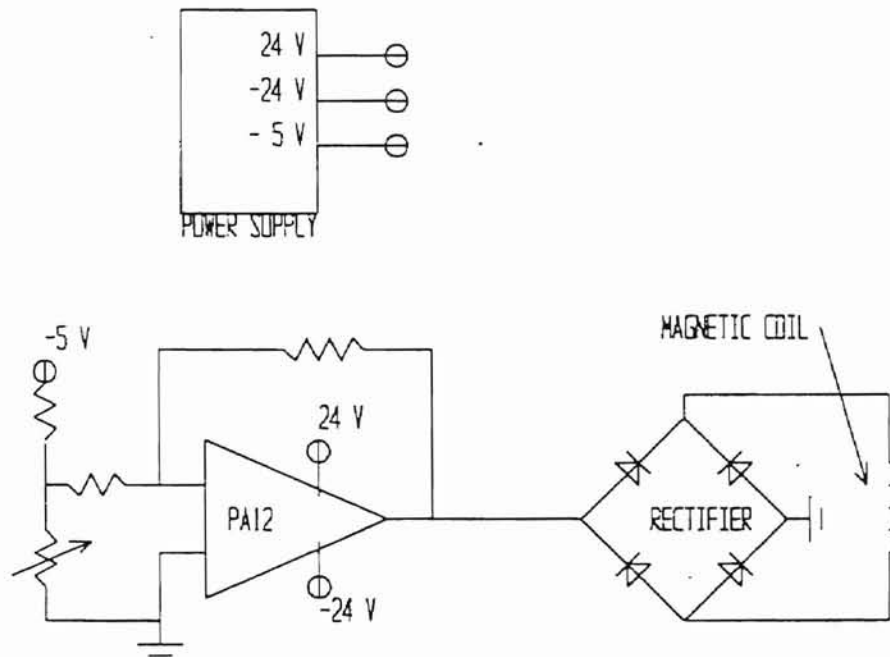


Figure 4.3 Schematic of the power system for electromagnetic field assisted polishing apparatus

The rationale behind Shinmura's design as a straight pole field was that the magnetic field conduction through the lower intensifier to the upper intensifier was found to be varying linearly inside the polishing chamber. The magnetic buoyancy forces which were measured with a 3-axis Kistler piezoelectric dynamometer and Kistler charge amplifier; were found to reach a saturation point where the bottom part of the float contacts with the polishing chamber. And at that point, the maximum buoyancy force obtained was 3.5 N which is not even close to what is obtained with the permanent

magnet. This was the major drawback of the straight field electromagnetic float polishing apparatus.

4.3 Finite Elements Analysis of the Straight Field Polishing Apparatus

In the initial stages of designing the magnetic float polishing apparatus, each parameter was established by trial and error since an FEM package was not available. It was especially difficult to determine the dimensions of the equipment and generate the required magnetic field orientation in order to provide reliable polishing equipment. The finite element method (FEM) was found to be a good tool to overcome this problem in the design stage. In the case of electromagnetic field assisted polishing, finite element analysis was used to determine buoyancy forces, stiffness of the magnetic field, the magnetic field strength and to estimate the magnetic field orientation inside the polishing chamber. In this investigation, the FEM package used was ANSYS 5.0. The ANSYS package uses Maxwell's equations for magnetic field analysis, and the magnetic flux density B , magnetic field intensity H ; and magnetic forces can be obtained from this program. During the evaluation of the electromagnetic field design, a 2D static magnetic analysis type of the solution was used. Even though the electromagnetic field assisted polishing apparatus has a three dimensional nature, by using the rules of symmetry and axisymmetry, FEM analysis can be conducted using 2D type magnetic field analysis.

During the evaluation of the straight field electromagnetic field assisted polishing apparatus, the main objective was to determine the optimum position of the upper magnetic intensifier and to find the maximum possible buoyancy forces. Figure 4.4

shows the geometry data entered into the ANSYS package in terms of real dimensions of the straight field design. The material properties of each element is also entered; including the permeability of air and steel. Material properties of the magnetic fluid were not taken into account which is an important feature for the equipment during the analysis. The relative permeability of air, which is 1, was also used to for the copper coil. The current density in the analysis was $1.5 \times 10^6 \text{ A/m}^2$ which is calculated using the number of turns times the current passing through the coil over the cross-sectional area of the coil which is shown as area 7 and 9 (A7, A9) in Figure 4.4.

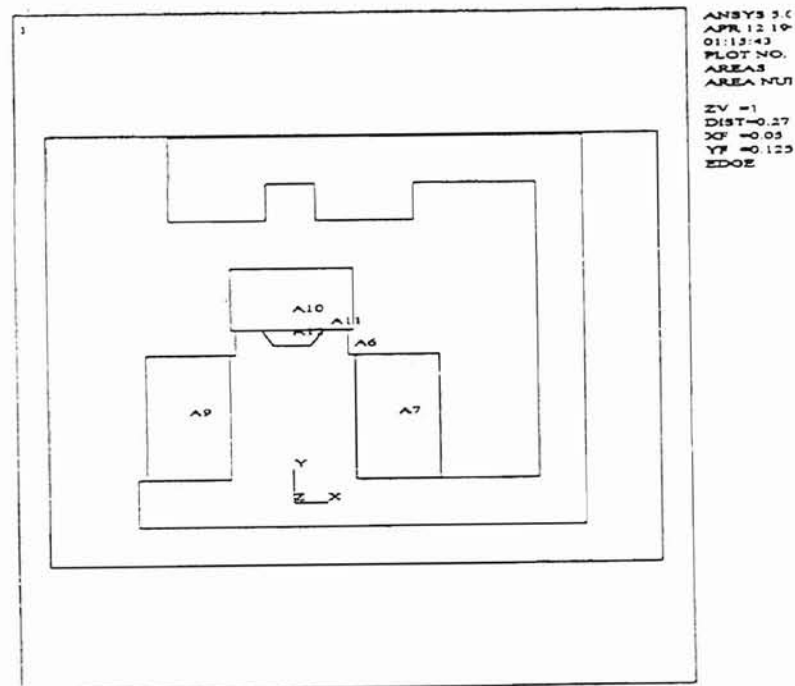


Figure 4.4 ANSYS model for straight field electromagnetic field assisted polishing apparatus [Dock, 1994]
The ANSYS model script generated by Dock [1994] is presented in Appendix A

including the geometry, meshing, material properties and solution script files. At the end, by running the solution script file, the variation in the magnetic field in terms of B and H are presented in Figures 4.5 and 4.6. Since the mesh generation depends upon the user in the ANSYS package, square elements of equal size were used inside of the polishing chamber in order to incorporate the results from the theoretical solution. After obtaining the theoretical solution from ANSYS, the magnitude of magnetic flux density, B, versus the height inside the polishing chamber can be plotted as presented in Figure 4.7. Also, by using magnetic field intensity, H, the buoyancy forces can be calculated using Equation (1) which is an integration over the surface of the immersed body.

$$F_{mf} = - \int_S \left(\frac{1}{2} M_n + \mu_0 \int_0^H M dH \right) n dS \quad (1)$$

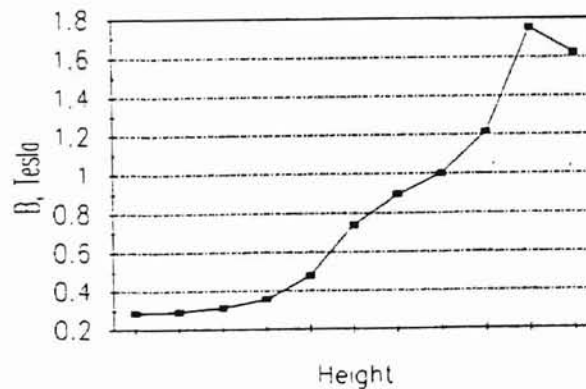


Figure 4.7 Magnetic Flux Density, B, versus the height inside the polishing chamber for straight field electromagnetic polishing apparatus [Dock, 1994]

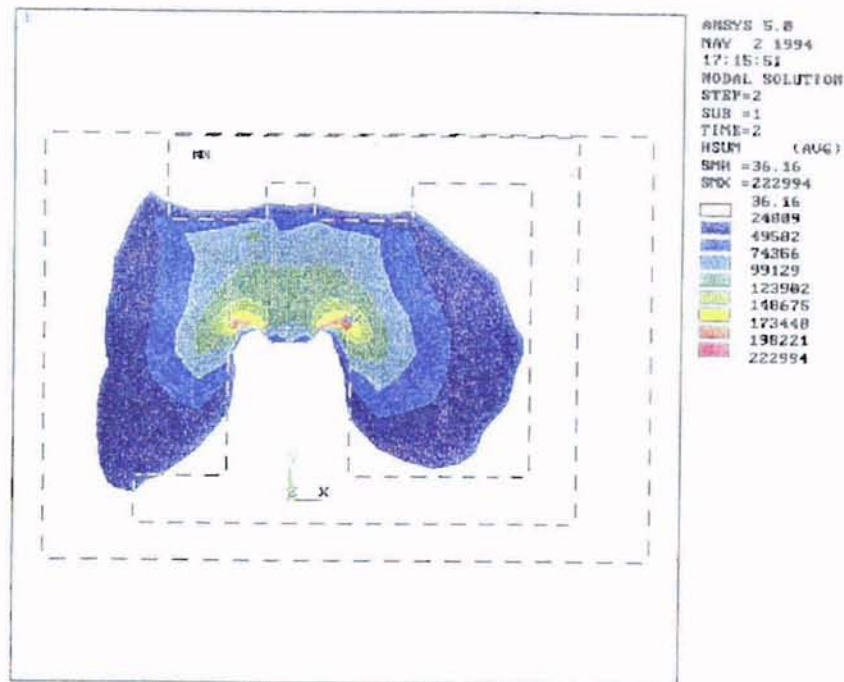


Figure 4.5 Theoretical solution with ANSYS for magnetic flux density, B , in straight field electromagnetic float polishing apparatus [Dock, 1994]

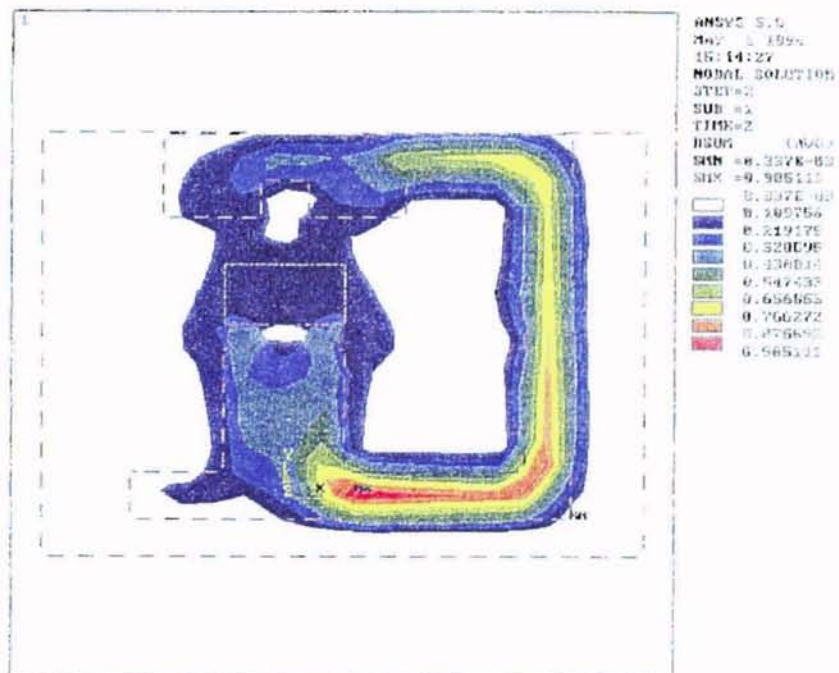


Figure 4.6 Theoretical solution with ANSYS for magnetic field intensity, H , in straight field electromagnetic float polishing apparatus [Dock, 1994]

As can be seen from Figure 4.8, the maximum calculated theoretical buoyancy force is approximately 2 N, which is found to be slightly over the experimental force values (~ 1.5 N). This variation is due to the effect of the magnetic fluid type which was not specified during the analysis, and the difference in the float material density. As shown in Figure 4.8, the obtained buoyancy forces are not even close to what was achieved in Umehara's permanent magnet design which is 7 N. This finding lead to a modification in the design of the electromagnetic field assisted polishing apparatus to obtain higher magnetic field strength and higher magnetic field gradients.

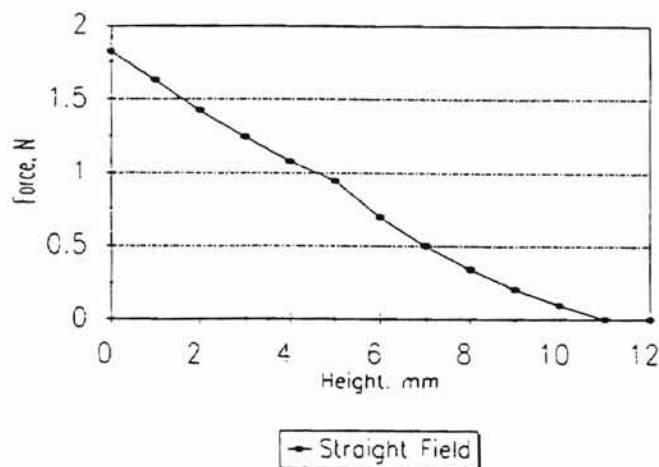


Figure 4.8 Variation in calculated theoretical buoyancy forces with height in straight field electromagnetic polishing apparatus [Dock, 1994]

4.4 Finite Element Analysis for Ring Pole Electromagnetic Polishing Apparatus and Modifications in the Analysis

In order to achieve the same magnetic field strength and magnetic field gradients as in the permanent magnet design of Umehara, modifications had to be made in the Shinmura's straight pole electromagnetic polishing apparatus. A ring pole electromagnetic polishing apparatus design was proposed by Dock [1994] in order to overcome the problems experienced in the straight pole electromagnetic polishing equipment. The rationale behind the proposition of this new design was understanding the importance of the magnetic field strength which increases as the gap between the lower and upper intensifier decreases. As the gap decreases between these intensifiers, magnetic field shorts in a smaller distance and therefore, provides higher magnetic field strength inside the polishing chamber. As the upper intensifier descends closer to the lower intensifier, the upper intensifier must be expanded so that the polishing chamber is encircled by a stronger magnetic field. Also, the low carbon steel plate conductors placed bilaterally of the magnetic core completes ring pole design.

Since the importance of the gap between the lower and upper intensifiers was recognized, the ANSYS analysis were carried out by varying the gaps between the bottom of the ring pole which functions as the upper intensifier and the lower intensifier.

During the initial finite element analysis, material properties (B-H Curve) of the magnetic fluid (which is an essential element in the polishing process) were not taken into account. Therefore, FEM analysis for the ring pole electromagnetic polishing apparatus was redone by considering magnetic flux density, B , and magnetic field

intensity, H , of the magnetic fluid that has been used during the polishing process. A similar approach was used to generate the geometry script file as was performed during the analysis of the straight pole design. The ANSYS geometrical model for the ring pole design is given in Figure 4.9, and the script files can be found in Appendix A.

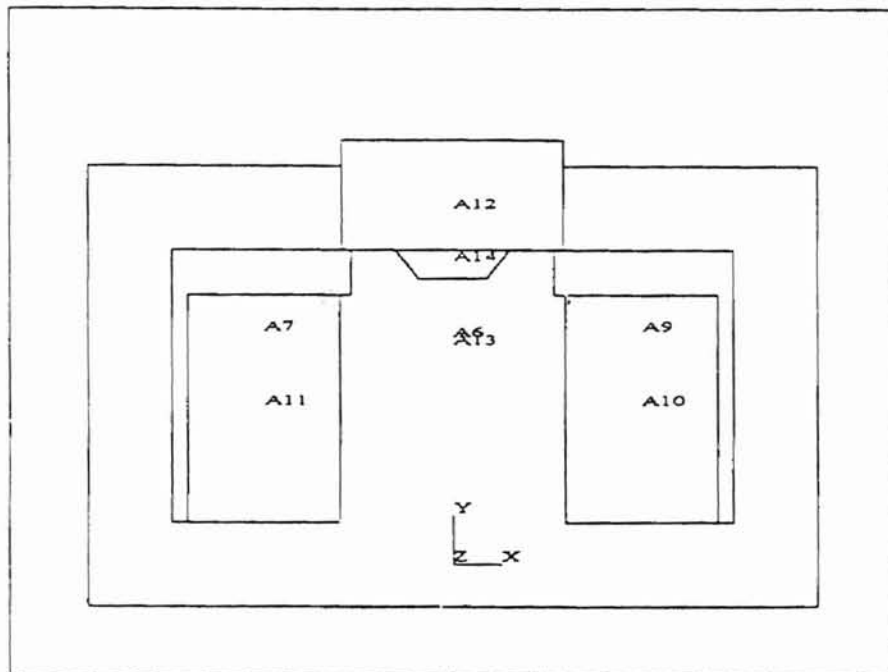


Figure 4.9 ANSYS geometrical model for the ring pole electromagnetic float polishing apparatus

Figures 4.10 and 4.11 show the magnetic flux density, B , and the magnetic field strength, H , plots for the modified ANSYS analysis results. These results clearly present the differences between the straight field and the ring pole designs in terms of the field

ANSYS 5.0.0
 JUN 21 1996
 10:32:04
 NODAL SOLUTION
 STEP=2
 SUB=1
 TIME=2
 BSUM = 0.922E-03
 SMX = 1.817
 (AUG)
 0.202E-03
 0.304E-03
 0.606E-03
 0.807E-03
 1.011
 1.213
 1.415
 1.617
 1.819

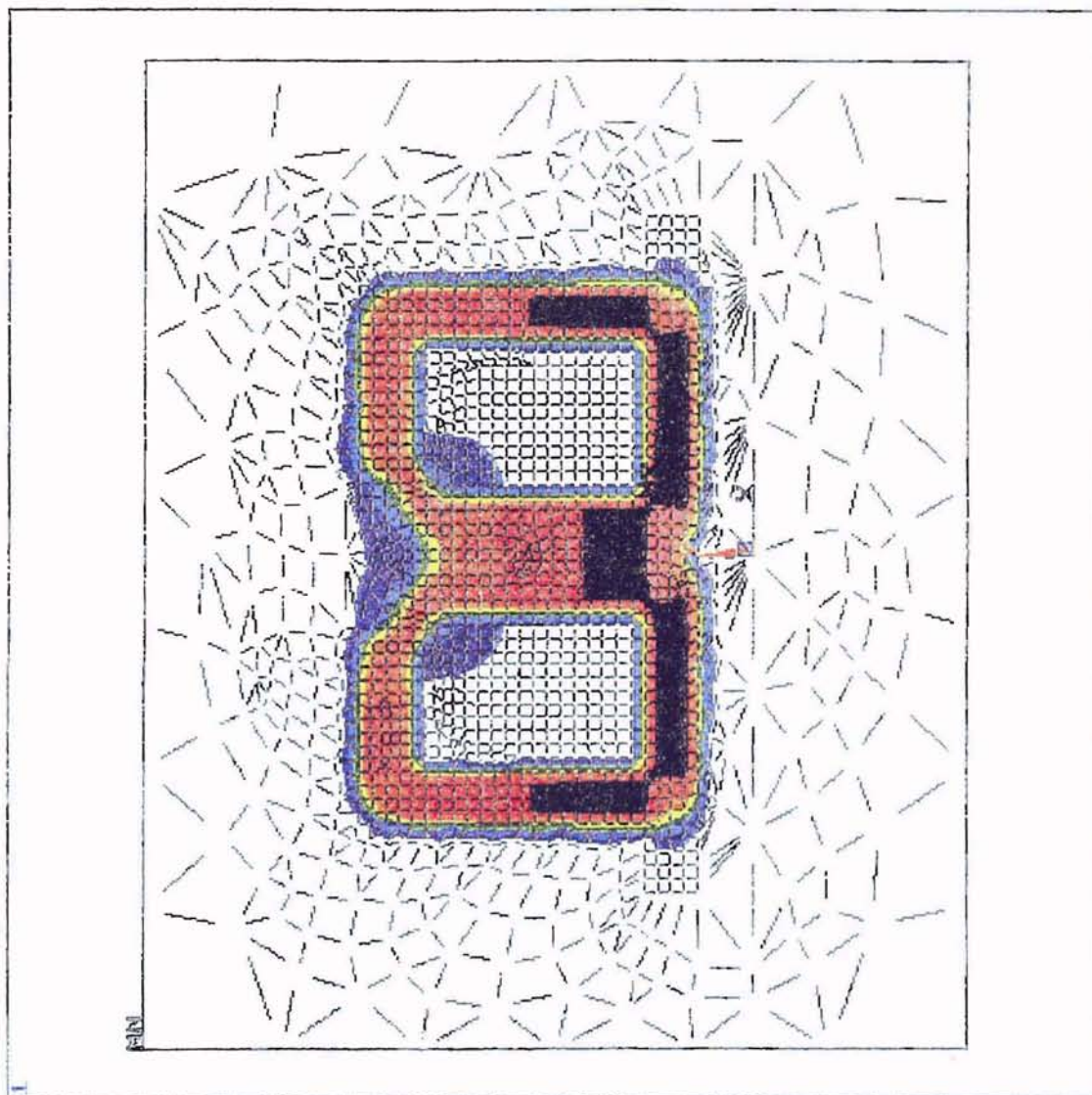


Figure 4.10 Modified magnetic flux density, B , results with ANSYS analysis for the ring pole electromagnetic polishing apparatus

ANSYS 5.0.0
 JUN 21 1996
 10:49:44
 MODAL SOLUTION
 STEP=2
 SUB=1
 TIME=2
 HSUM (AUG)
 SMN = 12.464
 SMX = 12.464
 105573
 211134
 316694
 4227816
 523337
 6338937
 844428
 950038

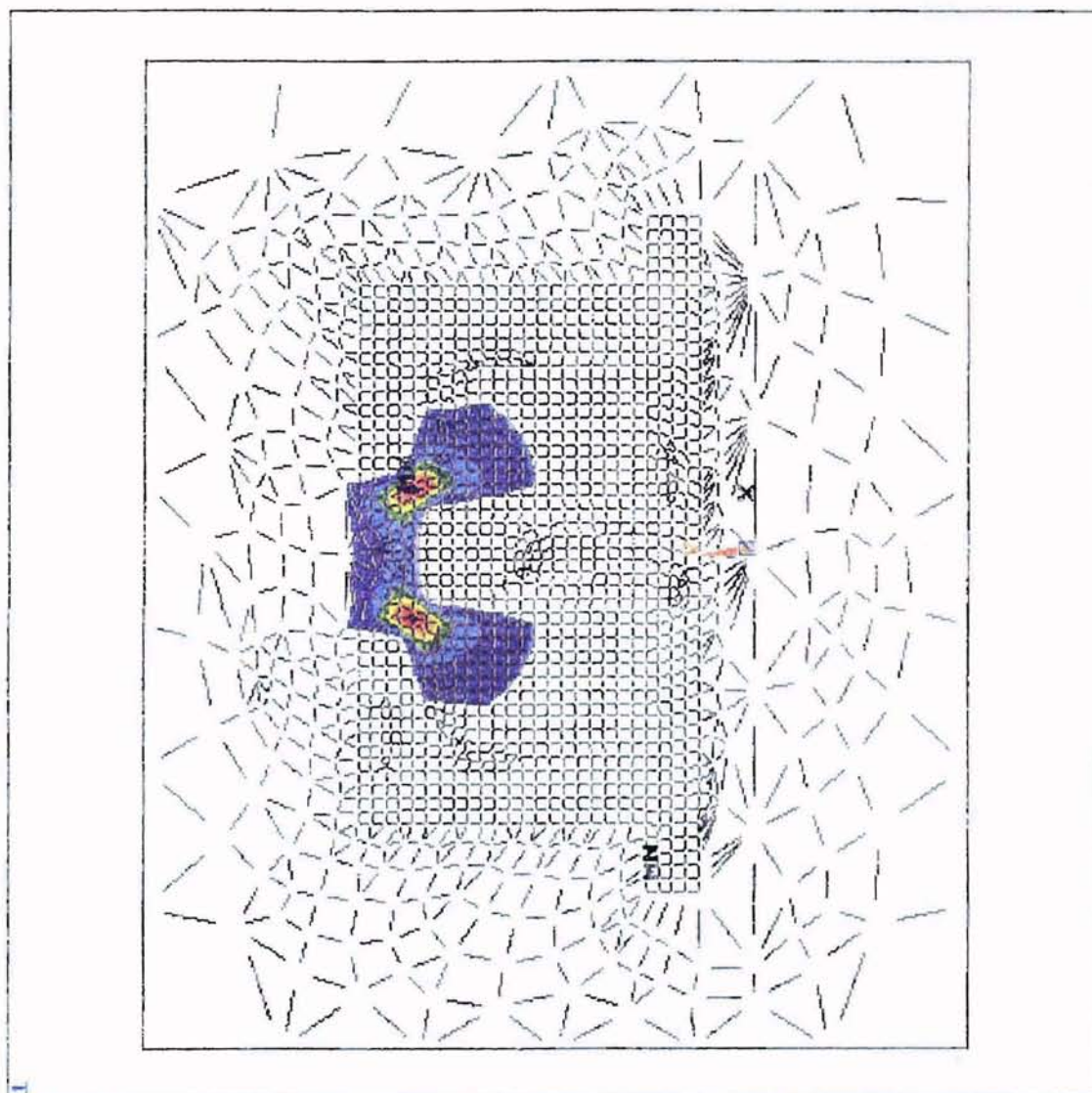


Figure 4.11 Modified magnetic field strength, H , results with ANSYS analysis for the ring pole electromagnetic polishing apparatus

strength and the field gradients. Figure 4.12 shows the magnetic field strength for a 6 mm ring pole, a 10 mm ring pole and the straight field designs. This figure clearly indicates that the 6 mm gap between the ring pole and the lower intensifier provides the strongest magnetic field strength.

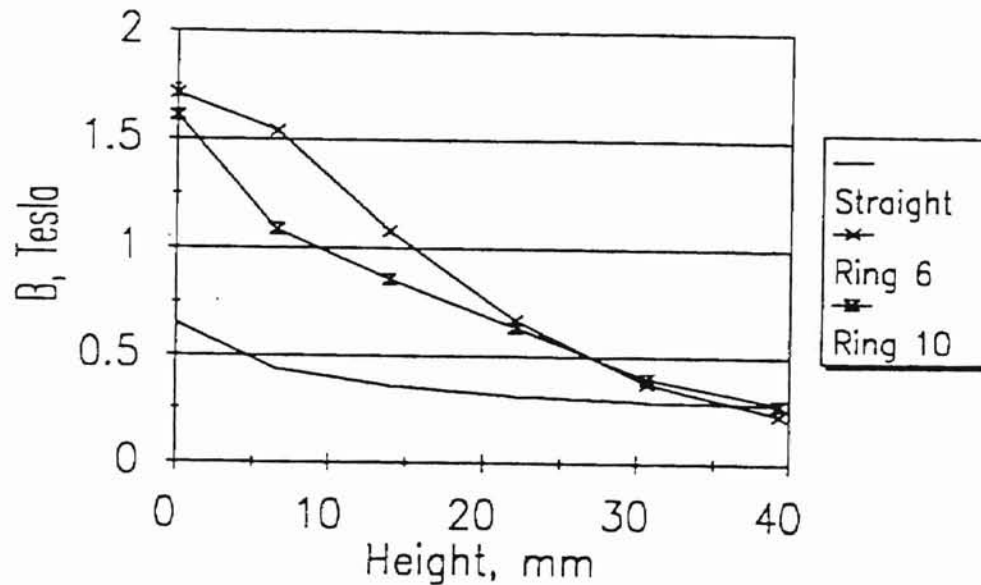


Figure 4.12 Magnetic flux density for the straight and ring pole designs

Figure 4.13 shows the variation in the buoyancy forces with the 0 and 3 mm ring pole and the straight field design. It can be seen from this figure that the straight field provides approximately 3 N at the bottom of the polishing chamber. On the other hand, the ring pole design shows different characteristics as the height decreases inside the polishing chamber. Especially when the trend of the 3 mm gap is noticed, it can be seen that the buoyancy force gradually increases toward the bottom of the polishing chamber, but then a decrease in the force followed by an increase at the bottom of the chamber occurs. This variation in the buoyancy force is due to the negative stiffness inside the

magnetic field. As far as the experimental results are concerned, this negative stiffness occurs when the gap is higher than 6 mm. If the gap is less than 6 mm, the balls inside the polishing chamber are pushed to the bottom rather than being pushed away from the bottom of the chamber. This negative stiffness region causes an increase in the sphericity of the balls. Hence, a zero gap between the ring pole and the lower intensifier must therefore be present in order to polish balls with the required quality of sphericity.

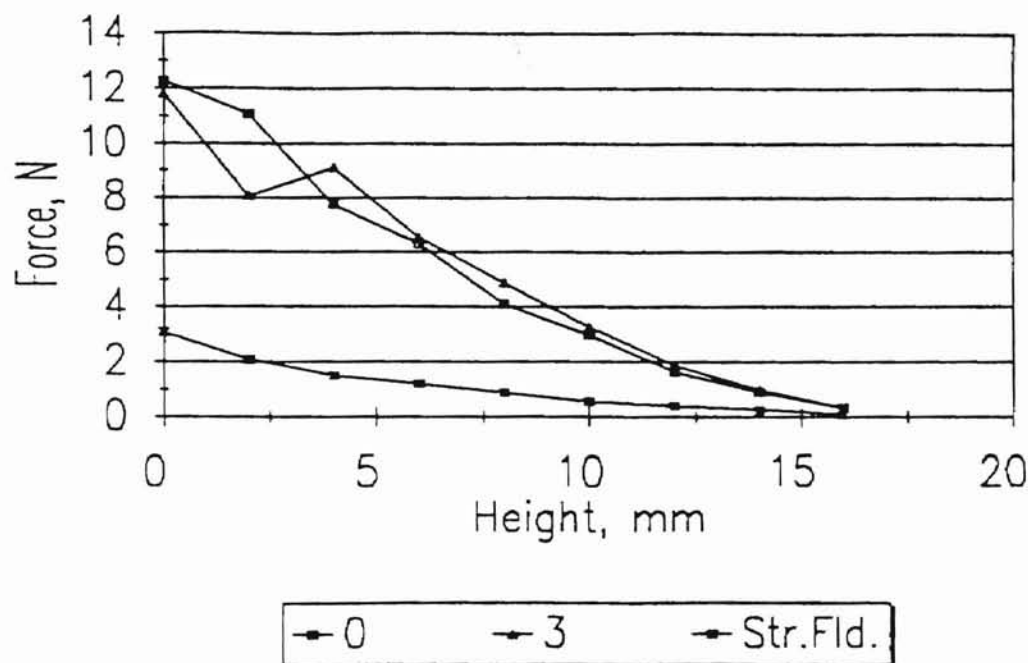


Figure 4.13 Variation in buoyancy forces with height for the straight field and ring pole designs

In Figure 4.14 illustrates the situation of the polishing chamber filled with the magnetic fluid. After analyzing the magnetic fluid generation inside the polishing chamber, it has been thought that the thickness of the ring pole has an effect on the magnetic field strength. After the current is applied to the coils, the magnetic fluid orients to a half donut shape. The magnetic fluid aligns itself due to magnetic field orientation, along the

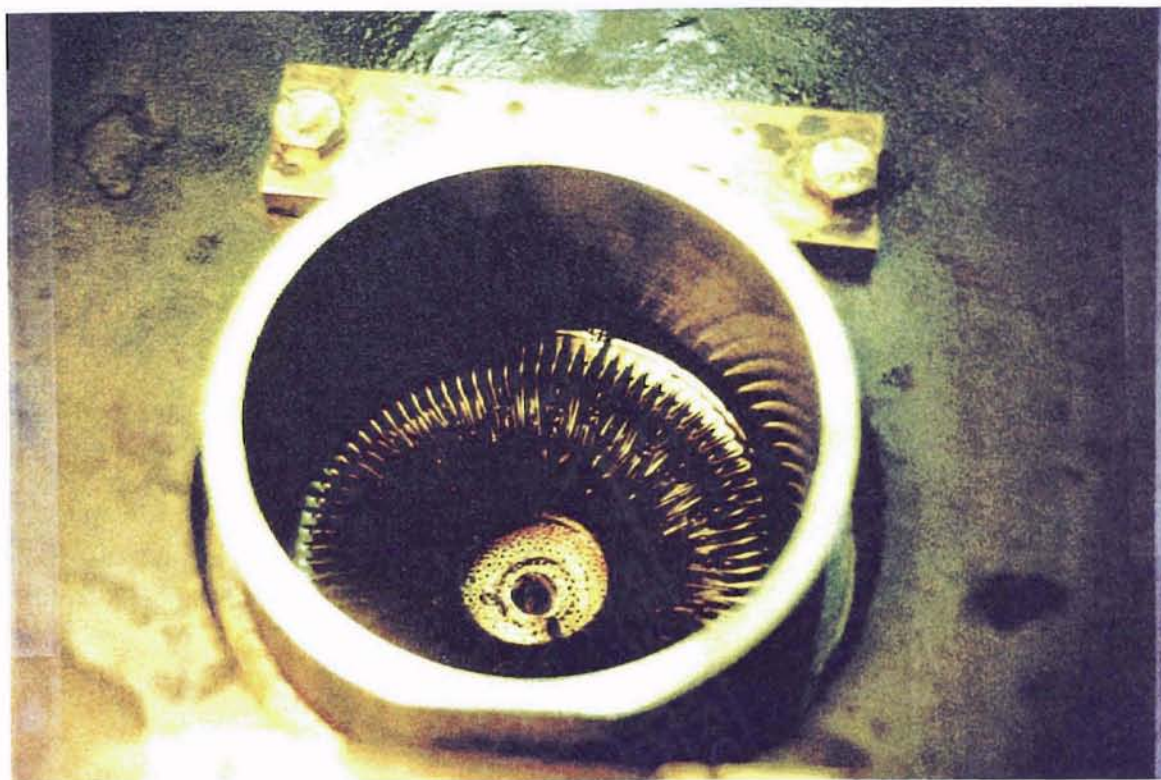


Figure 4.14 The situation of the polishing chamber filled with the magnetic fluid.

length of ring pole, neither going above nor below the thickness of the ring pole, which surrounds the polishing chamber. Therefore, ANSYS analysis was carried out in order to determine the thickness of the steel ring pole. During the analysis, four different ring pole thicknesses were used to determine the effect. In Figures 4.15, 4.16, 4.17 and 4.18, the variations among the different ring pole thicknesses in terms of magnetic flux density, B , are presented. In the initial ring pole design, the thickness that was used was 38.1 mm. As can be seen from these magnetic flux densities of different thicknesses, the ring pole thickness does not have a significant effect on the magnetic field strength. In other words, magnetic field shorts from the closest place from the lower intensifier to ring pole

independent of the ring pole thickness, and this shortest distance has the more dominant effect on the magnetic field strength.

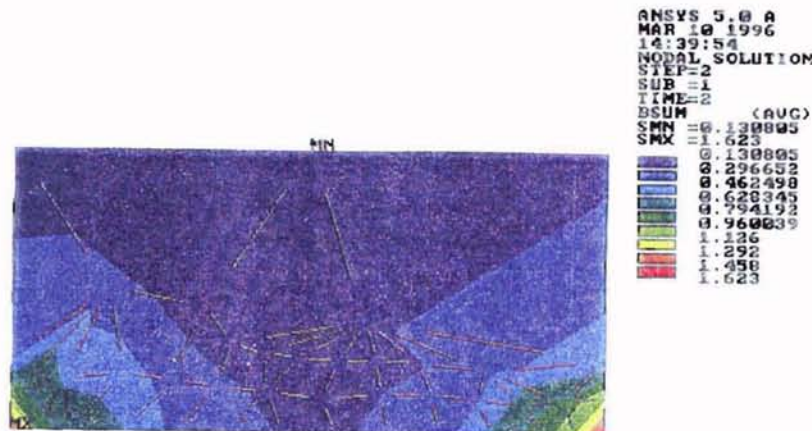


Figure 4.15 Magnetic flux density, B , of the ring pole with a thickness of 12.7 mm

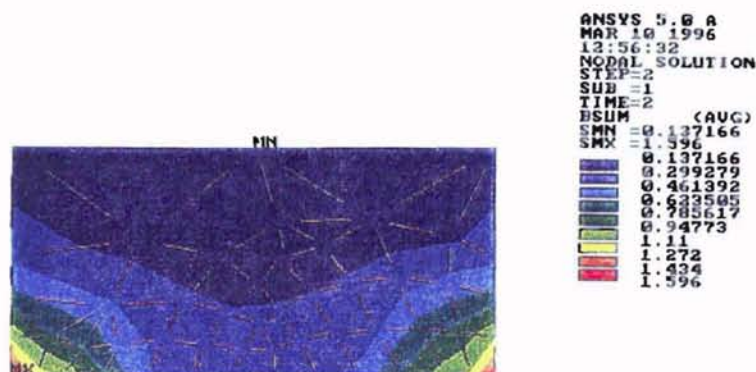


Figure 4.16 Magnetic flux density, B , of the ring pole with a thickness of 25.4 mm

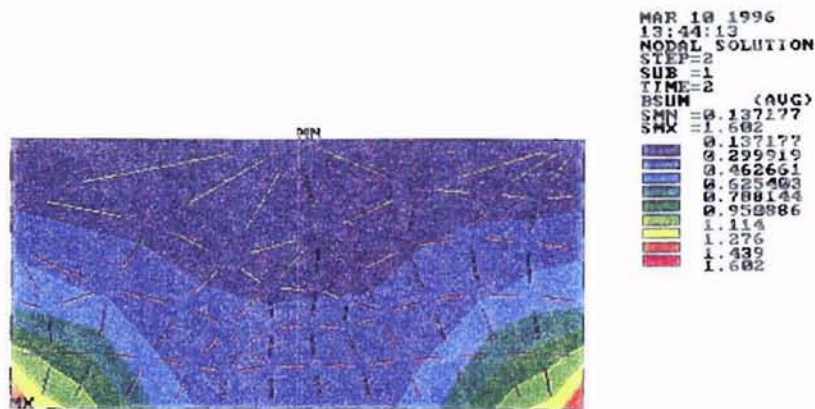


Figure 4.17 Magnetic flux density, B , of the ring pole with a thickness of 38.1 mm

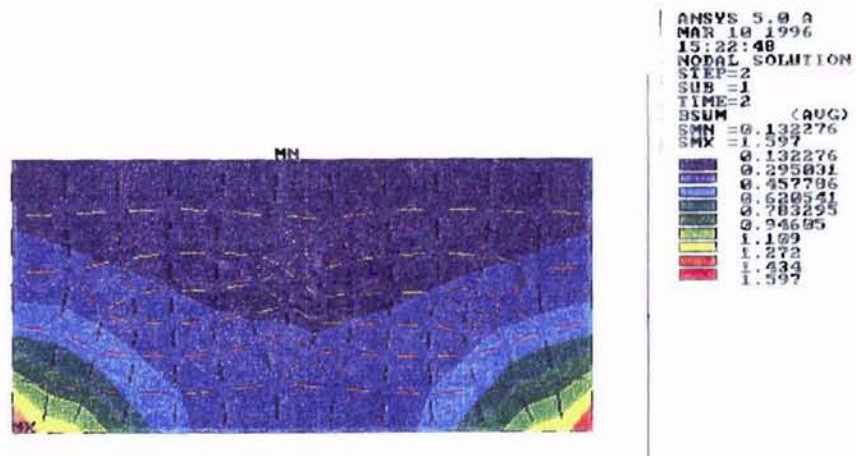


Figure 4.18 Magnetic flux density, B , of the ring pole with a thickness of 50.8 mm

4.5 Modified Ring Pole Electromagnetic Polishing Apparatus

While the ring pole electromagnetic polishing apparatus provides the closest magnetic field strength values to Umehara's permanent magnet design, it should also be noticed that the magnetic flux density, B , results inside the polishing chamber are far from reality. Inside that region, ANSYS analysis shows that the magnetic flux density values reach up to 1.6 Tesla, which is nearly the saturation point for magnetization in steel. It should be noted that the area filled with magnetic fluid has a permeability very close to that of air cannot provide this much magnetic flux density. When the magnetic flux density values are measured on the bottom of the ring pole, the average value of B is ~ 0.28 Tesla. It is almost $1/6$ of the theoretical solution obtained from ANSYS analysis. Part of this difference comes from the ANSYS analysis itself. Since the analysis carried out is a 2D analysis, the ANSYS package assumes that the magnetic coil and the surrounding parts such as the core, side plates and the ring pole steel plate are infinitely long elements. Yet, since the ring pole electromagnetic polishing apparatus has a three dimensional nature, it would be better to approach the problem in a more realistic fashion. The axi-symmetric analysis option in ANSYS package was found to be a better approach to the design problem. It is assumed that the magnetic coil is surrounded by a low carbon steel pipe with a thickness of 1.5 inch; and during the analysis, one fourth of this cross-sectional area is used as the total elements for the electromagnetic polishing apparatus. Area plot for the electromagnetic polishing apparatus in the axi-symmetric analysis option in ANSYS can be seen in Figure 4.19.

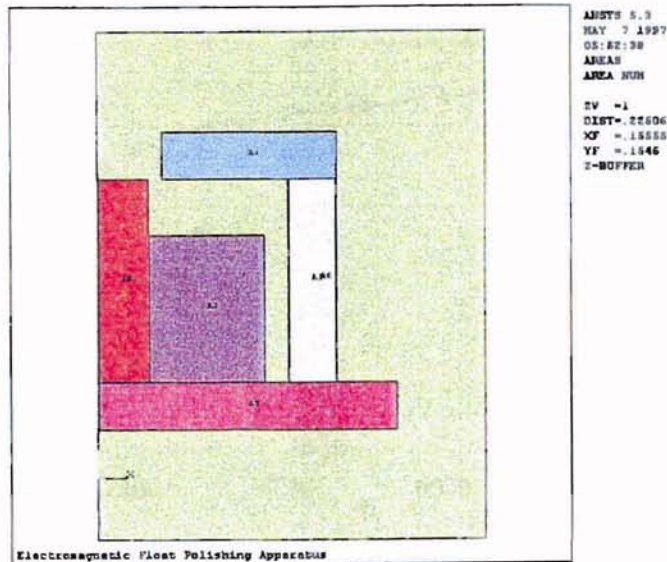


Figure 4.19 Area plot for electromagnetic polishing apparatus in axi-symmetric analysis option in ANSYS

It should be noted, that during the ANSYS analysis, the polishing chamber area was not taken into account. Because most of the FEM packages have their own mesh generators and depending on the mesh size specified, the packages mesh the areas automatically. Sometimes these mesh generators may cause problems which yield different kinds of problems in the solution. Even though, the polishing chamber area was initially defined, this lead to a negative value in the main diagonal of the stiffness matrix generated by the ANSYS package. This negative stiffness value can not be acceptable in the finite element solution. Another problem to be faced with ANSYS analysis is that the

BH curve, which must be entered as a material property of steel shown as in Figure 4.20.

As mentioned earlier, steel has a magnetic flux density saturation value of 1.75 Tesla.

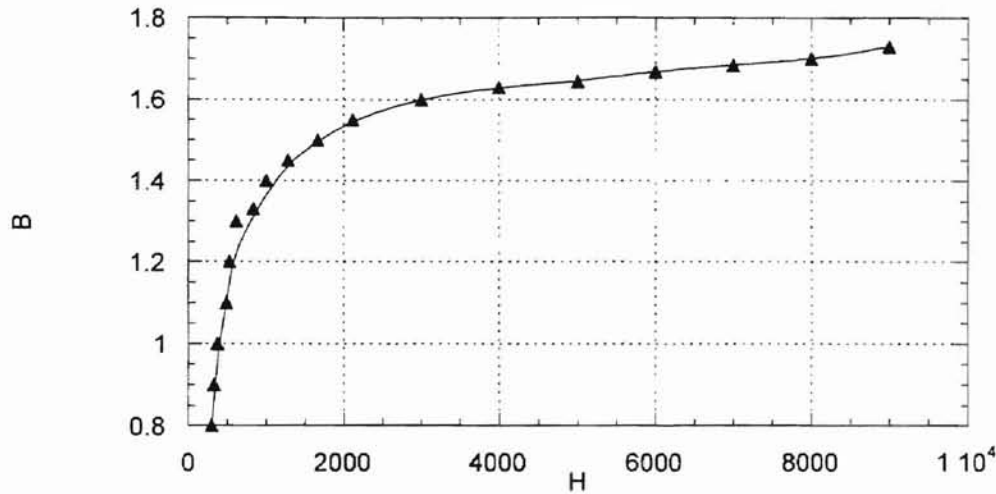


Figure 4.20 B-H curve for low carbon steel

During the solution process and after the magnetic field strength values exceeds 10000, the package extrapolates the corresponding values for magnetic flux density; and this leads to an incorrect solution. Therefore, during the definition of material properties (B-H Curve) for steel, the last data point was interpolated and entered as $H=1000000$ and $B=2.85$. The rationale behind this is that the basic magnetic field equation is $B=\mu_0 \times H$, and the relative permeability (μ_r) can be found from the slope of the B-H curve of steel.

Magnetic flux lines inside the modified electromagnetic polishing apparatus are presented in Figure 4.21 from the ANSYS solution. Magnetic flux density, B, and magnetic field strength, H, are presented in vector form and shown in Figure 4.22 and

4.23 sequentially. Also, total magnetic flux density and magnetic field strength can be seen in Figures 4.24 and 4.25.

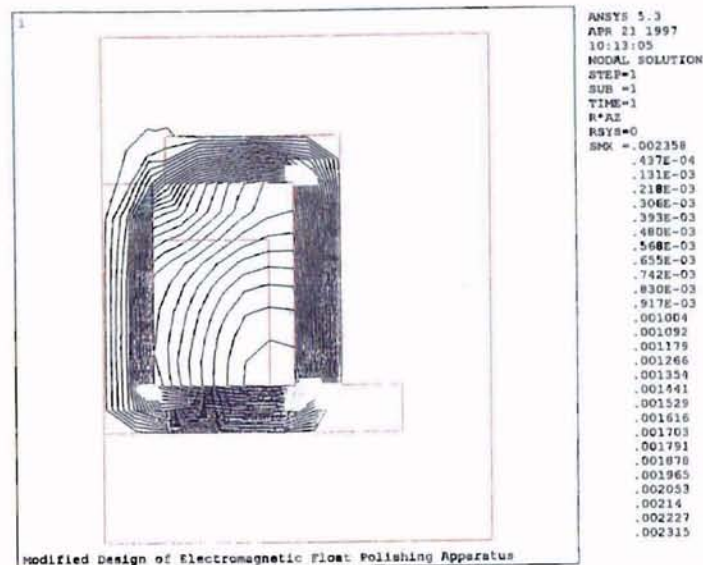


Figure 4.21 Magnetic flux lines inside the modified electromagnetic polishing apparatus.

In order to match with the results obtained from the axi-symmetric ANSYS analysis two conductor low carbon steel plates are placed with a 90 degree turn from the steel conductor plates. Even though this modified design does not meet the same conditions that were used in the ANSYS analysis, it was found that it would be a very close assumption in terms of theoretical analysis from the ANSYS package. It was also found that each of the three coils do not have the same resistance. Therefore, the current

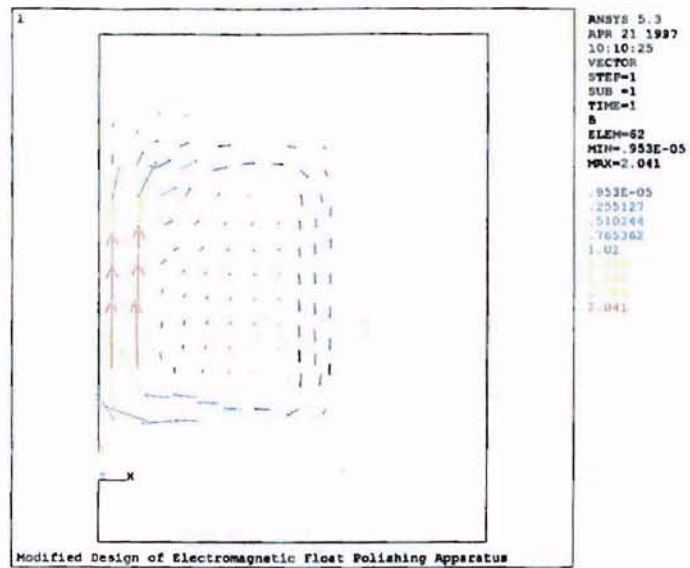


Figure 4.22 Vector form of magnetic flux density, B , in the modified electromagnetic polishing apparatus

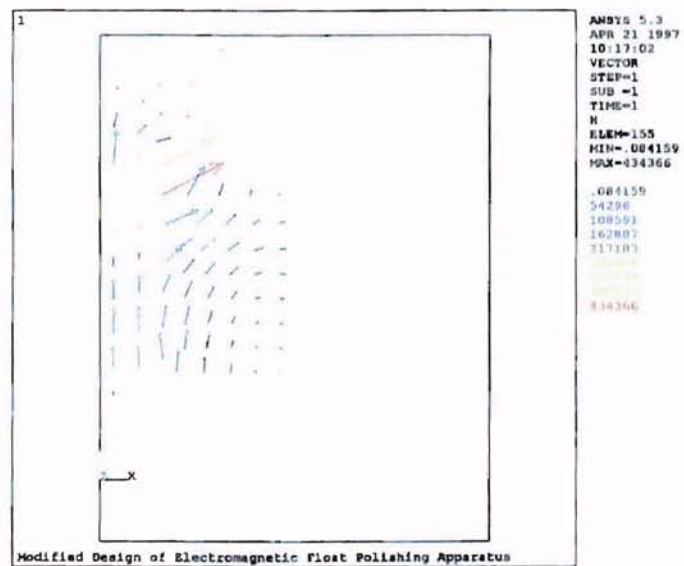


Figure 4.23 Vector form of magnetic field strength, H , in the modified electromagnetic polishing apparatus

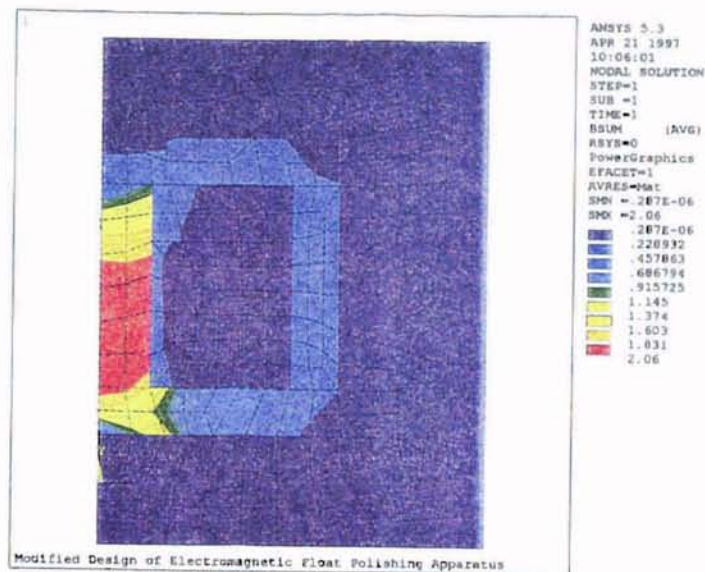


Figure 4.24 Total magnetic flux density, B , in the modified electromagnetic polishing apparatus

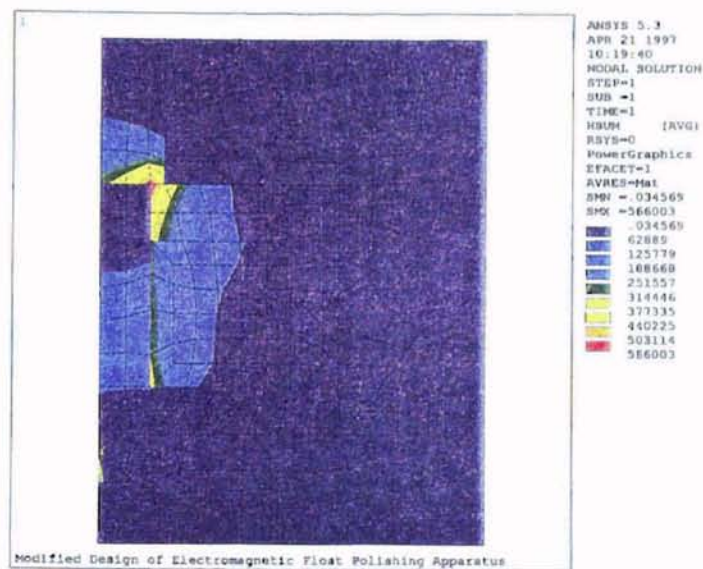


Figure 4.25 Total magnetic field strength, H , in the modified electromagnetic polishing apparatus.

density which is applied to the coil area should have been modified during the theoretical analysis. Even though these three coils have the same number of turns and supposedly should have the same amount of resistance; this variation does not affect the overall magnetic field. That is because the magnetic field generated by these three coils is basically a summation of the field provided by a particular coil. After all, this variation was found to be not much in terms of resistance of a single coil.

After obtaining the theoretical solution from the ANSYS package, the results were compared with the experimental setup. As can be seen from the magnetic flux density, B , results from the theoretical solution (Figure 4.24), the magnetic flux density is approximately 0.46 Tesla in the region corresponding to the bottom of the ring pole. After adding two more conductor side plates, magnetic flux density was measured in the same region with the same Tesla meter. These measurements were carried out by obtaining B values from four points with a 90 degree angle around the bottom of the ring pole. The average of the magnetic flux density was found to be 0.45 Tesla which is 0.01 Tesla less than what was obtained from the ANSYS analysis. This result proves that the assumption of adding two more conductor side plates can be adequate. Figure 4.26 shows the schematic of the modified ring pole electromagnetic polishing apparatus.

The only difference between the ring pole design and the modified ring pole design should be the magnetic field distribution on the ring plate. Three-dimensional ANSYS analysis is the only way to simulate this distribution on the ring pole plate. But when the size of the electromagnetic polishing apparatus is considered, the limited number of elements in the ANSYS package comes into the picture as a big problem. Since the mesh size plays a significant role on the accuracy of theoretical solution, a

limited number of element sizes may lead to an unrealistic result. On the other hand, three-dimensional analysis in the ANSYS analysis was found to be very difficult and tricky in terms creating the geometry and mesh. Since, the axi-symmetric analysis is not much different than a three-dimensional analysis, it is found to be the more realistic solution.

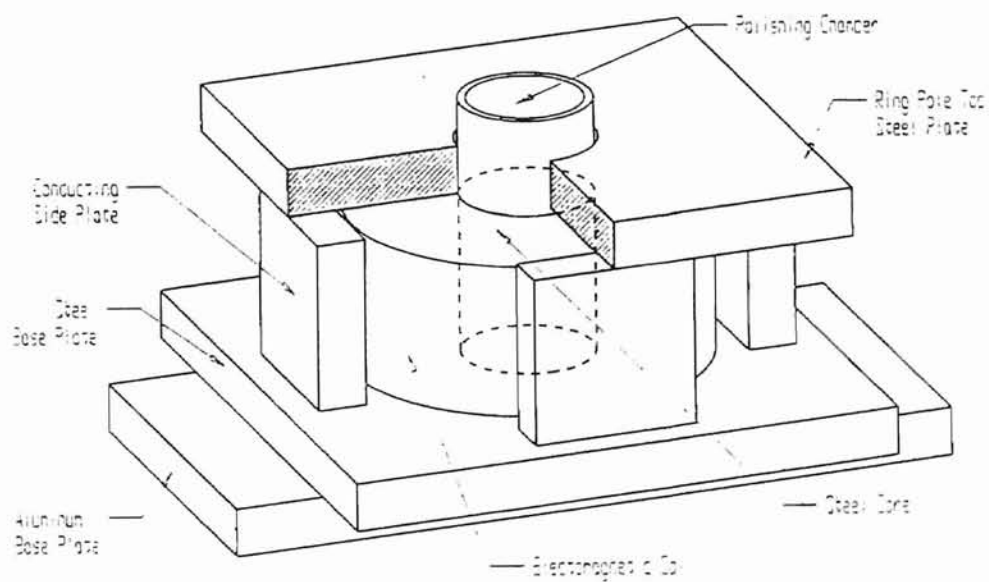


Figure 4.26 Modified ring pole electromagnetic polishing apparatus

4.6 Modifications in Force Measurement for the Electromagnetic Polishing Apparatus

In the case of the permanent magnet polishing apparatus, force measurements can be carried out by using a three-axis Kistler piezoelectric dynamometer hooked up to a charge amplifier and a voltmeter. This setup gives quite accurate results for the permanent magnet polishing apparatus in terms of force measurements. On the other hand, there are several restrictions that apply to the electromagnetic field assisted polishing apparatus. These restrictions are mainly due to the equipment's bulk and heavy nature. The electromagnetic field assisted polishing apparatus weighs approximately 400 pounds. As one can imagine, it is extremely difficult to place a dynamometer under the entire polishing equipment. Even if a dynamometer can be placed under the polishing apparatus, then the problem of locating the apparatus right at the center of the dynamometer comes into the picture. As stated earlier, polishing experiments were conducted on a Bridgeport NC milling center. The maximum length of the Bridgeport milling machine tool for the z axis is 411 mm. The height of the electromagnetic polishing apparatus is 300 mm. After placing the drive shaft in the tool holder, there is not enough space to place a dynamometer under the equipment due to limitation of the z-axis in the Bridgeport milling machine. Since the polishing force was recognized as an important parameter for the polishing process by the previous researchers, utilizing a force measurement system became also an essential challenge.

A uniforce sensor was placed between the polishing chamber and the lower intensifier to measure the forces applied to the silicon nitride balls (Figure 4.27 and

Figure 4.28). These uniforce sensors are about 0.076 mm thick in the sensing area. This thinness of the sensor allowed us to place it in a very small gap. The sensor is constructed with two layers of substrate, such as polyester or polyimide film. A layer of conductive material is applied to each substrate, then a layer of special pressure sensitive material is applied in the sensing area.

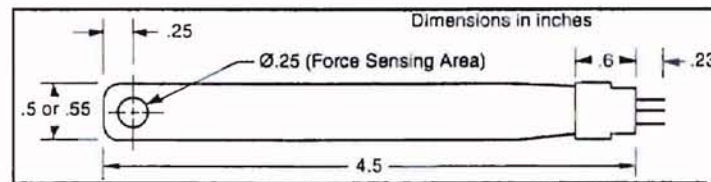


Figure 4.27 Dimensions of the uniforce sensor that was used to monitor the force applied to the silicon nitride balls in the electromagnetic field assisted polishing apparatus.



Figure 4.28 Uniforce sensor used in the electromagnetic float polishing

In order to protect the force sensor from scratches by the metallic surfaces of the lower intensifier and the polishing chamber, a transparency sheet was glued to the lower intensifier; and the force sensor was held on top of this sheet, and a sheet of rubber was placed on the force sensor. Then the sensor was connected to a multi-meter to monitor the force by basically reading the resistance values.

Force measurements were carried out by placing weights on top of the polishing chamber, then the resistance value was read and noted from the multimeter. The driving shaft then was brought down until the same resistance value read from the multimeter. Since the Bridgeport machine tool has an advantage of displaying the axis movements, force values can be monitored and compensated for, depending upon the wear on the edge of the drive shaft. Therefore, the difference of the z-axis value between two polishings was found to vary approximately between 0.020-0.040 of an inch, depending on the edge machining depth of cut. A calibration curve was also developed to monitor the buoyancy forces inside the polishing chamber in terms of the height from the bottom of the chamber for the ring pole design (Figure 4.29).

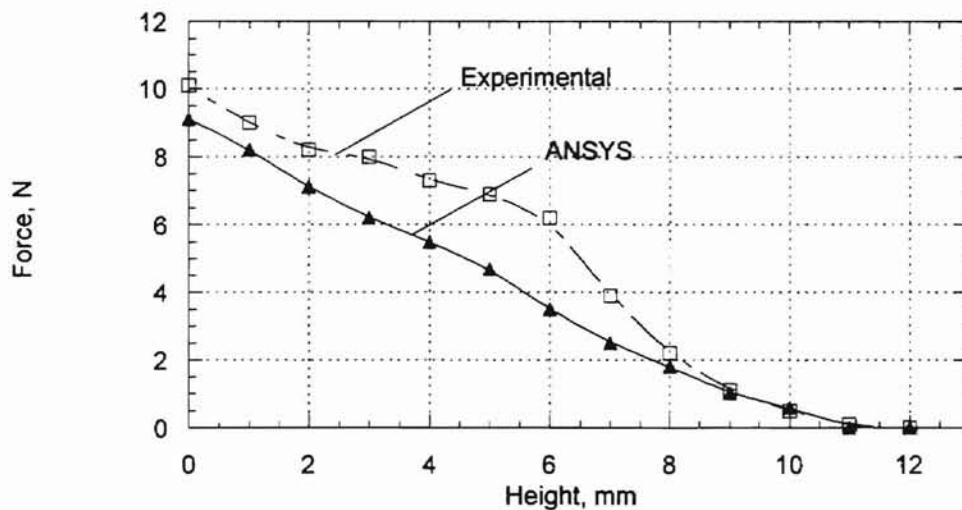


Figure 4.29 Experimental and theoretical buoyancy forces for the ring pole electromagnetic float polishing apparatus

This calibration curve was developed to determine the effectiveness of the ANSYS analysis and to compare the buoyancy forces obtained from the ring pole and the modified ring pole designs. The same procedure was followed to calculate the theoretical

buoyancy forces as in the straight field design. The difference between the ANSYS solution and the experimental results is attributed to varying density of the float material and the limited magnetic fluid volume and density when mixed with the abrasives. The same type of calibration curve was also developed for the modified ring pole design (Figure 4.30). In the case of the modified ring pole design, theoretical buoyancy forces could not be calculated because of meshing problems, which were discussed earlier in this chapter, experienced with the ANSYS package.

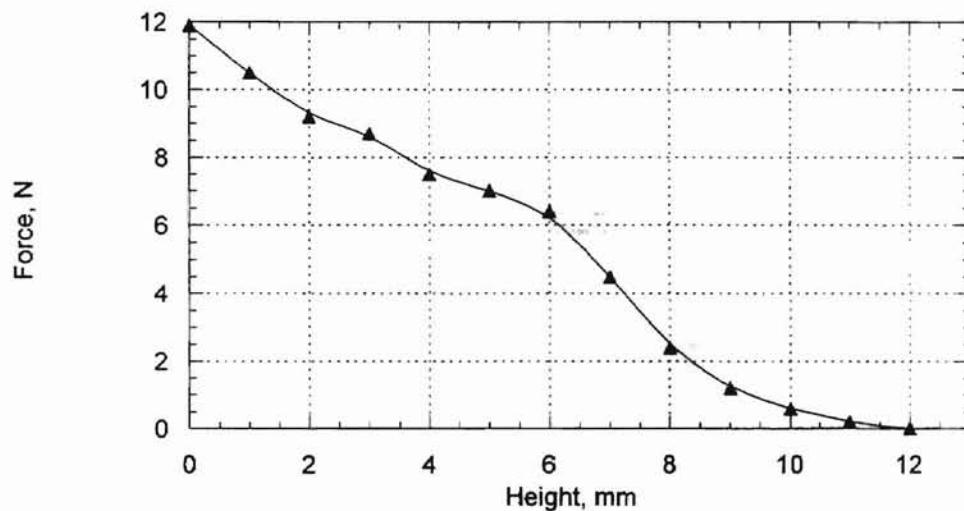


Figure 4.30 Experimental buoyancy force for the modified ring pole design

As can be seen from Figure 4.30, higher buoyancy forces can be obtained from the modified ring pole design. These higher buoyancy forces are due to the higher magnetic flux density obtained from the modified ring pole design. It should also be noted that these experimental buoyancy forces are averaged over 6 mm which is the thickness of the float used in the polishing process.

CHAPTER 5

EXPERIMENTAL STUDIES

In this chapter the experimental results are presented. In order to determine the effect of important process parameters on performance (material removal rate, surface finish and sphericity) and create the essential data base, several experiments were carried out. Since the material removal rate, the surface finish and the sphericity are the main criteria for a bearing ball, several parametric studies were also conducted to find the affect of variables involved in magnetic float polishing on these main criteria. Experimental set up can be seen in Figure 5.1.

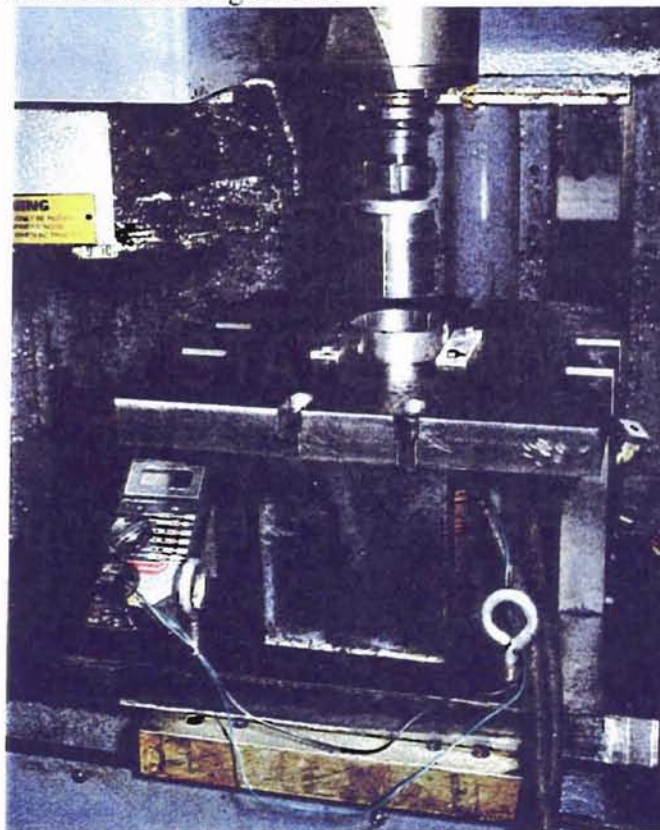


Figure 5.1 Experimental setup for electromagnetic field assisted polishing

5.1 Experimental Details and Procedure

Table 5.1 shows the variables involved in magnetic float polishing. Throughout the experimental studies, a standard producer was used in order to characterize the silicon nitride bearing balls and determine the effect of a particular experimental sequence. During the polishing tests, HIPped silicon nitride balls with diameters of $\phi 1/2''$, $\phi 3/8''$ were used. All the tests were conducted using water based ferrofluid (W-40). A Bridgeport NC milling machine was utilized throughout the research. Ball diameter measurements were carried out using a digital micrometer (Mitutoyo 293 Series) with an accuracy of 3 μm . Also, to monitor material removal rate; the ball weights were measured with a weighing instrument (Brinkmann Instruments Company Model 1712) with a resolution of 0.001 mg. Surface finish measurements were conducted with a stylus type measuring instrument (Rank Taylor Hobson Inc. from Talysurf 120 L).

Table 5.1 Variables involved magnetic float polishing

VARIABLES	TYPES
Rotational Speed	1000 rpm-6000 rpm
Abrasive Concentration	5-30 % by Volume
Abrasive Grain Size	1-40 μm
Abrasive Type	B_4C , SiC , Cr_2O_3 , CeO_2
Polishing Load	0.5-1.5 N/Ball

It is possible to measure both surface roughness and waviness with this instrument. Talysurf 120 L has a vertical resolution of 10.0 nm and a horizontal resolution of 0.25 μm . Several surface characterization parameters can be obtained, such as Ra (average surface roughness), Rt (maximum surface roughness), amplitude distribution, etc, with different cut-off lengths and filters. Another instrument used to characterize the surface finish was a laser interference microscope (Zygo Corporation, Zygo Maxim 3D) with a variety of resolutions depending upon the magnification and power used. With 400X system magnification, the lateral resolution is 1.68 μm , with 800X system magnification, the lateral resolution is 1.10 μm , and finally with 2000X system magnification, the lateral resolution is 0.82 μm . Sphericity measurements were conducted using a stylus based form accuracy measuring instrument (Rank Taylor Hobson Inc. Talyround 250). It is possible to measure roundness, vertical straightness, squareness, parallelism, flatness, cylindricity and concentricity. The gage has a range of $\pm 1\text{mm}$ and a resolution of 0.05 μm . Surface roundness calculations were performed using the least squares circle method.

Experimental studies were conducted using both the ring pole electromagnetic field assisted polishing apparatus and the modified ring pole electromagnetic field assisted polishing apparatus. Since material removal rate, surface finish, and sphericity are the main characteristics of a bearing ball, each of these characteristics and the variables that affect these characteristics are presented separately in this chapter. Test conditions for each experiment will be presented while discussed. Each test was performed two times to check the repeatability. For surface roughness and sphericity

three balls were selected and each ball was measured three times. The average values presented in this chapter are the results of these measurements. One also should understand that each parameter namely material removal rate, surface finish and sphericity is matter of the polishing stages. In other words material removal is the most parameter in the initial stages, where as sphericity is in the middle stages and the surface finish is in final stages. For example, the parameters namely speed, abrasive concentration, etc, involved during the in the initial stages may not be suitable for the final stages of polishing.

5.2 Effect on Material Removal Rate

As stated earlier, bearing balls made from silicon nitride have approximately two times higher Vickers hardness when compared to a SUJ 2 steel bearing ball. Therefore removal rates for silicon nitride are quiet low. In the conventional polishing techniques, it takes about 12-24 weeks to finish a batch of silicon nitride balls with the desired qualities. It has been reported by using a permanent magnet polishing apparatus, one batch of balls (15) can be finished in 16 hours [Raghunandan, 1996]. In the electromagnetic field assisted polishing apparatus, due to the orientation of the magnetic fluid under the generated magnetic field, it is possible to obtain material removal rates almost twice as much the permanent magnet design. As can be seen from Figure 5.2, because of the magnetic field orientation, balls are surrounded by the magnetic fluid and the abrasives; balls have greater chance to contact with the abrasives in the

electromagnetic field assisted polishing apparatus when compared to permanent magnet polishing apparatus. Consequently this leads to higher material removal rates.

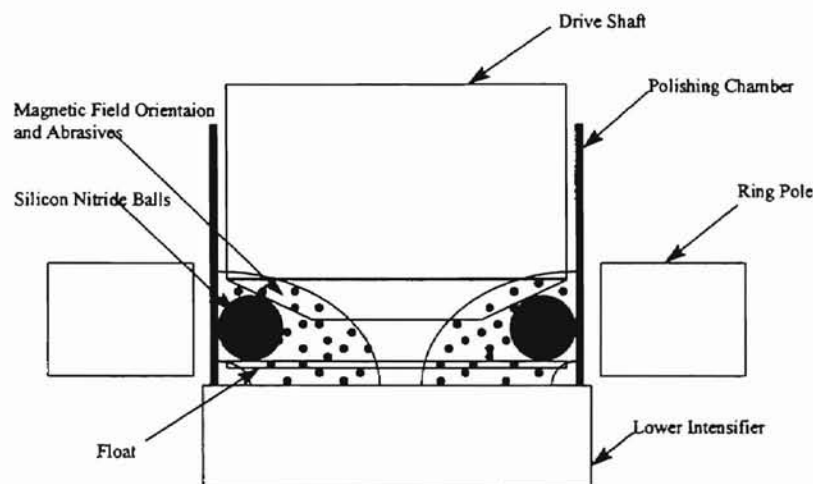


Figure 5.2 Orientation of the magnetic fluid and the abrasives under the applied magnetic field in the electromagnetic field assisted polishing apparatus.

5.2.1 Material Removal Rates in the Ring Pole Design

Various tests were conducted to investigate the best removal rate conditions in the ring pole electromagnetic field assisted polishing apparatus. In Figure 5.3, the effect of the rotational speed of the driving shaft on material removal rate can be seen. In order to determine the effect of the rotational speed, all other variables that are involved in the polishing process were kept constant for each experiment. Boron carbide (B_4C) 500 grit ($17\text{ }\mu\text{m}$) size was used as the polishing abrasive. In each experiment, the abrasive

concentration was 10% by volume, and the polishing load was 1.2 N/ball. The drive shaft was re-machined periodically due to the wear which occurred on the edge of the shaft. 50 ml of magnetic fluid was used as the polishing medium. All experiments were conducted on a Bridgeport NC milling center.

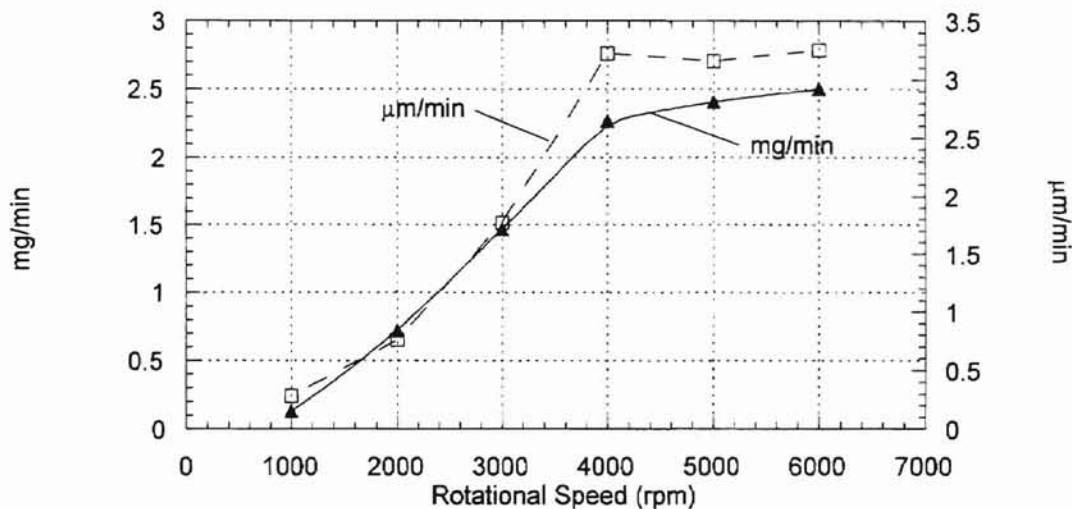


Figure 5.3 Effect of the rotational speed on material removal rate per ball in the ring pole electromagnetic field assisted polishing apparatus.

It can be seen from Figure 5.3 that the material removal rate increases linearly as the rotational speed of the driving shaft increases and reaches a saturation around 4000 rpm. When the material removal rates are compared with the permanent magnet polishing apparatus, it can be noted that the ring pole electromagnetic field assisted polishing apparatus provides almost two times higher removal rates [Raghunandan, 1996]. This is due to the difference in the magnetic field orientation as explained earlier. Another important factor that affects the material removal rate is the abrasive concentration. In Figure 5.4, the effect of abrasive concentration on material removal rate can be seen.

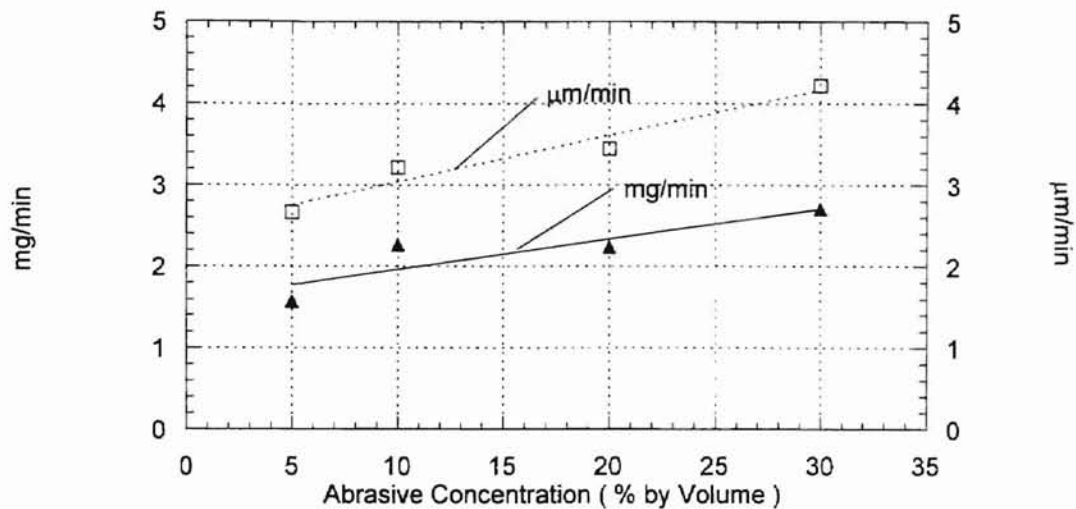


Figure 5.4 The effect of abrasive concentration on material removal rate per ball in the ring pole electromagnetic field assisted polishing apparatus.

Boron carbide (B4C) 500 grit size ($17 \mu\text{m}$) was used as the polishing abrasive in all the experiments that were conducted in order to determine the affect of the abrasive concentration. 1.2 N/ball was used as the polishing load. Like the previous characterization tests for rotational speed, the edge of the drive shaft was re-machined for each test. In order to find the maximum material removal rate achievable in the ring pole electromagnetic field assisted polishing apparatus, 4000 rpm was used as the rotational speed of the driving shaft due to the fact that this is the optimum speed found. Even though material removal rate seemed to be increasing with an increase in abrasive concentration, further tests were considered to be unnecessary because the achieved high removal rates were considered as sufficient for a polishing process. Another important parameter that affects the material removal rate is the abrasive type used during the

polishing process. In order to demonstrate this, the same set of balls with identical conditions were polished with silicon carbide (SiC) 400 grit size. Since the hardness of the silicon carbide is approximately 25% less than boron carbide, material removal rates obtained with silicon carbide were less with boron carbide (see Figure 5.3). Figure 5.5 shows the material removal rates that can be achieved by using silicon carbide 400.

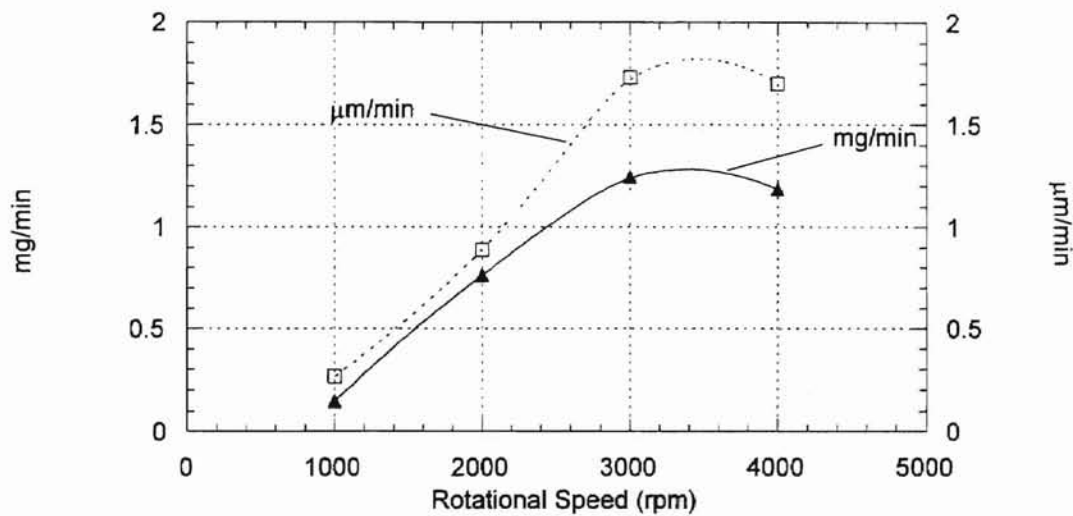
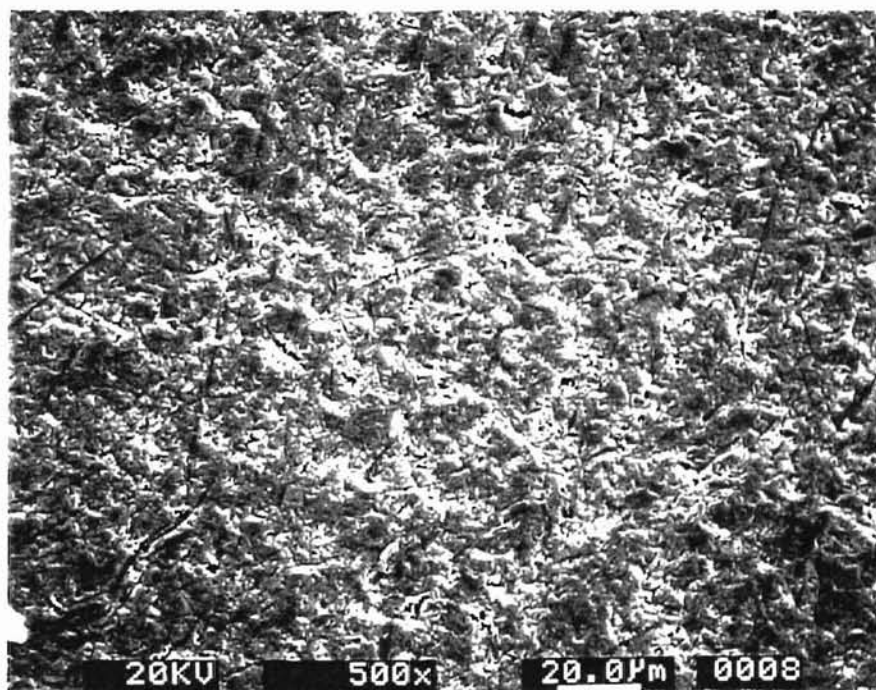


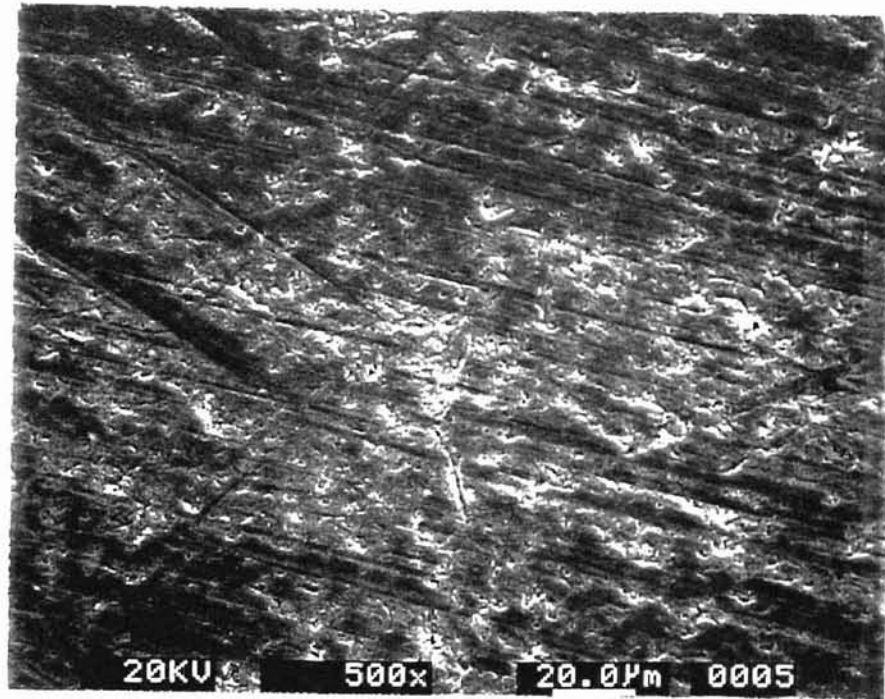
Figure 5.5 Material removal rate per ball with different rotational speeds by using SiC 400 grid size as the polishing abrasive in the ring pole electromagnetic field assisted polishing apparatus

As expected, when the abrasive hardness decreases, material removal rates decrease as well. It should be noted that the material removal rates accomplished by using silicon carbide 400 grit size were almost half of that with boron carbide 500 grit size. Of course, varying the grain size also affects the material removal rate; but there is not much of a difference when 400 grit size results and 500 grit size results were compared.

Surface morphology of the silicon nitride balls was also examined after the maximum material removal rate had been accomplished. Figures 5.6 (a) and (b) show the scanning electron microscope (SEM) images of a ball surface. Ball surface was found to be covered with pits and parallel scratches. These pits are caused by microfracture and also due to higher rotational speed (4000 rpm) parallel scratches formed due to higher sliding rates at the ball/shaft interface.



(a)



(b)

Figure 5.6 (a) Pits dominant SEM micrograph of a ball polished by using 4000 rpm and 30% volume abrasive concentration of B₄C 500 grit (17 µm). (b) Scratches dominant SEM micrograph of a ball polished by using 4000 rpm and 30% volume abrasive concentration of B₄C 500 grit (17 µm).

5.2.2 Material Removal Rates in Modified Ring Pole Design

In order to find the effect of the rotational speed on material removal rate, several experiments were conducted with the modified ring pole electromagnetic field assisted polishing apparatus. The results of these tests are shown in Figure 5.7. In all of these experiments the same test conditions were used as in the previous section to have a better comparison between the ring pole design and the modified ring pole design.

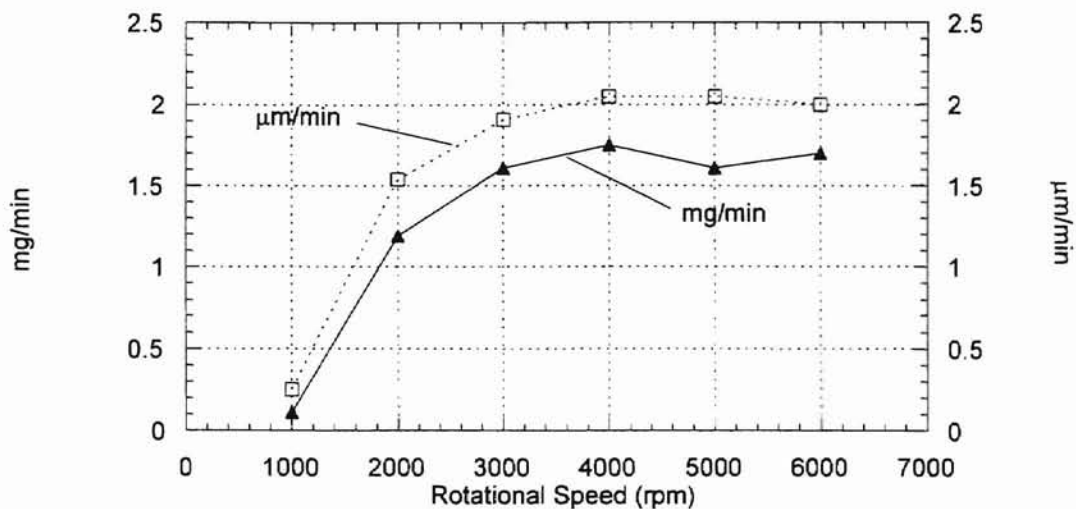


Figure 5.7 The effect of the rotational speed on material removal rate per ball in the modified ring pole electromagnetic field assisted polishing apparatus.

As shown in the Figure 5.7, material removal rates were relatively smaller in the modified ring pole design when compared with the original ring pole design (see Figure 5.3). As discussed in Chapter 4, magnetic field strength is smaller in the modified ring pole design due to the fact that the modified ring pole design's magnetic field strength generated by the coil was divided into 4 areas, whereas it was 2 areas in the ring pole design. Therefore, this reduced magnetic field strength leads to smaller material removal rates in the modified ring pole electromagnetic field assisted polishing apparatus.

The effect of abrasive concentration on material removal rates was discussed in the previous section for the ring pole design. The same type of effect on material removal rates can also be observed for the modified ring pole design. Figure 5.8 shows the effect

of abrasive concentration on the material removal rate in the modified ring pole electromagnetic field assisted polishing process.

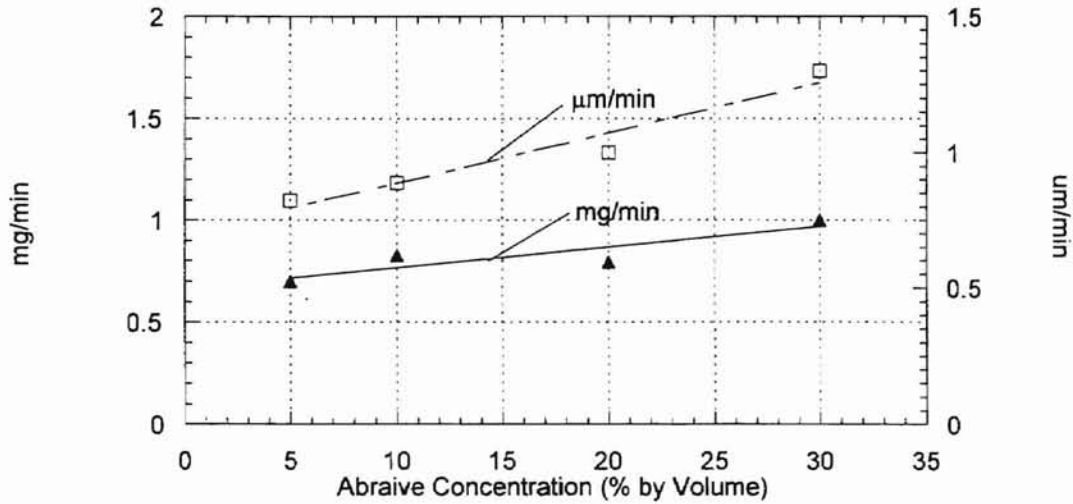


Figure 5.8 The effect of abrasive concentration on material removal rate per ball in the modified ring pole electromagnetic field assisted polishing apparatus

B_4C 500 grid ($17\ \mu m$) was used as the polishing abrasive during the evaluation of the effect of abrasive concentration on the material removal rate. The rotational speed of the drive shaft was 2000 rpm, which was 4000 rpm in the case of the ring pole design. The reason for the lower rotational speed is to keep the sphericity in an acceptable range which will be discussed later in detail in this chapter.

Another important factor affecting the material removal rate is the grain size of the abrasive used during the polishing process. In order to find the effect of grain size on the material removal rate, boron carbide (B_4C) was used as the polishing abrasive with varying grain sizes (500, 800, and 1500). All experiments were carried out by using 2000 rpm as the rotational speed of the drive shaft, and 1.2 N/ball was used as the polishing

load. In all experiments, the abrasive concentration was 5% by volume. The results of this study can be seen in Figure 5.9.

As shown in Figure 5.9, as the grain size of the abrasive increases, material removal rates increase, as can be anticipated.

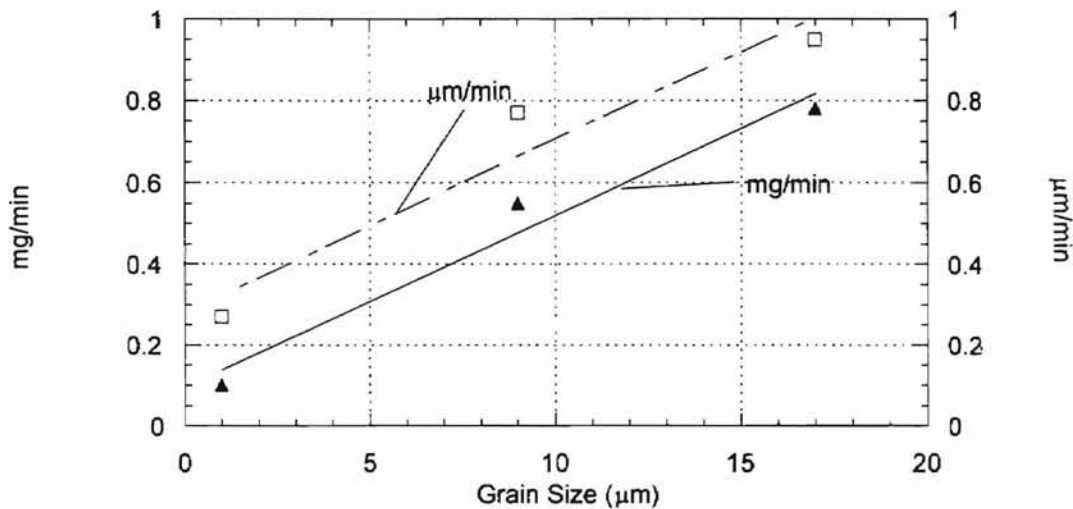


Figure 5.9 The effect of abrasive grain size on material removal rate per ball in the modified ring pole electromagnetic field assisted polishing apparatus.

5.3 Effect on Surface Finish

Surface roughness of a finished bearing ball is one of the most important parameters in terms of its quality requirements. In order to find out the parameters that affect surface finish, tests were conducted both with the ring pole design and the modified ring pole design.

One of the parameters that has an effect on surface roughness is the rotational speed of the driving shaft. The effect of the rotational speed on the surface roughness in

the ring pole design can be seen in Figure 5.10. All of these tests were conducted using B4C 500 (17mm) grid size as the polishing abrasive. Results of these tests are presented in terms of R_a (average surface roughness) and R_t (maximum surface roughness).

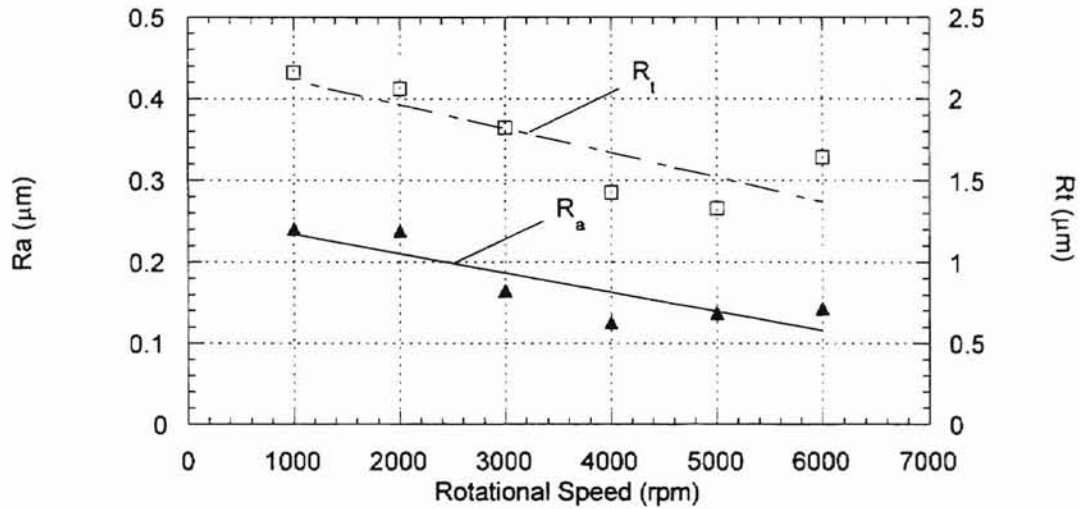
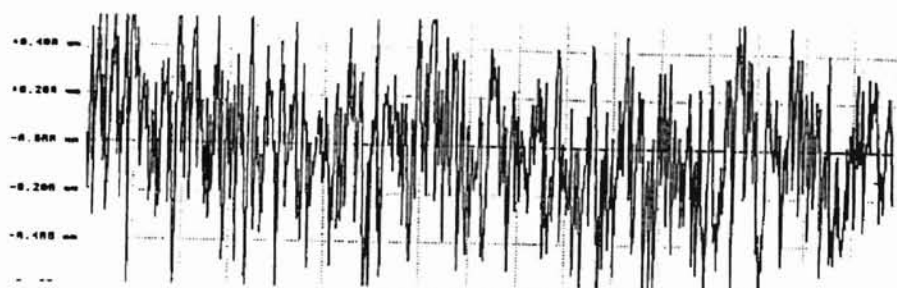


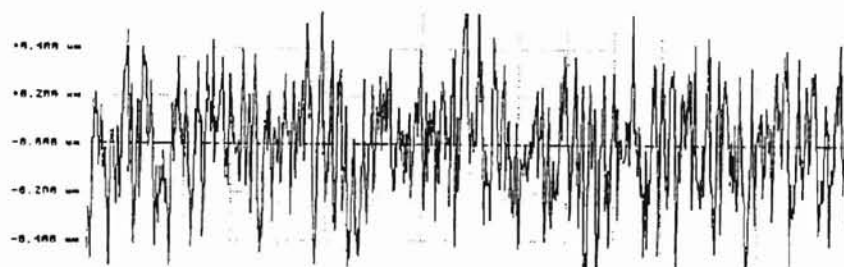
Figure 5.10 The effect of the rotational speed on surface roughness in the ring pole electromagnetic field assisted polishing apparatus.

As can be seen from Figure 5.10, as the rotational speed of the drive shaft increases, surface roughness of the silicon nitride ball also decreases in terms of average roughness (R_a) and maximum roughness (R_t). In Figure 5.11, surface traces obtained from Talysurf surface measurement instrument can be seen with different rotational speeds. In Figure 5.12 the effect of the rotational speed on surface roughness in the modified ring pole design is presented. Other parameters that are involved in polishing were kept constant the same as for the ring pole design characterization.



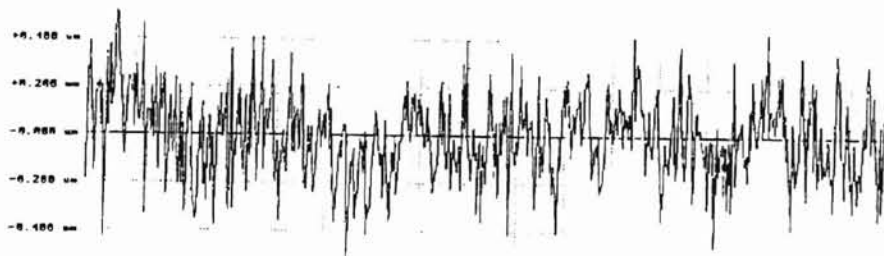
Ra	8.2188 um	Rq	8.2725 um	Rp	8.7976 um
Rv	8.9681 um	Rt	1.7658 um	Rt1	1.7802 um
Rt2	1.5979 um	Rt3	1.4212 um	Rt4	1.4284 um
Rsk	-8.1688 um	Rkw	2.9881 um	Rslq	5.1922 deg
Lamq	18.8415 um	S	7.2689 um	Sm	28.9672 um

(a) 1000 rpm



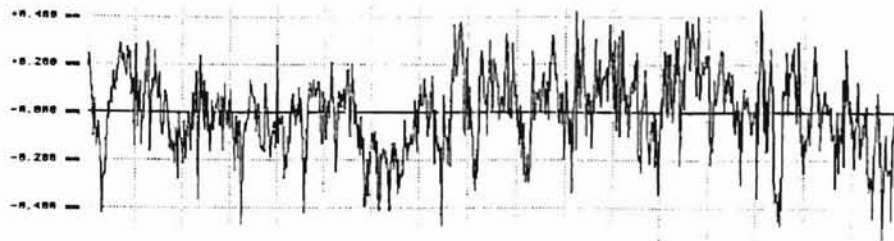
Ra	8.1885 um	Rq	8.2263 um	Rp	8.7228 um
Rv	8.8922 um	Rt	1.6152 um	Rt1	1.1734 um
Rt2	1.2843 um	Rt3	1.5258 um	Rt4	1.1398 um
Rsk	-8.2121 um	Rkw	3.2383 um	Rslq	3.8639 deg
Lamq	26.5688 um	S	13.7118 um	Sm	27.2985 um

(b) 2000 rpm



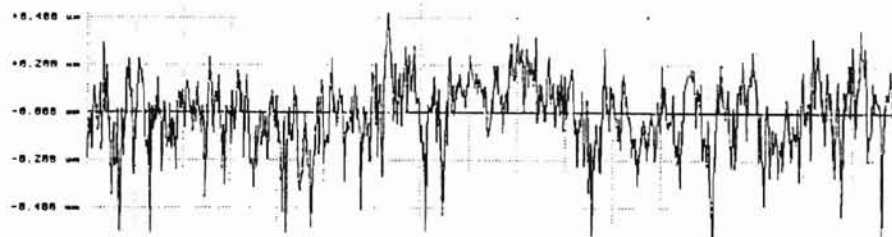
Ra	8.1735 um	Rq	8.1668 um	Rp	8.5563 um
Rv	8.5252 um	Rt	1.8815 um	Rt1	8.9817 um
Rt2	8.9243 um	Rt3	8.8643 um	Rt4	8.5156 um
Rsk	-8.9159 um	Rkw	2.8949 um	Rslq	2.2847 deg
Lamq	26.2733 um	S	14.1943 um	Sm	32.1325 um

(c) 3000 rpm



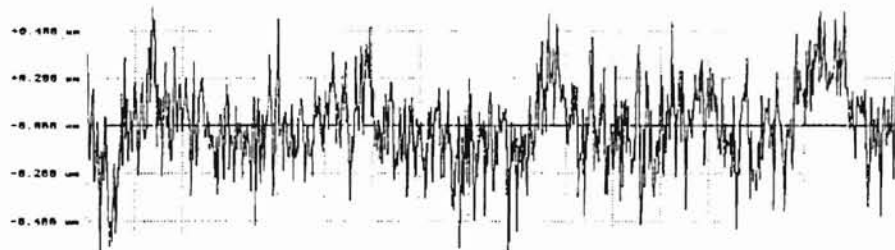
Ra	0.1007 um	Rq	0.1679 um	Sp	0.4378 um
Rv	0.5793 um	Rt	1.8163 um	Rt1	0.8677 um
Rt2	0.0856 um	Rt3	0.9227 um	Rt4	1.8163 um
Rsk	-0.2238 um	Rku	2.9155 um	Sm	3.0784 um
Lamq	19.6622 um	S	6.8978 um		23.3658 um

(d) 4000 rpm



Ra	0.1204 um	Rq	0.1559 um	Sp	0.4248 um
Rv	0.9262 um	Rt	1.3518 um	Rt1	0.9188 um
Rt2	1.3518 um	Rt3	0.9622 um	Rt4	1.8515 um
Rsk	-0.0148 um	Rku	4.7871 um	Sm	2.8844 um
Lamq	20.0038 um	S	7.3319 um		24.8744 um

(e) 5000 rpm



Ra	0.1346 um	Rq	0.1716 um	Sp	0.5496 um
Rv	0.7242 um	Rt	1.2739 um	Rt1	1.1524 um
Rt2	0.9673 um	Rt3	1.2739 um	Rt4	0.9259 um
Rsk	-0.0002 um	Rku	3.3181 um	Sm	3.7567 um
Lamq	16.4198 um	S	6.4648 um		18.2757 um

(f) 6000 rpm

Figure 5.11 Surface traces obtained from Rank Taylor Hobson 120L Talysurf instrument of the silicon nitride balls with varying rotational speed of the driving shaft in the ring pole design

Like the ring pole design, the modified ring pole also has same kind of effect on surface roughness with an increase in the rotational speed of the drive shaft, as expected.

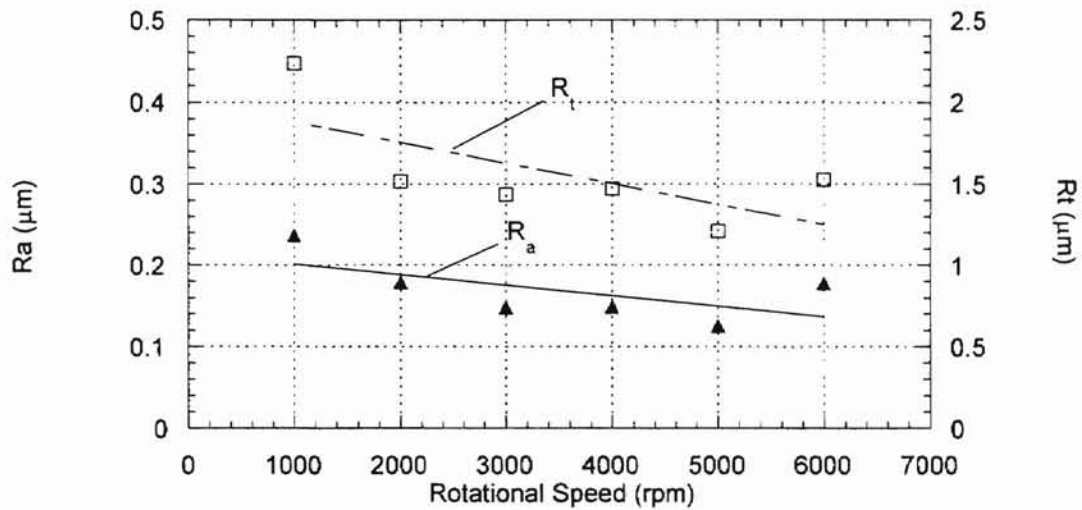
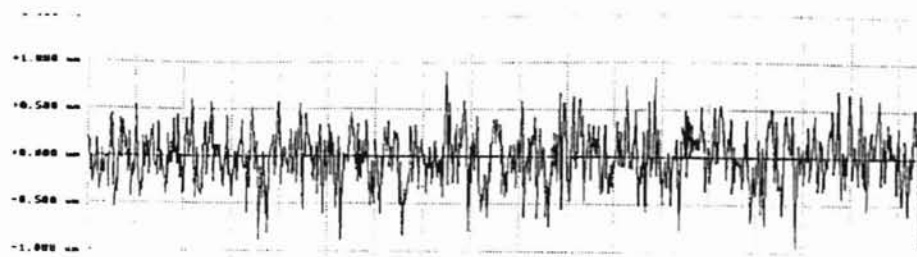


Figure 5.12 The effect of the rotational speed on surface roughness in the modified electromagnetic field assisted polishing apparatus.

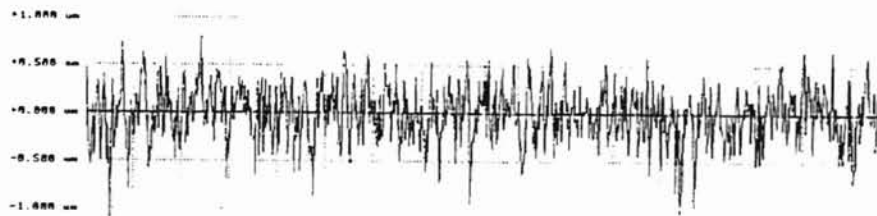
Surface roughness traces with the effects of varying rotational speeds of the driving shaft which are in the modified ring pole electromagnetic polishing apparatus can be seen in Figure 5.13.

Of course one should realize that the desired quality of a ball is not limited to the surface roughness. Therefore, other considerations such as material removal rate and sphericity should be taken into account. Even though the higher rotational speeds of the



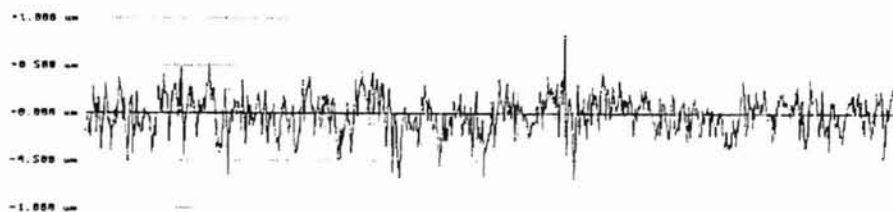
Ra	8.2325 μm	Rq	8.2924 μm	Rp	8.9893 μm
Rv	1.1681 μm	Rt	2.8695 μm	Rt1	1.4158 μm
Rt2	1.9318 μm	Rt3	1.6738 μm	Rt4	1.9289 μm
Rsk	-8.1587 μm	Rku	3.1289 μm	Smq	6.8536 deg
Lamq	17.3214 μm	S	7.4875 μm	Sm	19.2545 μm

(a) 1000 rpm



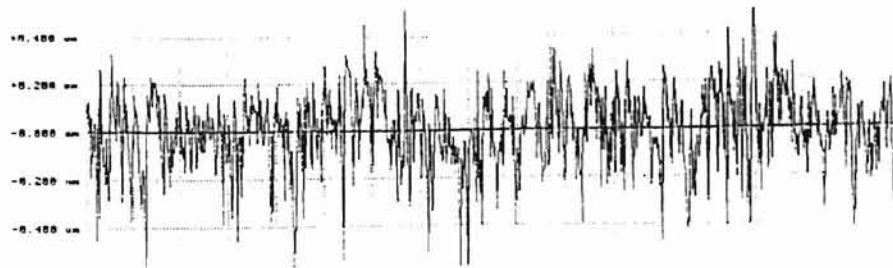
Ra	8.2361 μm	Rq	8.2951 μm	Rp	8.9893 μm
Rv	1.1632 μm	Rt	2.8724 μm	Rt1	2.8724 μm
Rt2	1.7398 μm	Rt3	1.6556 μm	Rt4	1.7938 μm
Rsk	-8.2696 μm	Rku	3.1548 μm	Smq	6.8514 deg
Lamq	15.8818 μm	S	6.7246 μm	Sm	17.8379 μm

(b) 2000 rpm



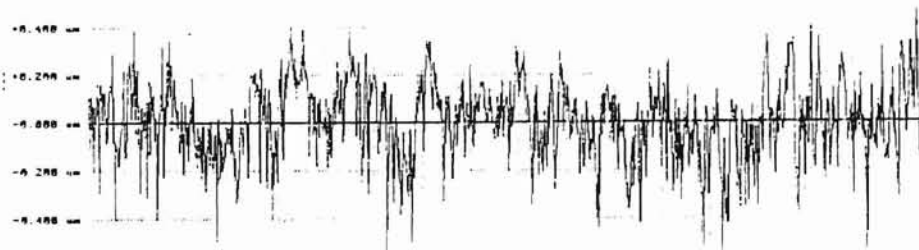
Ra	8.1568 μm	Rq	8.1999 μm	Rp	1.1473 μm
Rv	8.8824 μm	Rt	7.9497 μm	Rt1	1.1837 μm
Rt2	7.2644 μm	Rt3	1.3578 μm	Rt4	8.8858 μm
Rsk	-8.1584 μm	Rku	3.8831 μm	Smq	4.2752 deg
Lamq	16.8851 μm	S	6.7339 μm	Sm	19.3657 μm

(c) 3000 rpm



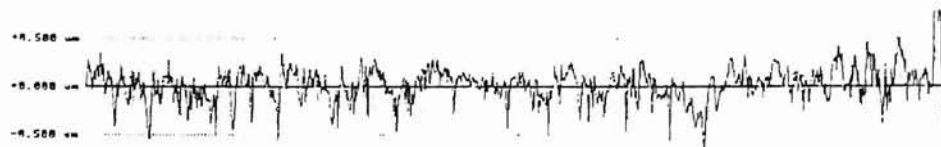
Ra	8.1315 um	Rq	8.1712 um	Rp	4.7726 um
Rv	8.7113 um	Rt	1.4839 um	Rt1	8.9329 um
Rt2	1.2681 um	Rt3	1.4651 um	Rt4	1.4239 um
Rsk	-0.5284 um	Rku	4.4378 um	Rsk1	4.8988 um
Lam	15.8414 um	S	4.6988 um	Su	17.1286 um

(d) 4000 rpm



Ra	8.1321 um	Rq	8.1667 um	Rp	4.5327 um
Rv	8.6294 um	Rt	1.1621 um	Rt1	8.8861 um
Rt2	1.8883 um	Rt3	8.8969 um	Rt4	1.1621 um
Rsk	-0.1525 um	Rku	3.1244 um	Rsk1	3.9898 um
Lam	15.3277 um	S	6.2618 um	Su	1.1621 um
Rt150	1.8863 um	RtD1H	8.9859 um	Su	17.1238 um

(e) 5000 rpm



Ra	8.1376 um	Rq	8.1863 um	Rp	1.3283 um
Rv	8.7828 um	Rt	2.8222 um	Rt1	4.5928 um
Rt2	8.8824 um	Rt3	8.9985 um	Rt4	1.5839 um
Rsk	8.4911 um	Rku	7.1876 um	Rsk1	3.2937 um
Lam	28.2428 um	S	7.3847 um	Su	1.9839 um
Rt150	1.2942 um	RtD1H	1.2122 um	Su	26.3844 um

(f) 6000 rpm

Figure 5.13 Surface traces obtained from Rank Taylor Hobson 120L Talysurf instrument of the silicon nitride balls with varying rotational speed of the driving shaft in the modified ring pole design

drive shaft provide a better surface finish this does not necessarily mean that these conditions yield optimum manufacturing quality.

Another important factor that affects the surface finish is the grit size of the abrasive used during the polishing process. In order to find the effect of the abrasive grain size, tests were carried out using boron carbide 500 grit ($17\text{ }\mu\text{m}$) size and boron carbide 800 grit ($9\text{ }\mu\text{m}$) size and boron carbide 1500 grit ($1\text{-}5\text{ }\mu\text{m}$) size. The effects of the grain size on the surface finish can be seen in Figure 5.14.

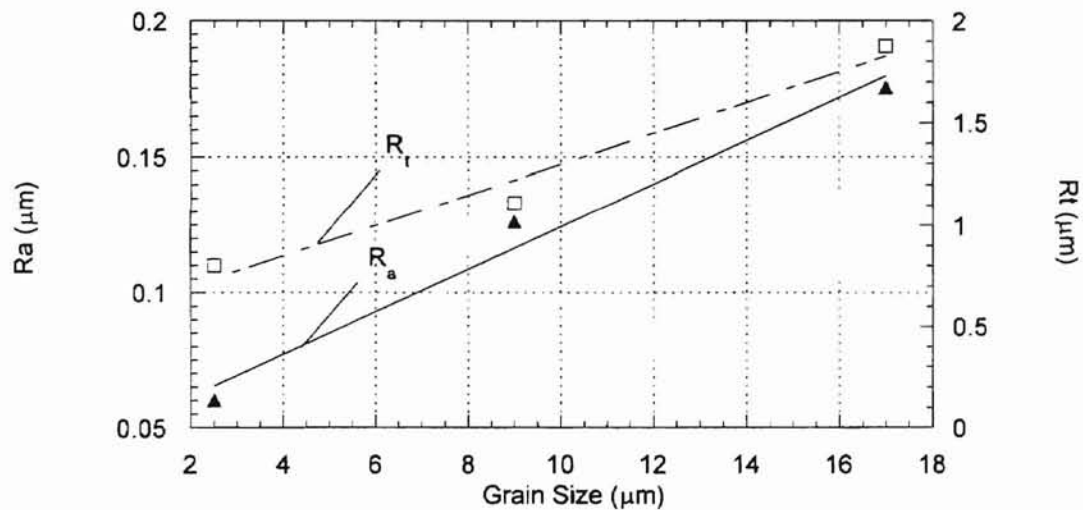
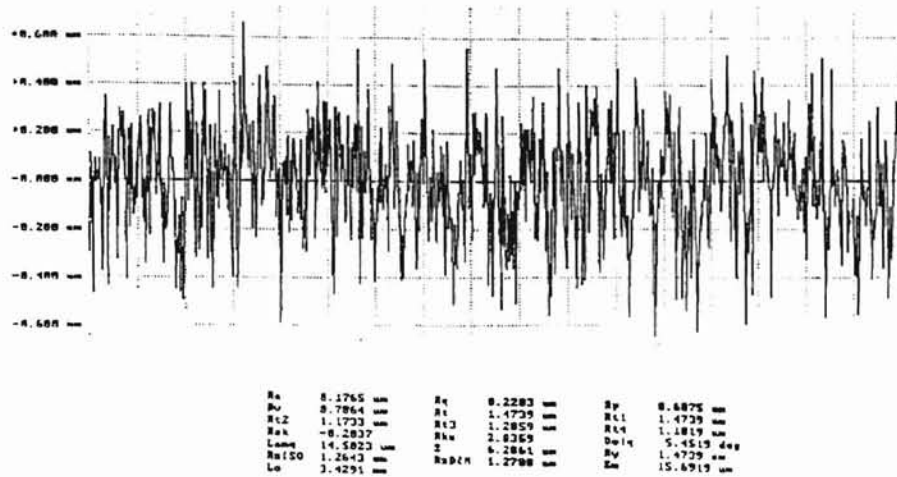
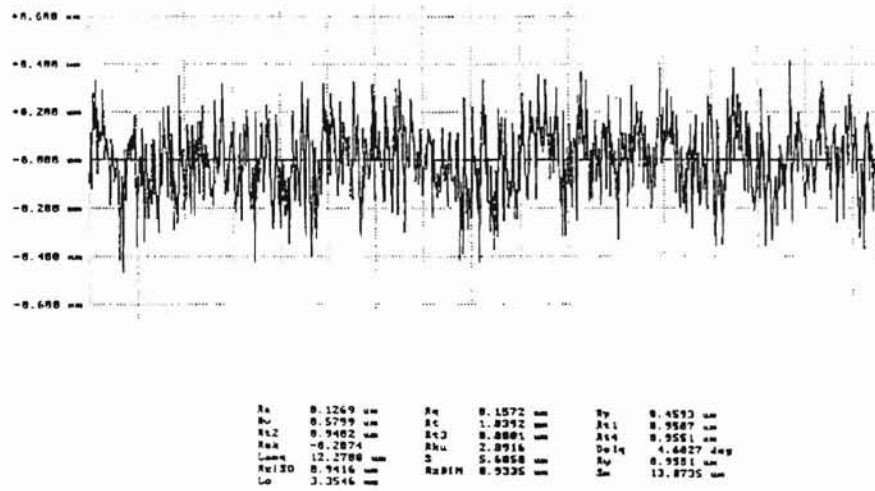


Figure 5.14 Effect of abrasive grain size on surface finish in the modified ring pole electromagnetic field assisted polishing apparatus.

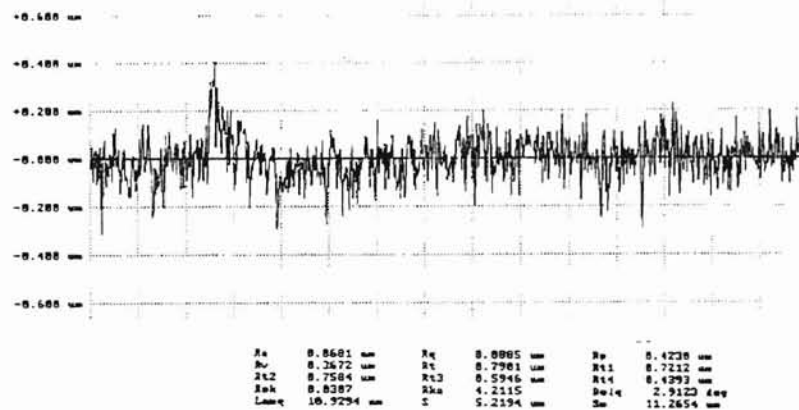
As can be seen from Figure 5.14, as the grain size decreases, surface roughness also decreases as expected. These results are also in agreement with the results presented by Raghunandan [1996]. Surface traces with varying grain size can be seen in Figure 5.15.



(a) B₄C 500 grid (17 μm)



(b) B₄C 800 grid (9 μm)



(c) B₄C 1500 grid (1-5 μm)

Figure 5.15 Surface traces obtained from Rank Taylor Hobson 120L Talysurf with varying grit sizes in the modified ring pole electromagnetic polishing apparatus.

5.3.1 Optimum Surface Finish Sequence

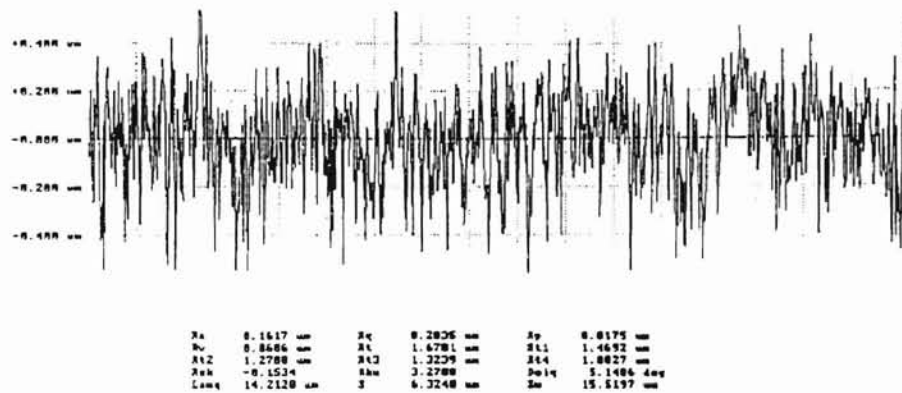
In order to achieve the optimum surface finish, it was found that there is a specific operations sequence that should be followed. With this sequence, it is possible to obtain approximately 13 nm of R_a surface roughness. The optimum sequence that needs to be followed is presented in Table 5.2.

Table 5.2 Polishing process sequence for optimum surface finish in the electromagnetic field assisted float polishing

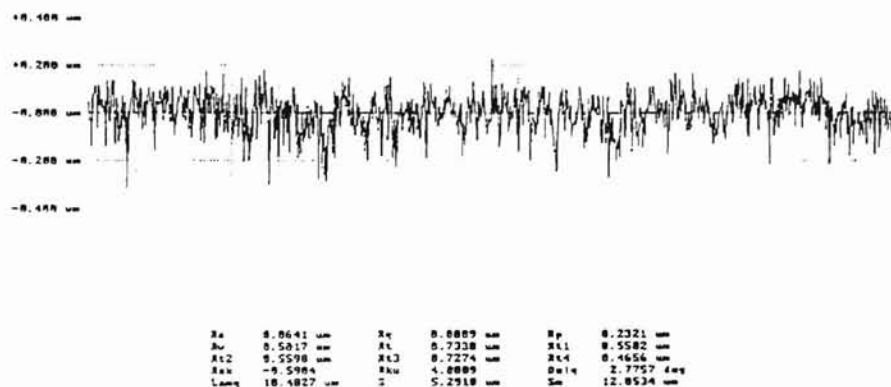
STEP NUMBER	ABRASIVE TYPE	GRAIN SIZE	POLISHING LOAD	POLISHING TIME	AVERAGE R_a	AVERAGE R_T
1	B ₄ C 500, 5% Vol.	17 μ m	1.25 N/ball	45 min.	167.7 nm	1529.1 nm
2	SiC 1000, 5% Vol.	5 μ m	1.25 N/ball	90 min.	65.7 nm	803.3 nm
3	SiC, 5% Vol.	1 μ m	1.25 N/ball	90 min.	35 nm	352.8 nm
4	Cr ₂ O ₃ 10% Vol.	1-5 μ m	1.25 N/ball	90 min.	13.6 nm	220.3 nm

As can be seen from Table 5.2, surface roughness continuously improves with each stage of the polishing process. In the first polishing step with boron carbide (B₄C), surface waviness can be eliminated, so that real average surface roughness can be

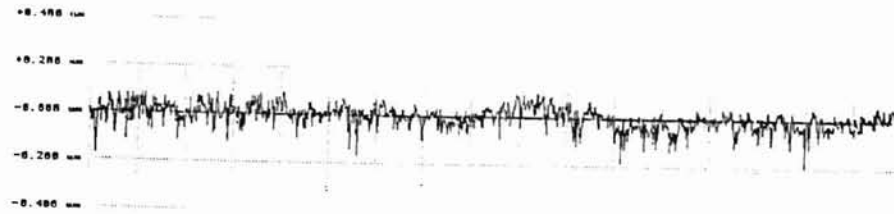
obtained properly. In the second and third steps, due to use of the smaller grain sizes of silicon carbide (SiC), surface roughness shows improvement compared to larger grain size boron carbide (B_4C). Even though the abrasive grain size is similar in step four when compared to step three, due to chemo-mechanical polishing action with the chromium oxide (Cr_2O_3) an optimum surface finish can be obtained. Surface roughness traces of this specific sequence can be seen in Figure 5.16.



Step 1 (B_4C , 17 μm)

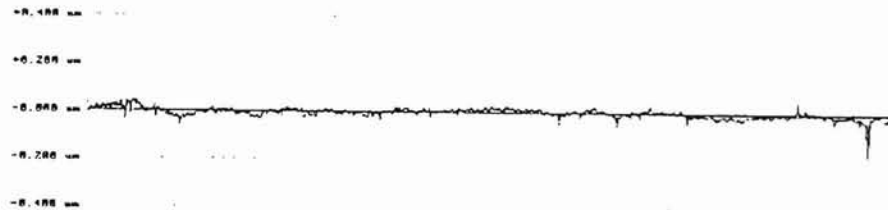


Step 2 (SiC, 5 μm)



Ra	0.0248 μm	Rq	0.0435 μm	Rp	0.1264 μm
Rv	0.1953 μm	Rt	0.3219 μm	Rt1	0.2874 μm
Rt2	0.2889 μm	Rt3	0.3187 μm	Rt4	0.2917 μm
Rsk	-0.2387	Rku	3.6861	Sm1q	1.5764 deg
Ln1q	9.9426 μm	S	4.8828 μm	Sm	11.1474 μm

Step 3 (SiC, 1 μm)



Ra	0.0123 μm	Rq	0.0173 μm	Rp	0.0568 μm
Rv	0.1139 μm	Rt	0.2788 μm	Rt1	0.1243 μm
Rt2	0.0683 μm	Rt3	0.1282 μm	Rt4	0.2661 μm
Rsk	-2.4397	Rku	24.2984	Sm1q	0.4654 deg
Ln1q	13.3883 μm	S	4.8498 μm	Sm	0.2661 μm
Ra150	0.1479 μm	RaD1H	0.1467 μm		17.8318 μm

Step 4 (Cr₂O₃, 1-5 μm)

Figure 5.16 Surface roughness traces from Rank Taylor Hobson 120L Talysurf in optimum surface finish sequence in the electromagnetic field assisted polishing apparatus

In order to compare and evaluate this specific polishing sequence several experiments were conducted. The results of these tests can be seen in Table 5.3.

Eventhough, all the other variables were kept constant, it can be seen that the final surface roughness is approximately 10 nm worse when compared with the optimum surface polishing sequence. Among these two set of experiments, the only difference is

the elimination of the third step in the polishing order. These final surface roughness results obtained by using the electromagnetic field assisted polishing apparatus results are in agreement with what is accomplished and reported for the permanent magnet polishing equipment [Raghunandan, 1996].

Table 5.3 Comparison of the optimum surface polishing sequence with another set of polishing tests.

STEP NUMBER	ABRASIVE TYPE	GRAIN SIZE	POLISHING LOAD	POLISHING TIME	AVERAGE R_A	AVERAGE R_T
1	B ₄ C 500, 5% Vol.	17 μ m	1.25 N/ball	45 min.	185.4 nm	1672.6 nm
2	SiC 1000, 5% Vol.	5 μ m	1.25 N/ball	90 min.	64.9 nm	709 nm
3	Cr ₂ O ₃ 10% Vol.	1-5 μ m	1.25 N/ball	90 min.	22.8 nm	338.8 nm

In order to obtain the best results with electromagnetic field assisted polishing apparatus in terms of surface finish, chromium oxide (Cr₂O₃) was used as the polishing abrasive. Even though the hardness of the chromium oxide is very close to the workpiece material silicon nitride, it has been reported that material removal is due to chemo-mechanical action rather than abrasion. In Figures 5.17 and 5.18, ZYGO plots at different magnifications of a ball polished with silicon nitride (SiC 1-5 μ m) can be seen. Then in Figures 5.19 and 5.20, ZYGO plots at different magnifications of a ball polished with chromium oxide (Cr₂O₃ 1-5 μ m) can be seen. As reported in the literature, the best

surface finish values in the electromagnetic field assisted polishing apparatus were also obtained by using chromium oxide.

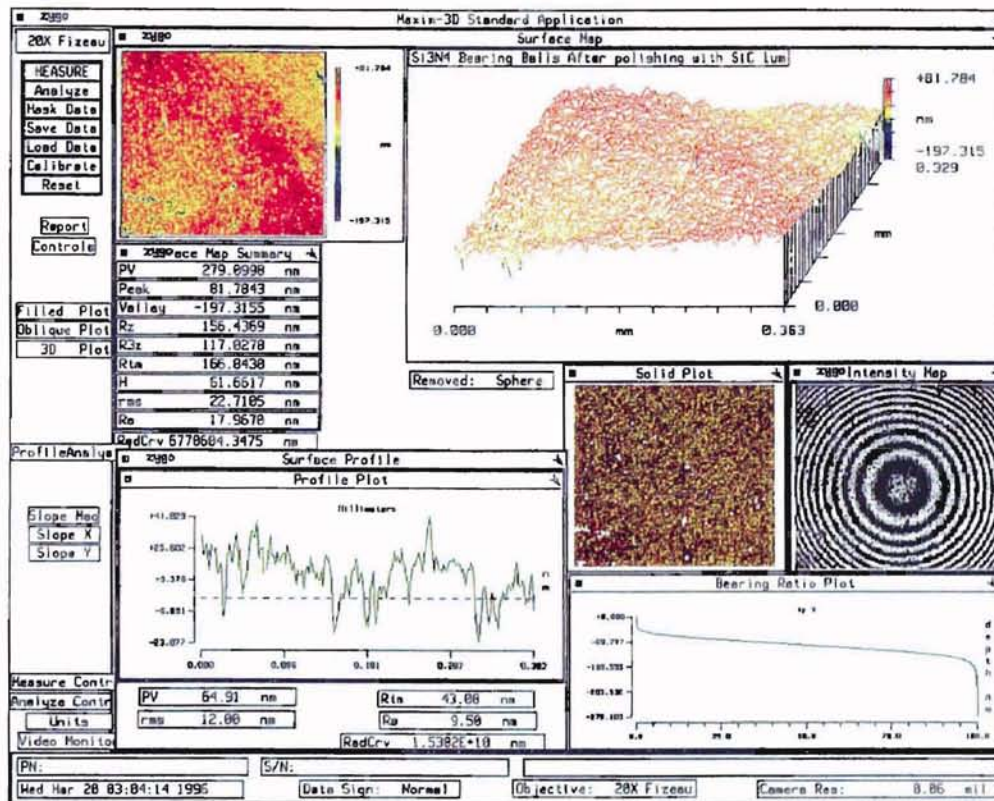


Figure 5.17 ZYGO plots at a lower magnification (20X Fizeau) of a ball polished with SiC (1-5 μm) with the ring pole electromagnetic field assisted polishing apparatus

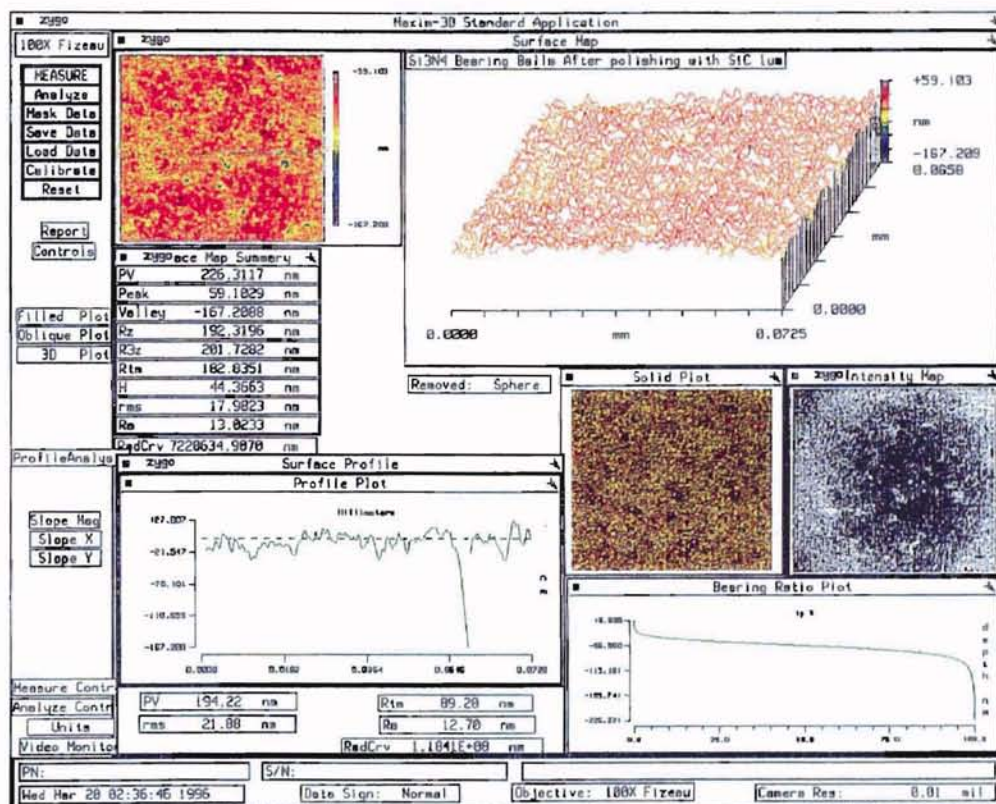


Figure 5.18 ZYGO plots at a higher magnification (100X Fizeau) of a ball polished with SiC (1-5 μm) with the ring pole electromagnetic field assisted polishing apparatus

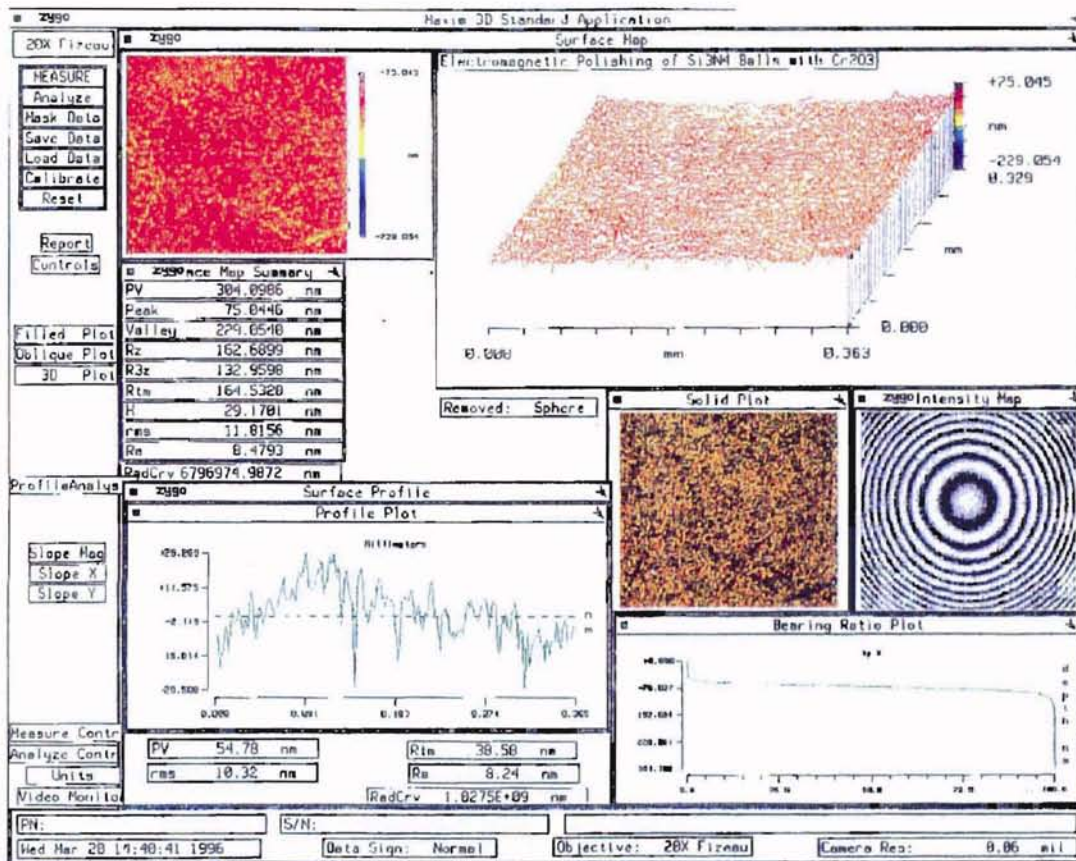


Figure 5.19 ZYGO plots at lower magnification (20X Fizeau) of a ball polished with Cr_2O_3 (1-5 μm) with the ring pole electromagnetic field assisted polishing apparatus

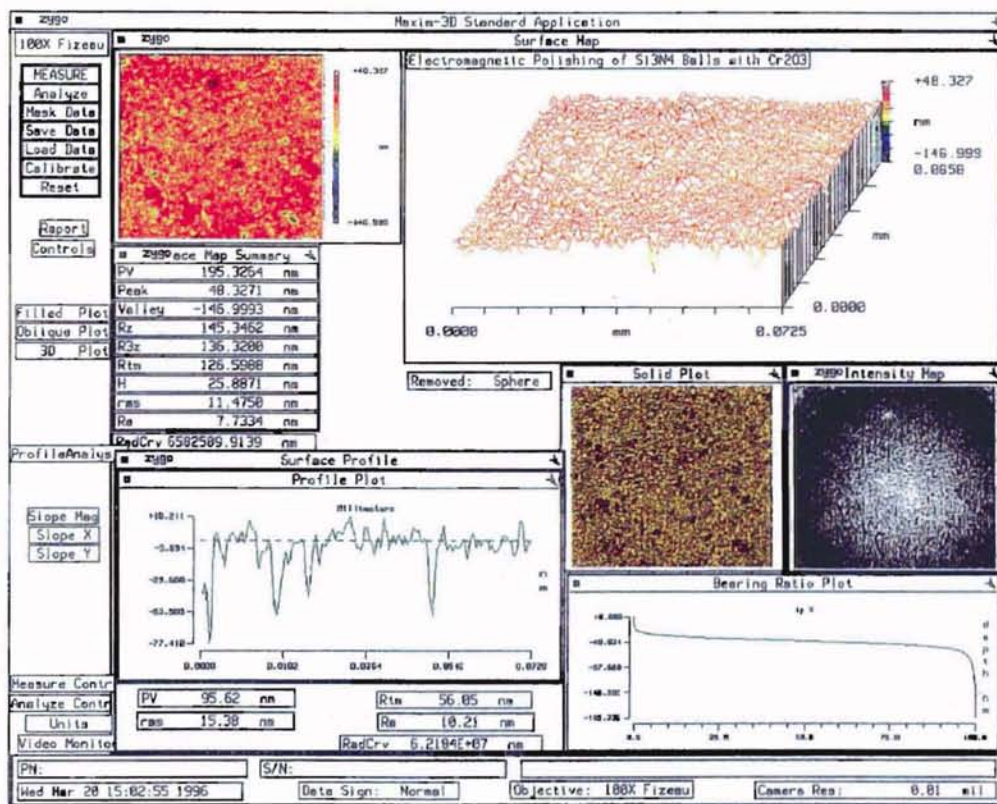


Figure 5.20 ZYGO plots at a higher magnification (100X Fizeau) of a ball polished with Cr_2O_3 (1-5 μm) with the ring pole electromagnetic field assisted polishing apparatus

Surface morphology of the finished balls was also examined and compared with a conventionally finished silicon nitride bearing ball by using a scanning electron microscope (SEM) at different magnifications (Figure 5.21 and Figure 5.22). These micrographs show deep surface damages and fractures in the case of the conventionally finished silicon nitride with hard diamond abrasives, whereas in the case electromagnetic float polishing, the surface appears to be covered with relatively less deep pits and is smoother when polished with chromium oxide abrasives. These pits are believed to be due to previous polishing tests which were conducted with larger size abrasives.

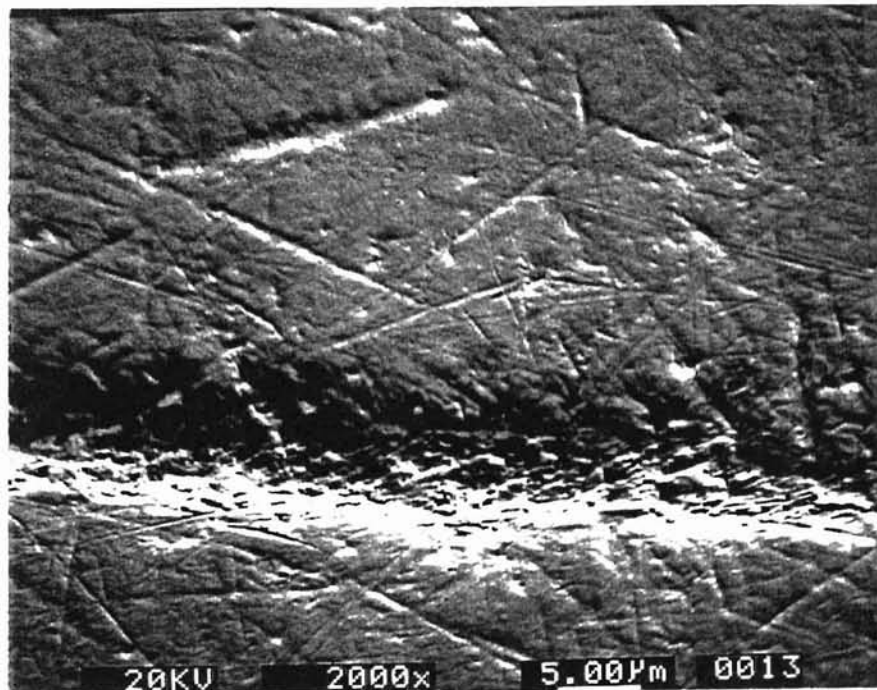


Figure 5.21(a) SEM micrograph at 2000X magnification polished with conventional polishing methods

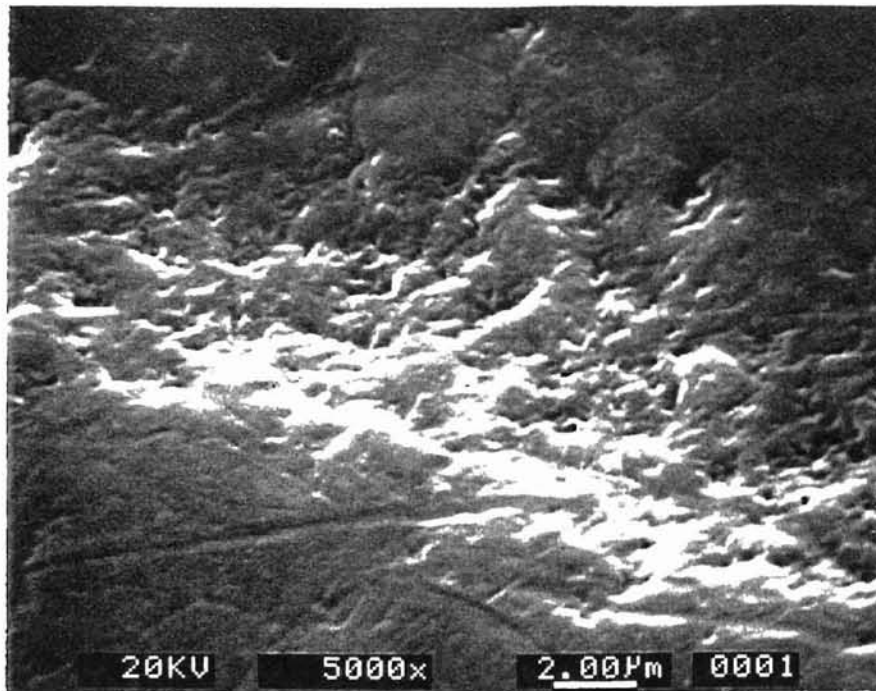


Figure 5.21(b) SEM micrograph at 5000X magnification polished with conventional polishing methods

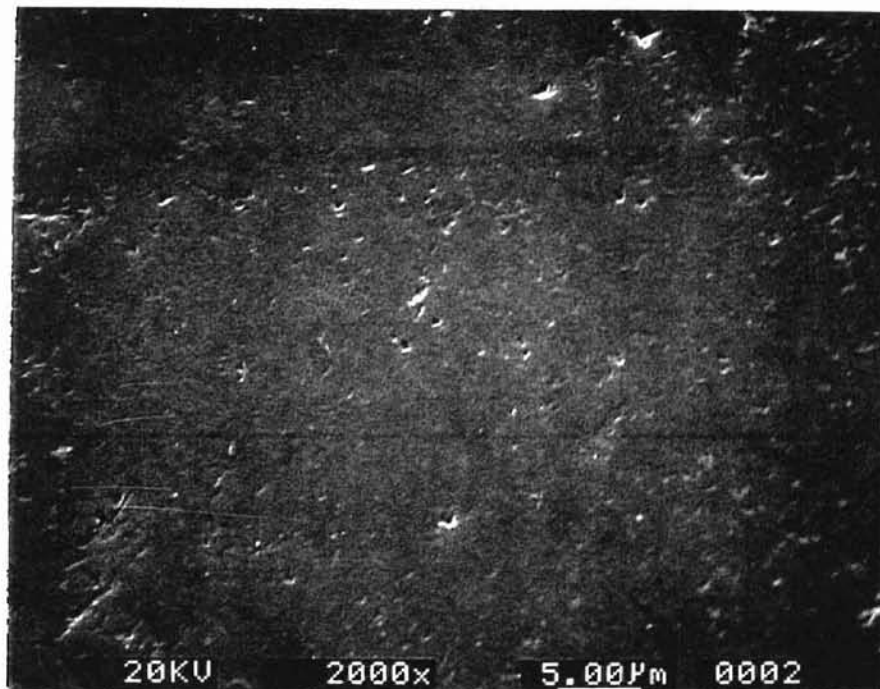


Figure 5.22(a) SEM micrograph at 2000X magnification polished with 1-5µm Cr_2O_3 in the electromagnetic float polishing apparatus

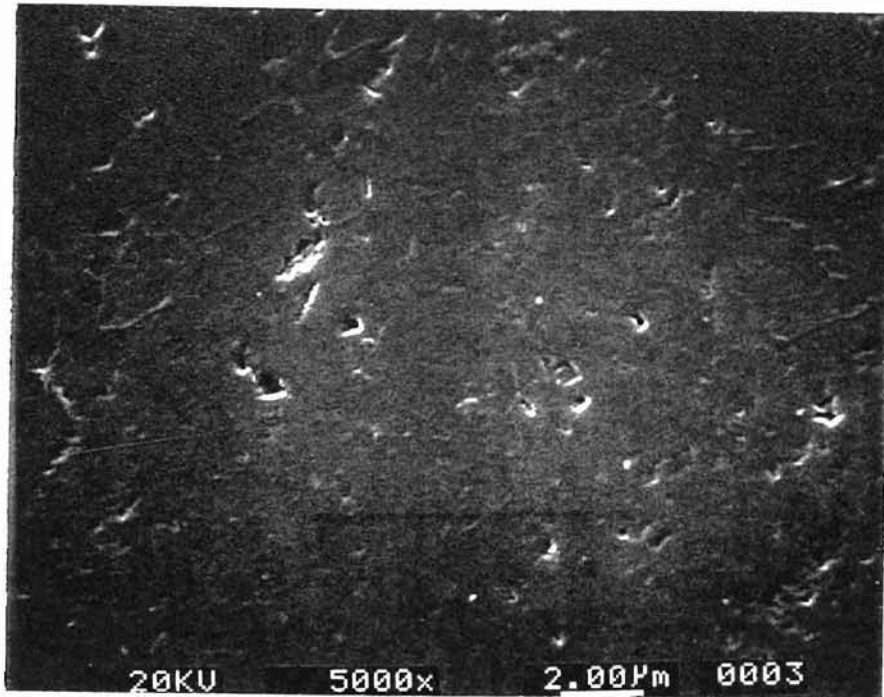


Figure 5.22(b) SEM micrograph at 5000X magnification polished with 1-5µm Cr_2O_3 in the electromagnetic float polishing apparatus

Cerium oxide (CeO_2) 3 µm grit was also found to be effective in the final stages for the polishing process in terms of surface finish. Even though the hardness of the cerium oxide (625 MPa) is less than both silicon nitride (1600-2200 MPa) and chromium oxide (2000-2200 MPa), it provides as good surface finish roughness in the electromagnetic field assisted polishing process. Surface morphology of the balls was also examined at different magnifications by using the scanning electron microscope (SEM) as shown in Figure 2.23. Comparing to a silicon nitride ball finished by conventional polishing techniques, ball surface was found to be much smoother and as good as that with a ball polished by using chromium oxide abrasive with the electromagnetic field assisted float polishing apparatus.

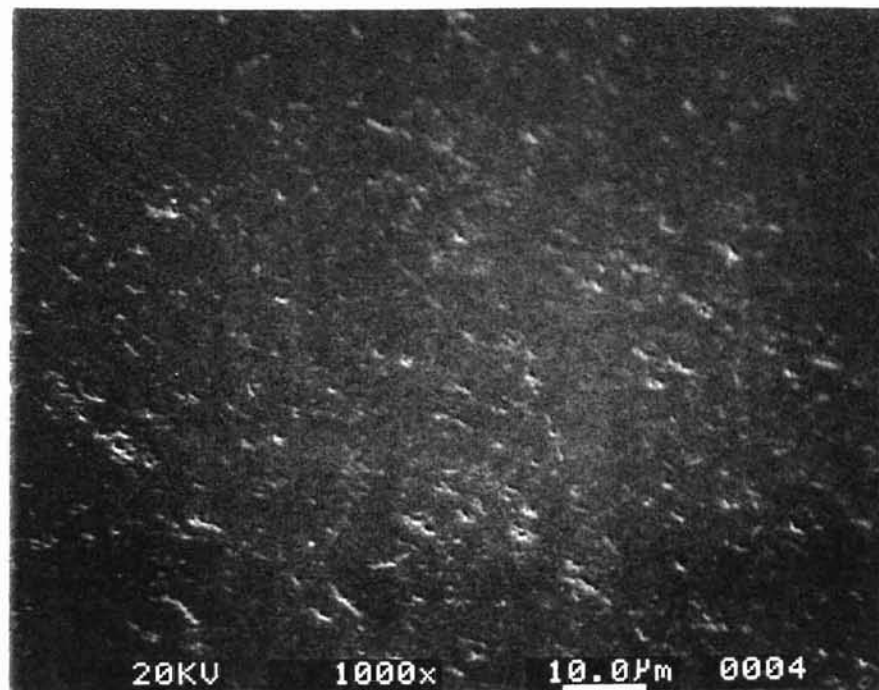


Figure 5.23(a) SEM micrograph at 1000X magnification polished with 3 μm CeO_2 in the electromagnetic float polishing apparatus

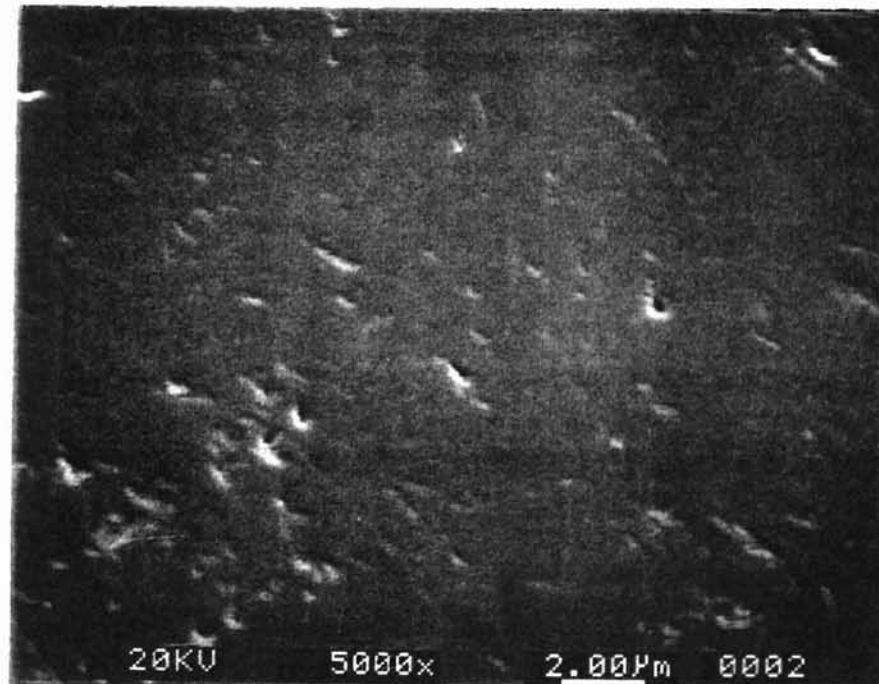


Figure 5.23(b) SEM micrograph at 5000X magnification polished with 3 μm CeO_2 in the electromagnetic float polishing apparatus

Similar test conditions were used during the evaluation of the surface roughness obtained with cerium oxide. Zygo plots of a ball finished by using cerium oxide at different magnifications are presented in Figure 5.24 and surface traces obtained from Talysurf in Figure 5.25.

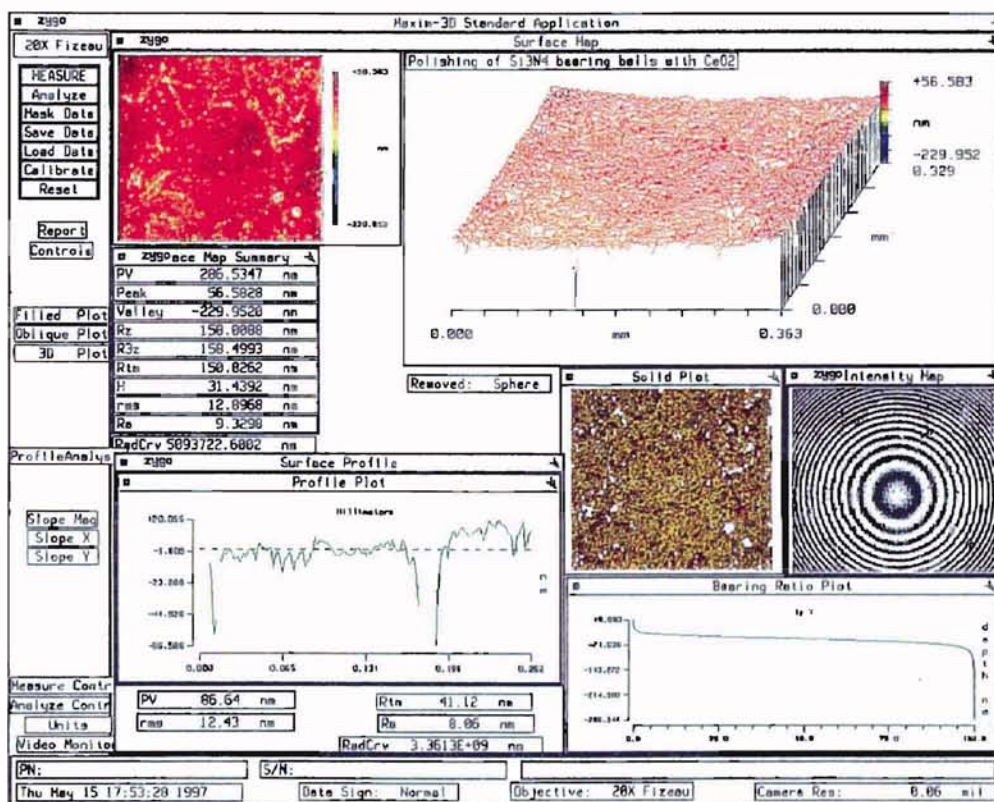


Figure 5.24 (a) ZYGO plots at low magnification (20X Fizeau) of a ball polished with CeO₂ (3 μ m) with the ring pole electromagnetic field assisted polishing apparatus.

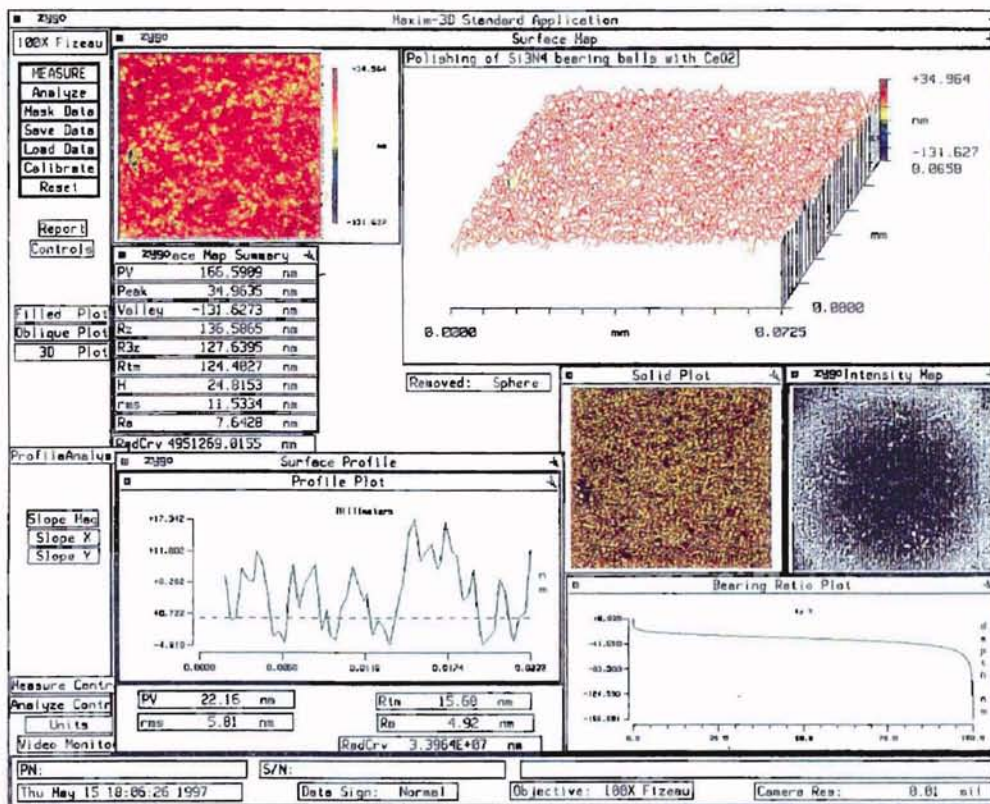


Figure 5.24(b) ZYGO plots at high magnification (100X Fizeau) of a ball polished with CeO_2 ($3 \mu\text{m}$) in the ring pole electromagnetic field assisted polishing apparatus.

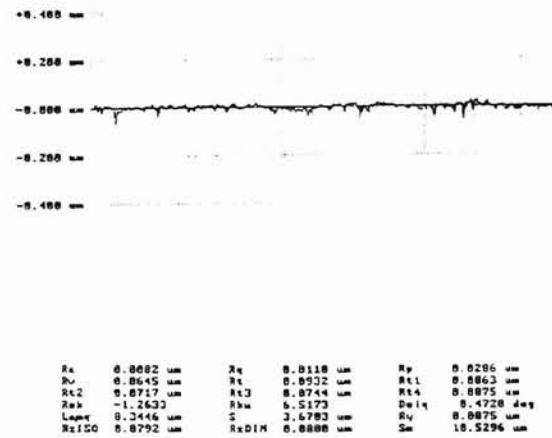


Figure 5.25 Talysurf trace of a silicon nitride bearing ball polished with CeO_2 ($3 \mu\text{m}$) in the ring pole electromagnetic field assisted polishing apparatus

5.4 Sphericity

In a bearing ball, sphericity (roundness) is defined as the maximum deviation from the minimum sphere diameter. The roundness of a bearing ball is an important factor in terms of its quality, and it is an important challenge for the magnetic float polishing technique. There are several other factors which have a significant effect on sphericity in the electromagnetic field assisted polishing apparatus. These factors were determined and grouped by Raghunandan [1996]. Although these factors are defined for the permanent magnet polishing apparatus, they are also found to be applicable to the electromagnetic field assisted polishing apparatus with some minor differences. These factors can be seen in Figure 5.26.

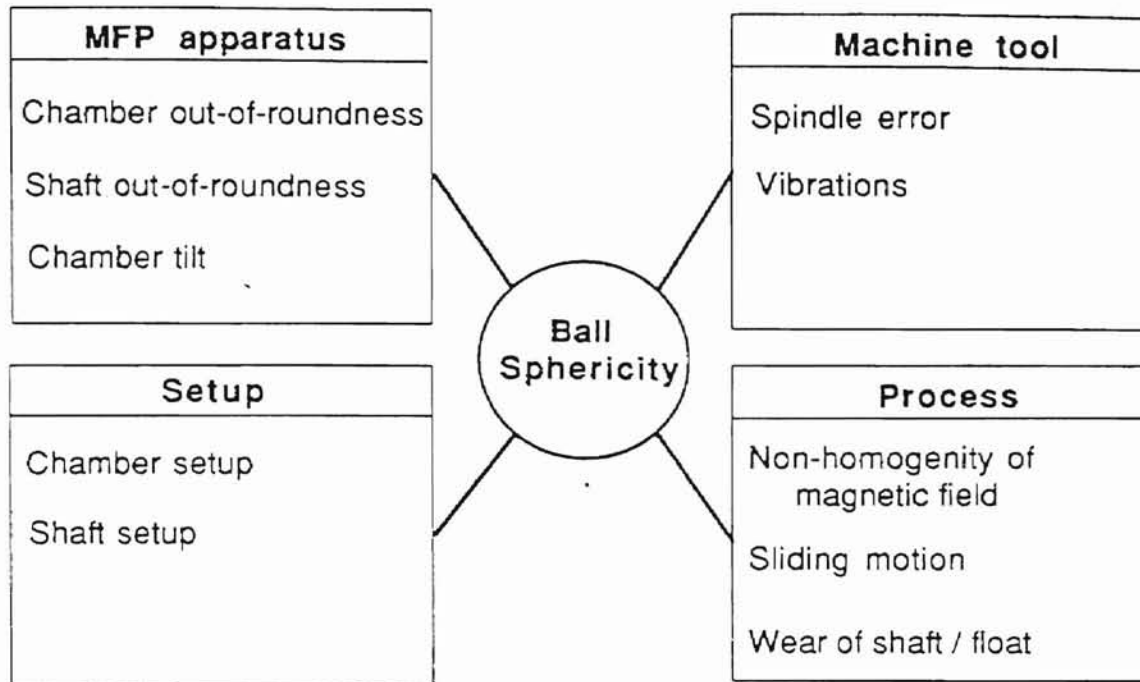


Figure 5.26 Factors affecting the ball sphericity in magnetic float polishing [Raghunandan, 1996].

Apparatus and setup related problems can be addressed and solved relatively easily when compared to the machine tool and process related problems. In the case of the electromagnetic field assisted polishing apparatus, there are three important process related parameters found to affect the ball sphericity most. These parameters are the abrasive concentration, the rotational speed of the driving shaft and the polishing force applied to the balls. Several characterization tests were conducted in order to find out how these parameters affected the ball roundness.

The effect of the rotational speed on the ball sphericity in the modified ring pole electromagnetic field assisted polishing apparatus can be seen in Figure 5.27.

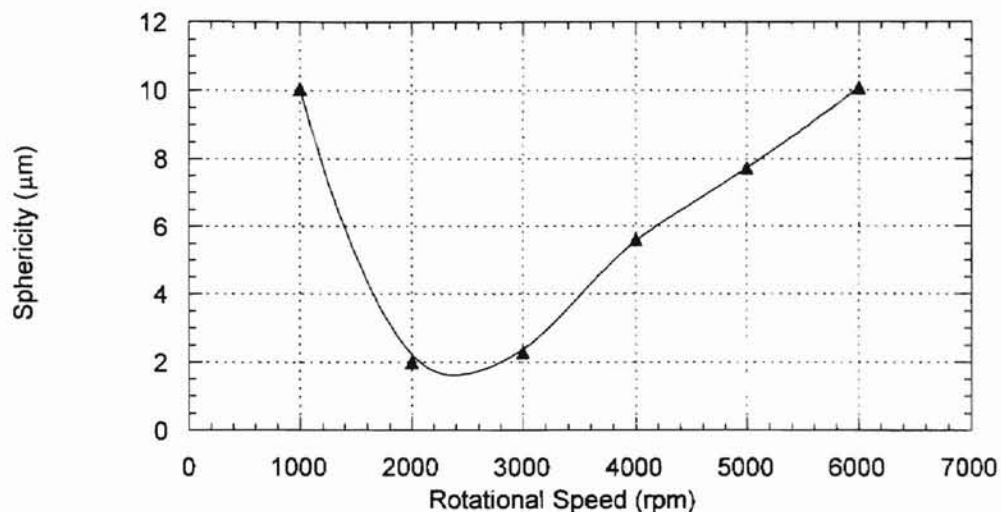


Figure 5.27 Effect of the rotational speed on the ball sphericity in the modified ring pole electromagnetic field assisted polishing apparatus.

These experiments were carried out by using boron carbide (B_4C) 500 grit size as the polishing abrasive. Figure 5.27 indicates that a rotational speed of 2000 rpm is the optimum polishing speed in terms of the best sphericity in the case of the electromagnetic field assisted polishing apparatus. A similar result was also reported for the permanent magnet polishing apparatus.

As stated earlier, the abrasive concentration was also found to have an important effect on the sphericity. Figure 5.28 shows the effect of the abrasive concentration on sphericity in the ring pole electromagnetic field assisted polishing apparatus.

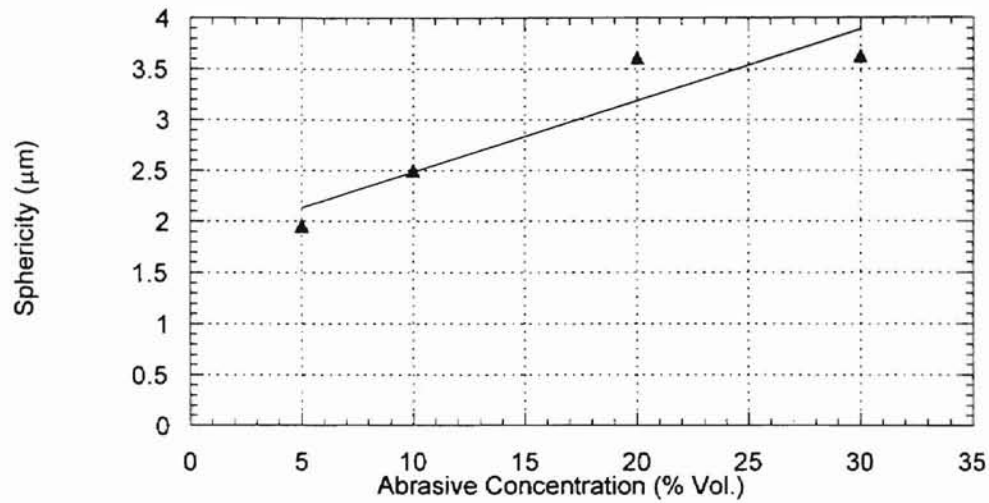
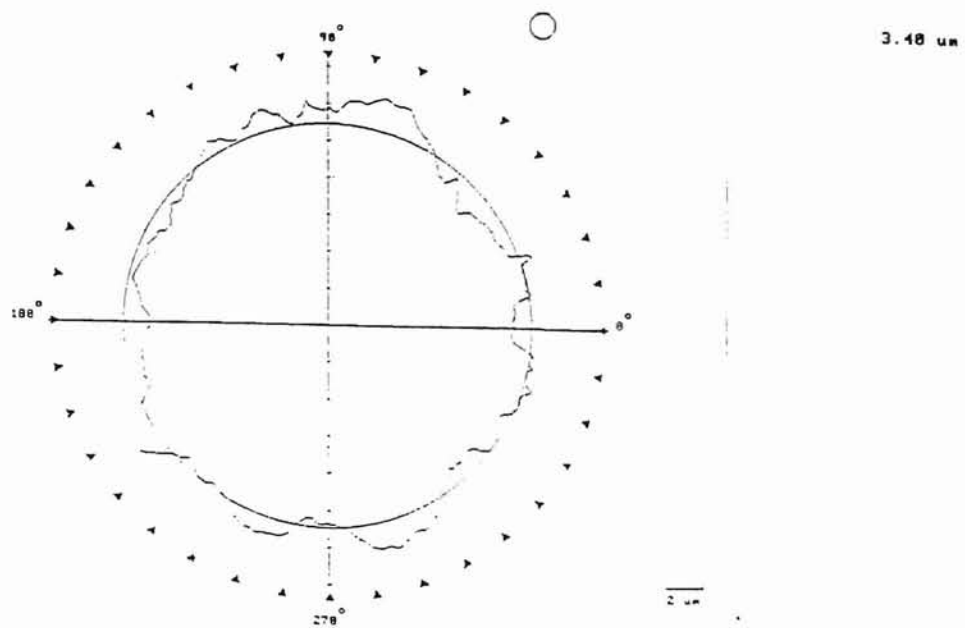
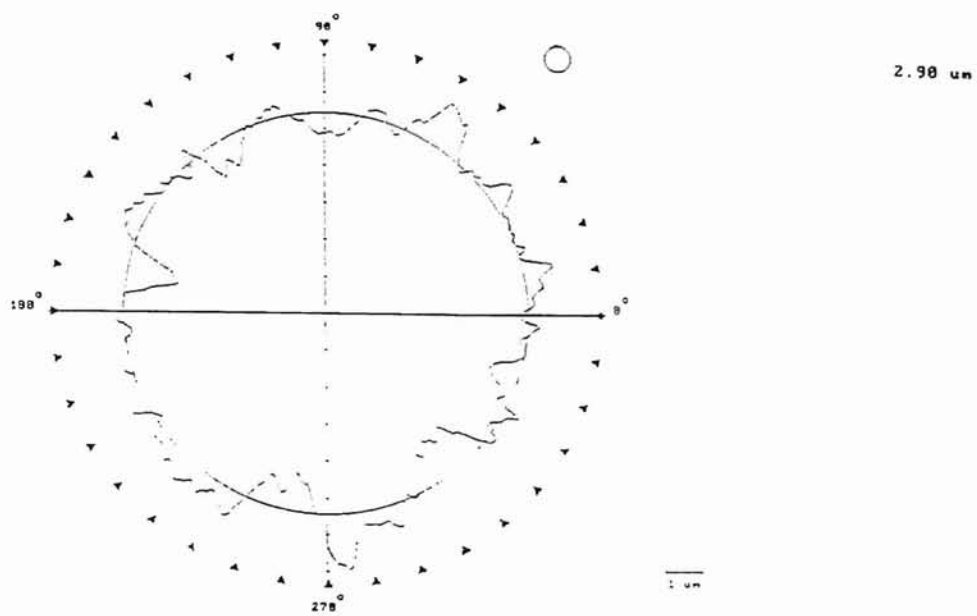


Figure 5.28 Effect of abrasive concentration on sphericity in the ring pole electromagnetic field assisted polishing apparatus.

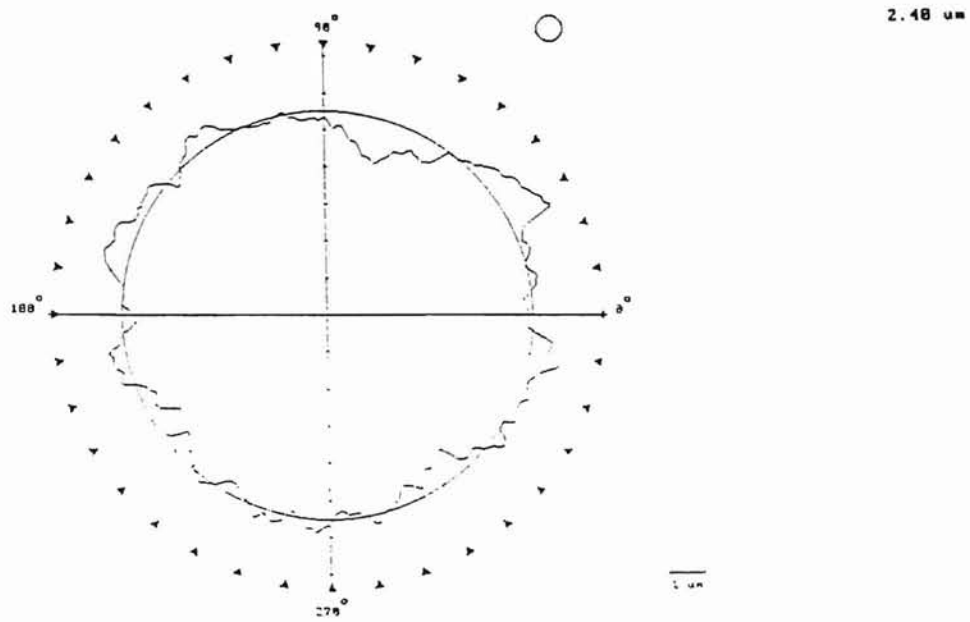
As can be seen from Figure 5.28, sphericity shows improvement as the abrasive concentration decreases. During the experiments, the speed of the drive shaft was 4000 rpm. The polishing abrasive was boron carbide (B_4C) 500 grid size and the polishing load was 1.2 N/ball. Talyround roundness traces of these tests can be seen in Figure 5.29.



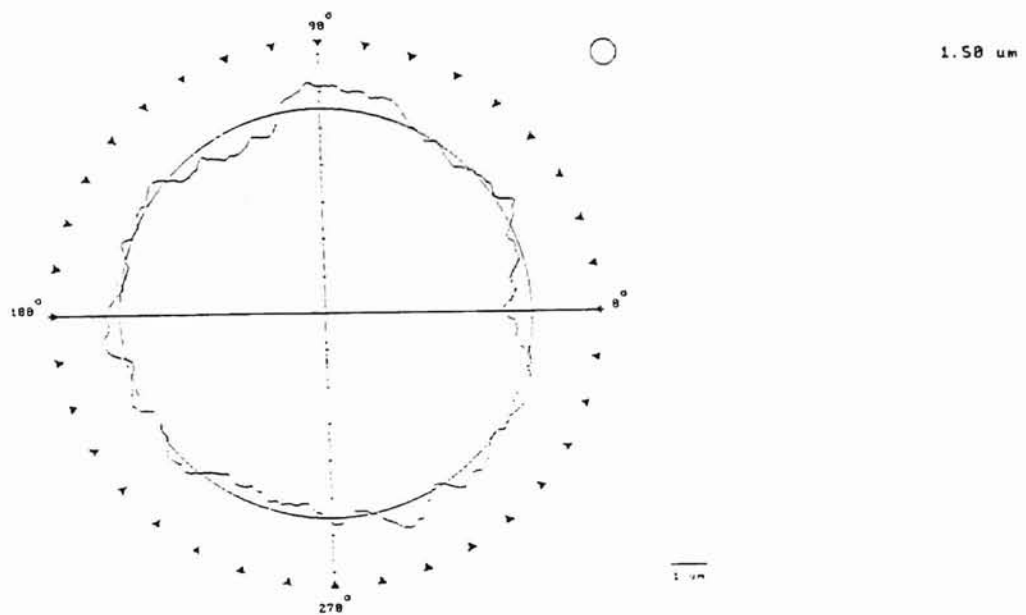
(a) 30% Vol. Abrasive Concentration



(b) 20% Vol. Abrasive Concentration



(c) 10%Vol. Abrasive Concentration



(d) 5%Vol. Abrasive Concentration

Figure 5.29 Talyround roundness traces of a ball with different abrasive concentrations in the ring pole design.

The same characterization tests were also conducted by using the modified ring pole design. The results of these tests can be seen in Figure 5.30.

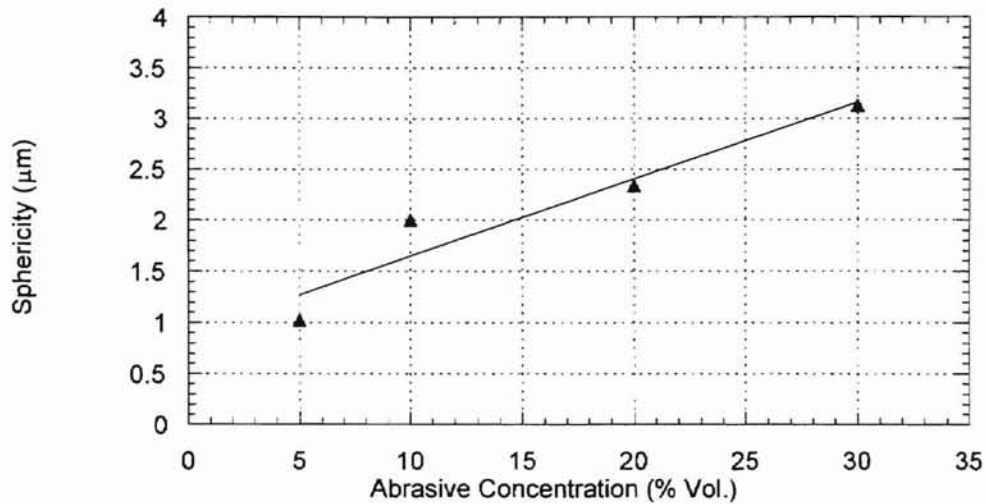
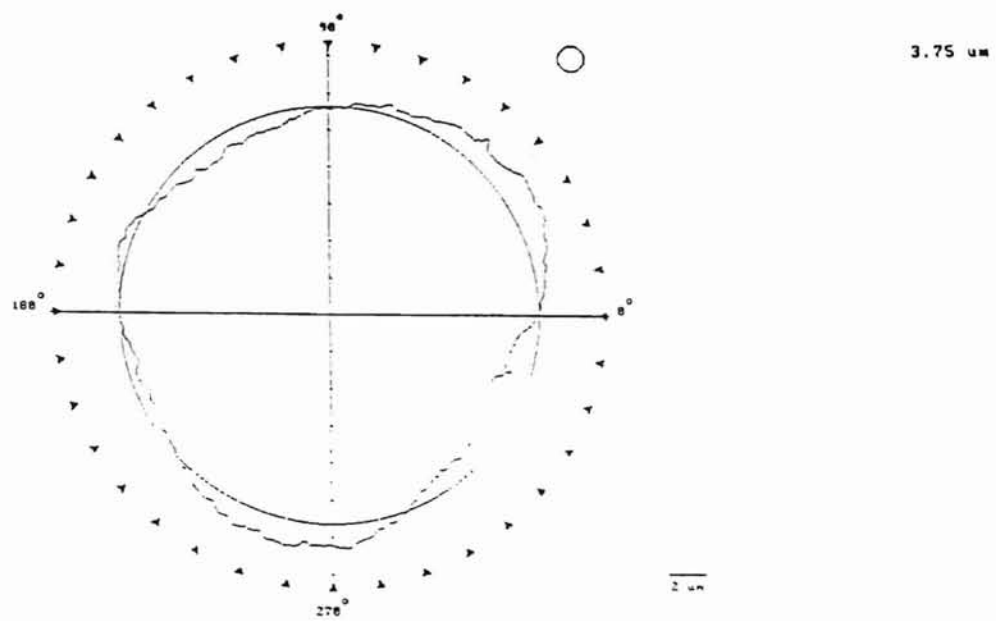
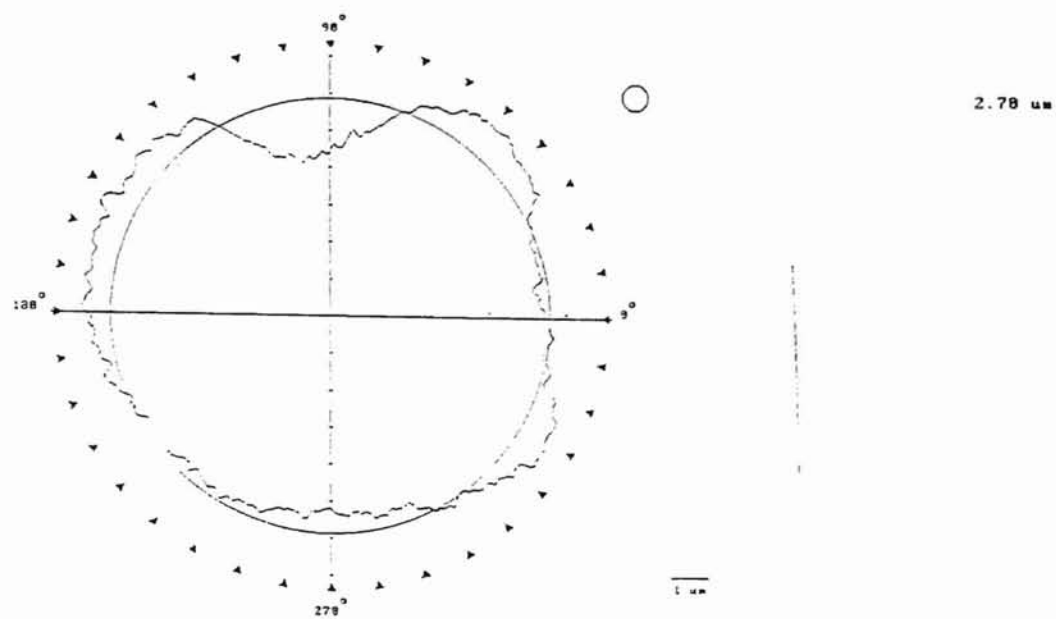


Figure 5.30 Effect of abrasive concentration on sphericity in the modified ring pole electromagnetic field assisted polishing apparatus.

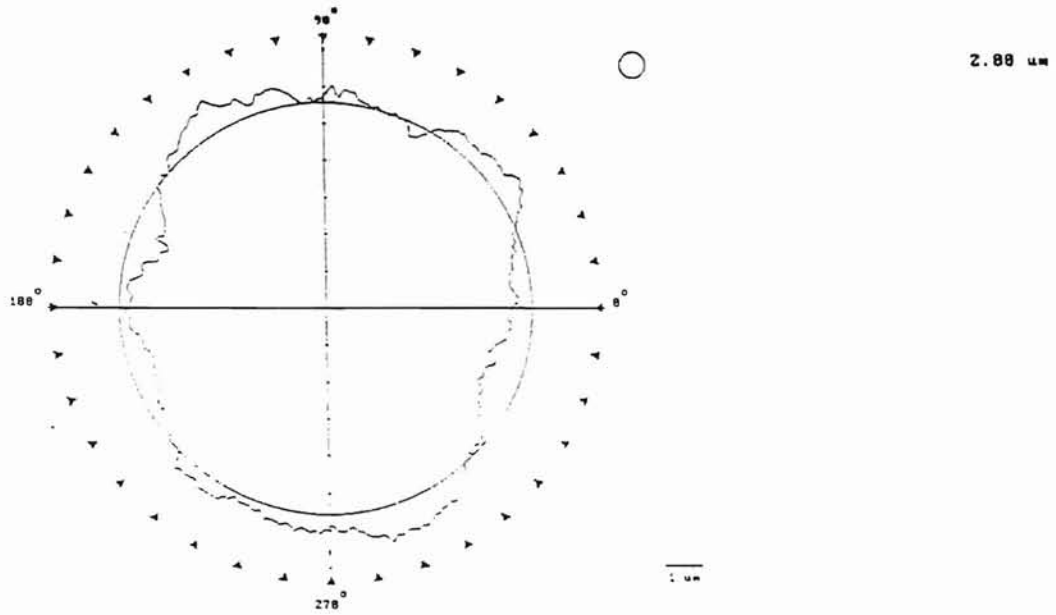
A similar behavior was also observed in the modified ring pole design when the abrasive concentration was altered. It should be noted that the average sphericity values are less when they are compared with the ring pole design. This is because during the tests, the rotational speed of the drive shaft was set to 2000 rpm. In other words, the results presented in Figure 5.27 are also in agreement with the optimum speed for good sphericity discussed earlier. Talyround roundness traces of these tests can be seen in Figure 5.31 for the modified ring pole design.



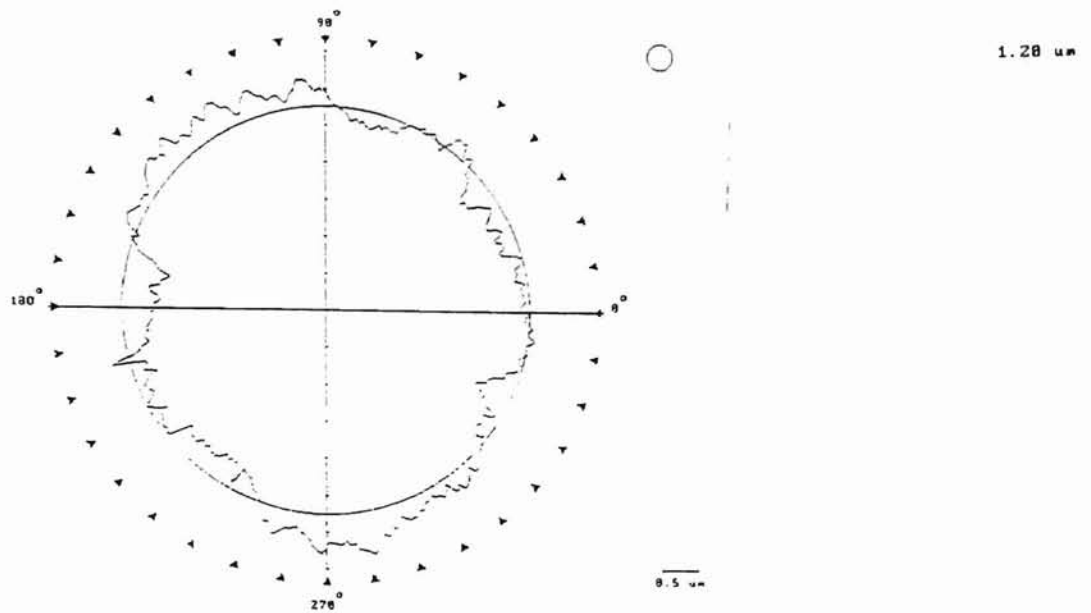
(a) 30% Vol. Abrasive Concentration



(b) 20% Vol. Abrasive Concentration



(c) 10% Vol. Abrasive Concentration



(d) 5% Vol. Abrasive Concentration

Figure 5.31 Talyround roundness traces of a ball with different abrasive concentrations in the modified ring pole design.

Another important factor that affects the sphericity is the polishing load applied to the balls during the polishing process. In order to determine the effect of the polishing load, tests were conducted by varying the force applied. During these tests, boron carbide (B4C) 500 grit was used as the polishing abrasive and a 2000 rpm rotational speed was used. The abrasive concentration was 5% by volume during the tests. Results of these experiments are shown in Figure 5.32.

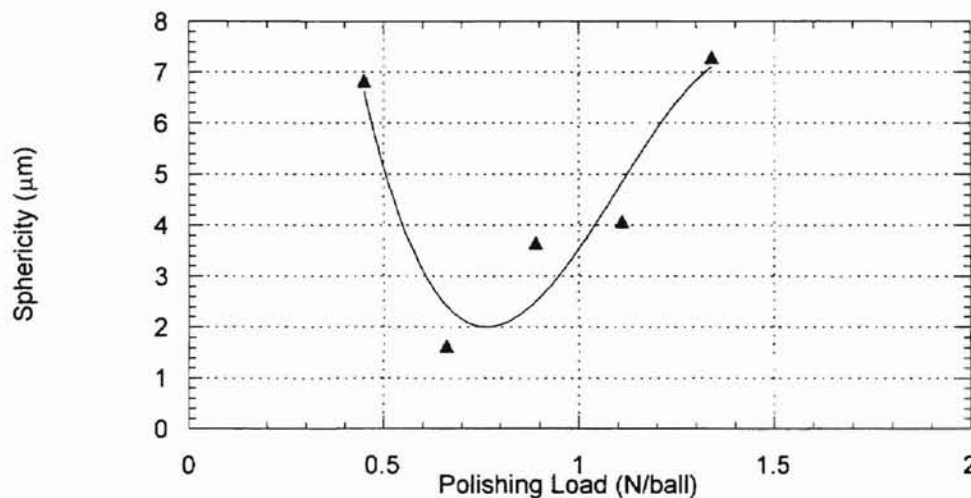


Figure 5.32 Effect of the polishing load on sphericity in the modified ring pole electromagnetic field assisted polishing apparatus.

It can be seen from Figure 5.32 that optimum polishing load is found be 0.65 N/ball in terms of obtaining a better sphericity in the modified ring pole design.

It should also be realized that obtaining better sphericity is also a function of the polishing time. By applying the optimum conditions discussed earlier, longer polishing times lead to better sphericity values. In order to illustrate the importance of the polishing

time, Figure 5.33 is presented for the ring pole design and Figure 5.34 is for the modified ring pole design.

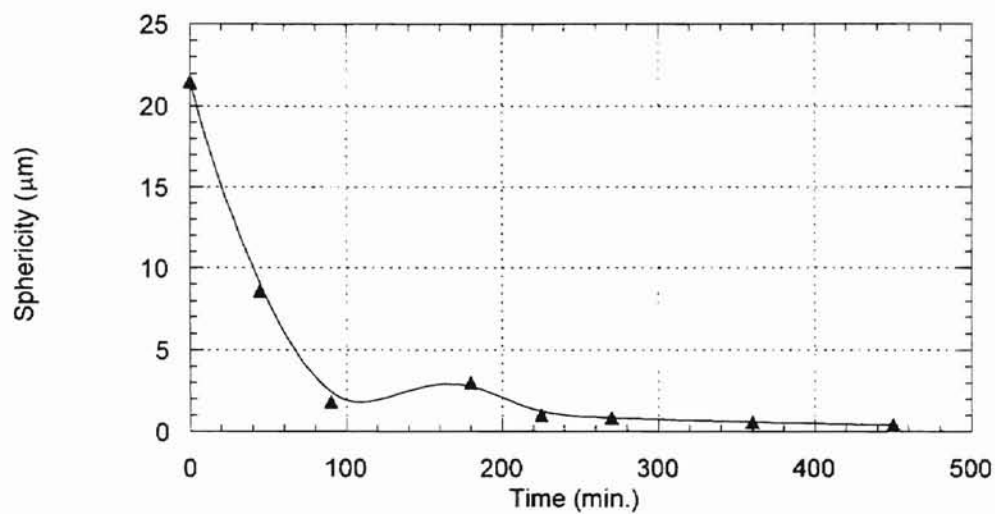


Figure 5.33 Change in sphericity with time in the ring pole design

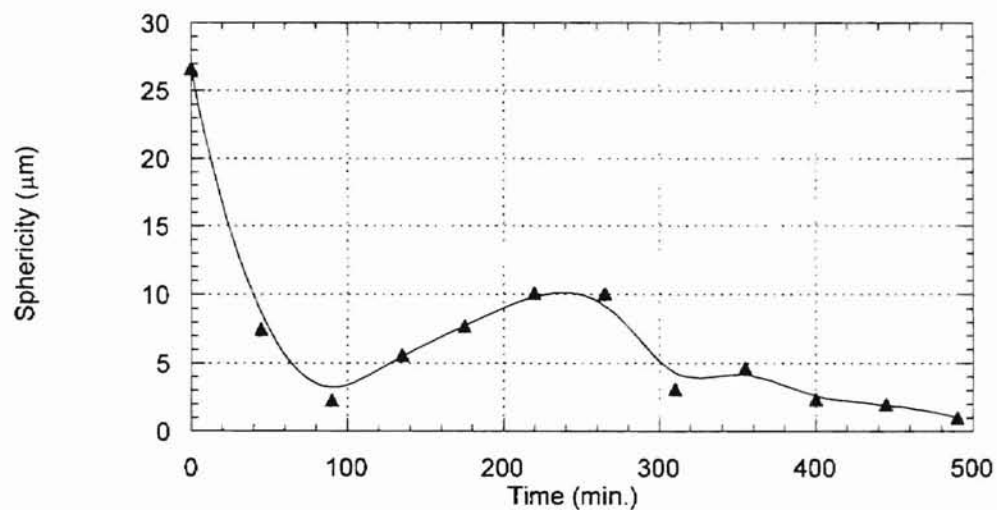
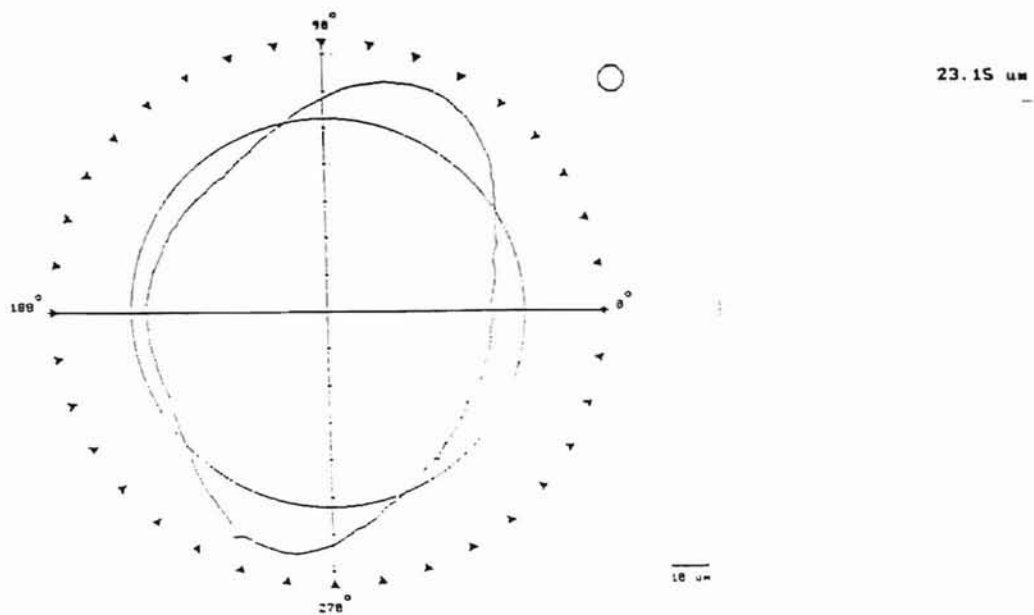
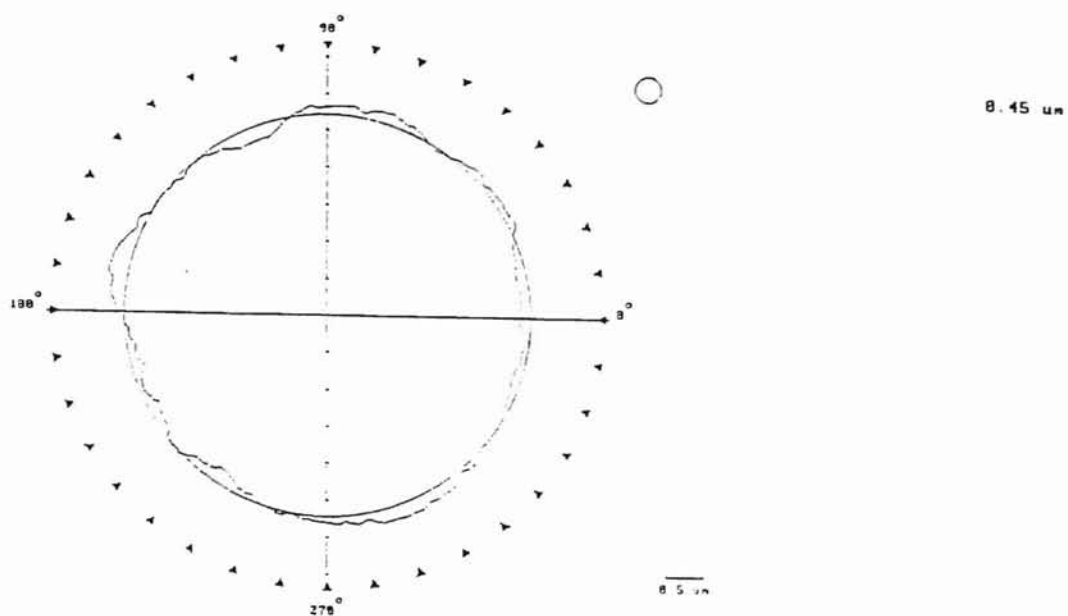


Figure 5.34 Change in sphericity with time in the modified ring pole design

In Figure 5.35, Talyround traces for the initial and the final average sphericity values obtained with the ring pole design can be seen.



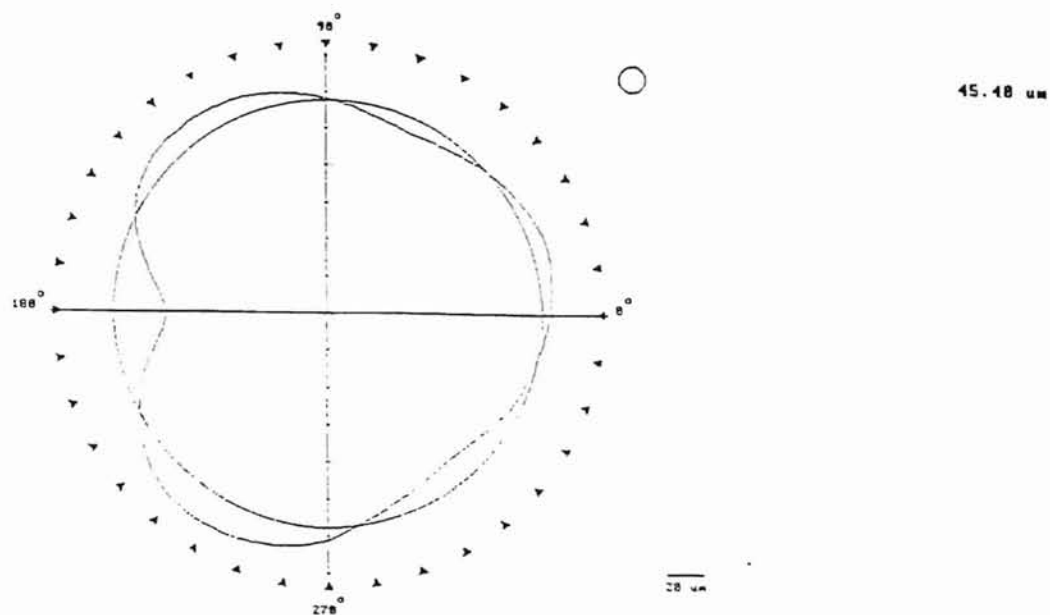
(a) Initial average sphericity



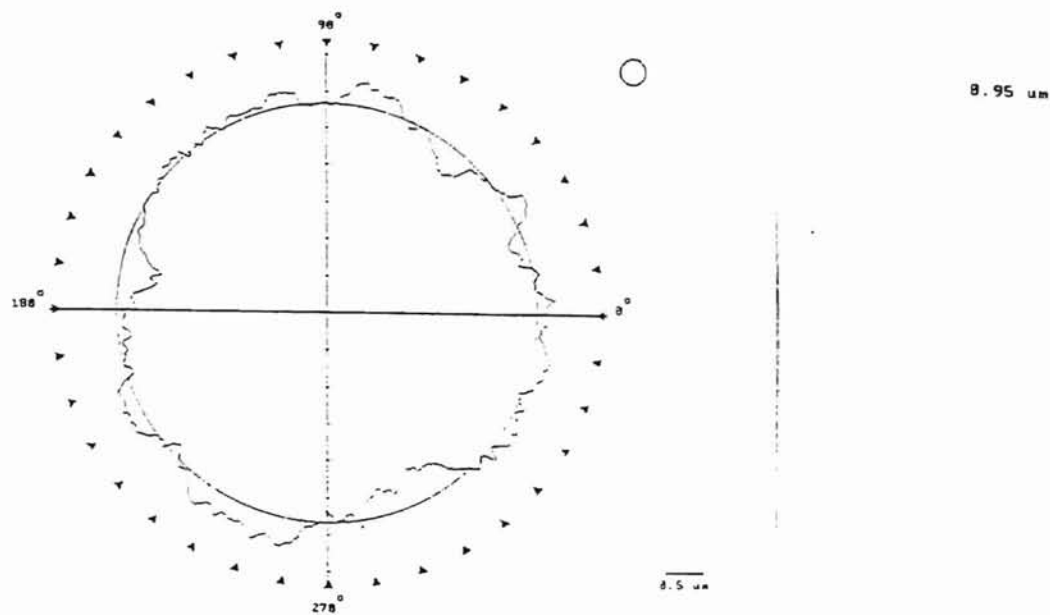
(b) Final average sphericity

Figure 5.35 Talyround traces for the ring pole design

In Figure 5.36 Talyround traces for the initial and the final average sphericity values obtained with the ring pole design can be seen.



(a) Initial average sphericity



(b) Initial average sphericity

Figure 5.36 Talyround traces for the modified ring pole design

CHAPTER 6

DISCUSSION

A straight field electromagnetic field assisted polishing apparatus was conceived and designed by Shinmura and Komanduri incorporating Umehara's permanent magnet design and built by Mr. M. Dock. The initial design was evaluated by Dock and found to provide less buoyancy forces (3.5 N) when compared to permanent magnet apparatus (7 N), as discussed earlier. Therefore, modifications were made to the upper intensifier in order to obtain better and improved magnetic field strength and buoyancy forces (10 N).

In the evaluation stage of the ring pole design, FEM analysis was employed. Even though ANSYS analysis provided valuable design optimization characteristics without multiple construction iterations, theoretical results obtained from the ANSYS package were found to be far from reality in terms of magnetic flux density and magnetic field strength. The main reason for the difference between the theoretical and experimental results was due to the 2D analysis option in the ANSYS solution. ANSYS analysis was also employed to determine the effect of the ring pole thickness on the magnetic field strength. It was found that magnetic field shorts from the closest distance from the lower intensifier to ring pole. Therefore, the thickness of the ring pole steel plate does not affect the overall magnetic field strength inside the polishing chamber. Axi-symmetric solution in the ANSYS package provided more realistic results and lead to a modified ring pole design which yielded experimental results comparable to the theoretical

solution. Since the polishing load was found to be an important factor in magnetic float polishing, a new force monitoring system was developed. In the case of the permanent magnet, force measurements were performed using a 3-axis dynamometer. Due the heavy size of the electromagnetic polishing apparatus, difficulty in balancing the apparatus on the dynamometer and limited z-axis distance in the Bridgeport NC milling machine necessitated a different force measurement system. Even though the developed system is not as accurate as the Kistler piezoelectric dynamometer in the permanent magnet apparatus, it provides adequate force measurement results which can also be monitored using the calibration curve in terms of height inside the polishing chamber.

Due to the higher buoyancy forces and the donut shaped magnetic field orientation inside the polishing chamber (Figure 6.1), higher material removal rates (up to 4.5 $\mu\text{m}/\text{min}$) were accomplished with the ring pole design. This donut shaped magnetic field orientation was found to be the key factor in terms of high material removal rates. During the polishing process, silicon nitride balls are fully covered with the magnetic fluid mixed with the abrasives. Since the ball surfaces are covered with the magnetic fluid and the abrasives, the balls have a greater possibility to contact with the abrasives and therefore higher rates of abrasion occurs. In the case of permanent magnet apparatus, the balls have less chances of contacting the abrasives due its specific magnetic field orientation (Figure 6.2). Hard abrasives, such as boron carbide (B_4C) provide higher material removal rates for a given grain size as compared to softer abrasives namely, silicon

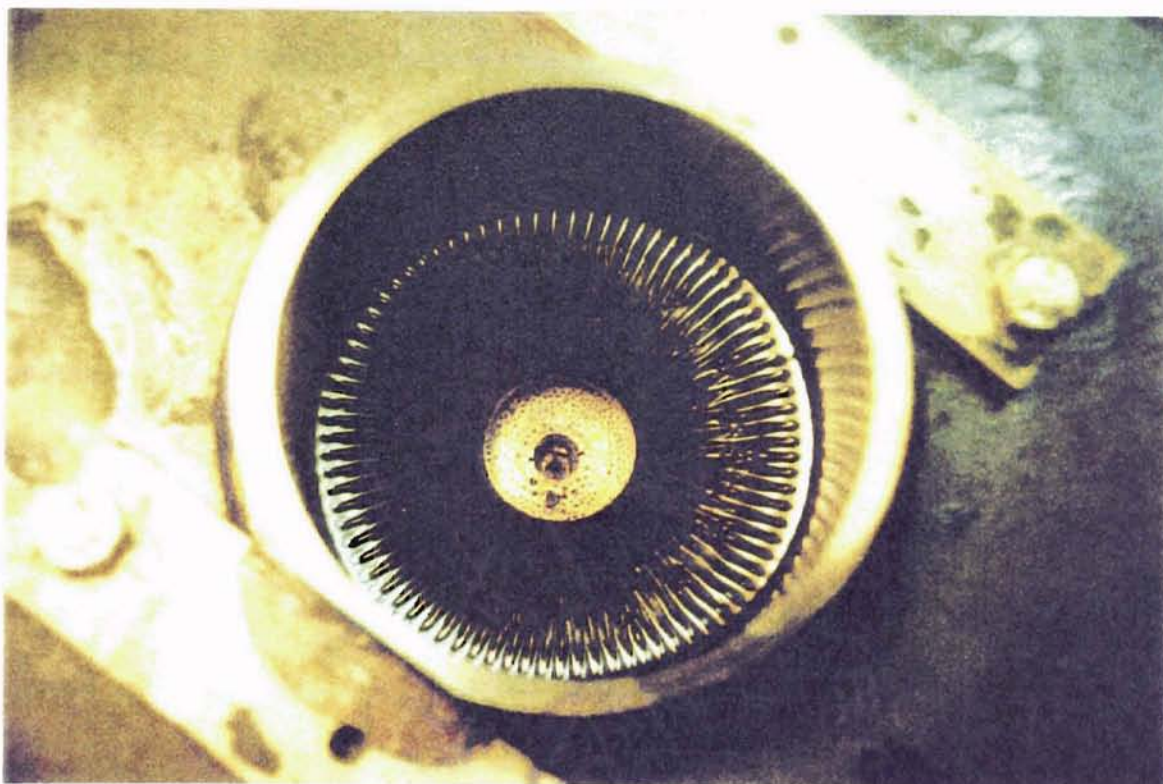


Figure 6.1 Situation of the magnetic fluid and the abrasives under the magnetic field in the electromagnetic float polishing apparatus.

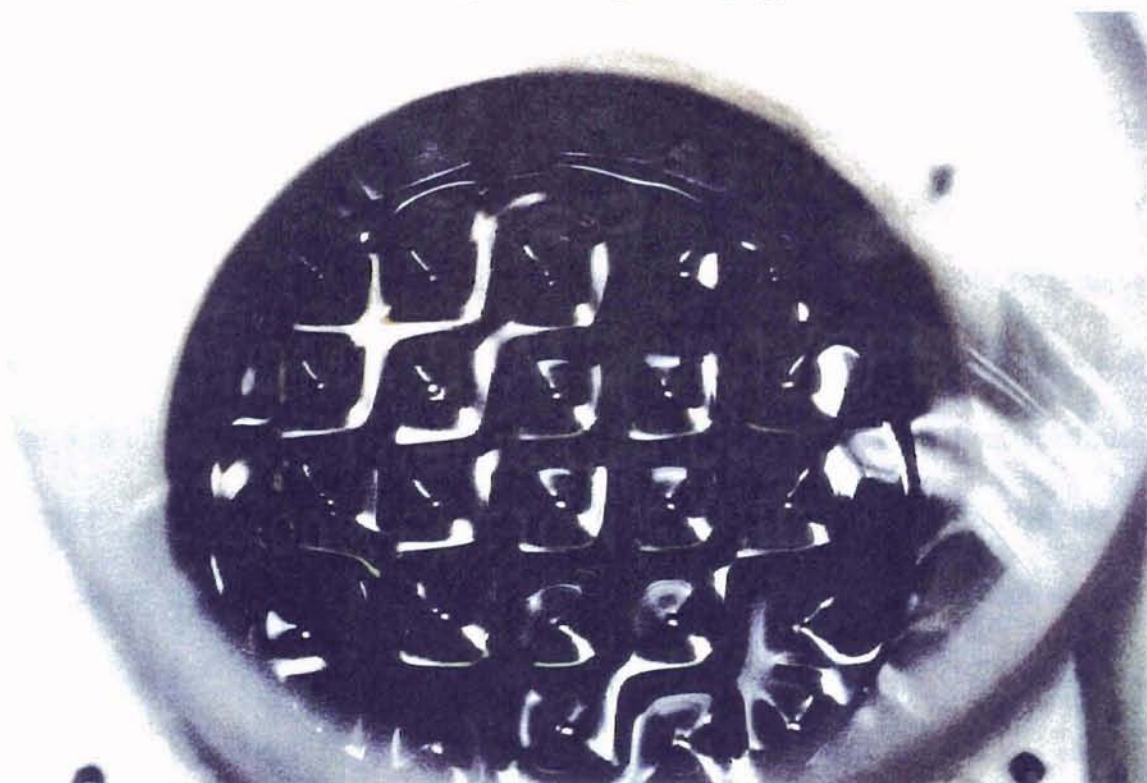


Figure 6.2 Situation of the magnetic fluid and the abrasives under the magnetic field in the permanent magnet float polishing apparatus.

carbide (SiC) and chromium oxide (Cr_2O_3). Also, higher rotational speeds for the drive shaft lead to higher material removal rates but also showed signs of vibrational instabilities. Higher rotational speeds also lead to higher evaporation rate of the magnetic fluid which caused irregularities in the shape of the silicon nitride balls. Higher abrasive concentrations provided higher material removal rates but 10% by volume concentration is considered as adequate in terms of desired material removal rates.

Material removal mechanisms in the electromagnetic polishing apparatus were found to be similar to the permanent magnet apparatus. Microfracture, scratch formation due to abrasion, and chemo-mechanical action are the three material removal mechanisms in the case of electromagnetic polishing apparatus. In the literature, the material removal mechanism was reported to be a 2-body abrasion process, but this may not be so in practice.

The surface finish obtained in the electromagnetic field assisted polishing apparatus was found to be similar to ones obtained using a permanent magnet design. By using chromium oxide (Cr_2O_3) and chemo-mechanical action, it is possible to achieve fracture free and sub-surface damage free bearing balls. Cerium oxide (CeO_2) was also employed as a final stage polishing abrasive and found to provide excellent surface finish (average surface roughness R_a of 8 nm). Since the hardness of the cerium oxide is significantly less than silicon nitride work material, it is also believed that chemo-mechanical action is the dominant mechanism of material removal.

In the electromagnetic field assisted polishing apparatus, it is also possible to obtain similar sphericity values when compared to permanent magnet apparatus. Abrasive concentration was found to have a significant effect on sphericity in the case of

electromagnetic field assisted polishing apparatus. Less abrasive concentration (5% by volume) leads to a better sphericity. Since less abrasive concentration provides lower viscosity for the magnetic fluid, surface traction forces are believed to be decreasing and therefore providing more uniform rolling and sliding action for the balls inside the polishing chamber. As mentioned earlier, all of the experiments were conducted on a Bridgeport CNC milling machine. A PI air bearing spindle was employed for the reported sphericity values obtained with permanent magnet design. Comparing with the PI spindle, the Bridgeport spindle was found to have relatively higher lateral vibrations which has a significant effect on sphericity. Sphericity values would have been better if the PI spindle had been used in the case electromagnetic polishing apparatus. Repeatability in sphericity values was another problem faced with the electromagnetic polishing apparatus which is believed to have been caused by the magnetic field generation and the power system.

Diameter deviation was found to be around 4-5 μm in a particular batch. This variation is also believed to be due to the lateral vibration of the Bridgeport spindle.

CHAPTER 7

CONCLUSIONS

- The straight field electromagnetic field assisted polishing apparatus proposed and designed by Shinmura and Komanduri was reviewed. The ring pole design proposed by Dock was reanalyzed and modified using the ANSYS FEM package and a modified ring pole design was introduced using the axi-symmetric solution of the ANSYS package
- A new force monitoring system was developed for the electromagnetic field assisted polishing apparatus
- Experimental tests were conducted using the modified ring pole electromagnetic field assisted polishing apparatus as well as the ring pole design to determine the important process parameters in the electromagnetic float polishing apparatus.
- An average sphericity of 0.45 μm with the ring pole design and 0.95 μm with the modified ring pole design was obtained. An average surface roughness of 13 nm was produced using chromium oxide (Cr_2O_3) abrasive with both of the designs and 8 nm with cerium oxide (CeO_2). Variation in diameter of 4-5 μm in a batch was obtained.
- Up to 4.5 $\mu\text{m}/\text{min}$ material removal rate was accomplished using both the ring pole design and the modified ring pole design.

- Higher buoyancy forces were obtained using the electromagnetic design (12 N) than by the permanent magnet polishing apparatus (7 N).

7.1 Future Work

A high precision spindle needs to be used in conjunction with the electromagnetic float polishing apparatus to reduce the sphericity and variation in diameter among the balls in a batch.

To determine the full potential of the electromagnetic float polishing apparatus, further work needs to be done. In order to provide a more uniform magnetic field inside the polishing chamber, possible design alterations should be considered to have better control on the polishing process and to achieve the desired qualities of a bearing ball.

Material removal mechanisms should also be clearly identified to have a better understanding for the process. The effect of the magnetic fluid viscosity on sphericity should also be investigated. Even though the magnetic field provided by the three coils is the summation of all of them, it would be better to have a new coil system, since each coil has a different resistance.

Cerium oxide was also found be performing well in the final stages of the polishing process. It would be better to investigate the actual material removal mechanism with this abrasive.

Since it is possible to alter the current passing through the coils, the effect of different current densities should also be investigated. By increasing the magnetic field

gradients, stiffness of the magnetic polishing apparatus could be improved to obtain better sphericity values. It would be also a better comparison with the permanent magnet design if the polishing process was carried out by using the PI air bearing spindle.

Using the 3D analysis option in ANSYS package, might give a better idea to see the distribution of the magnetic field on the ring pole steel plate.

BIBLIOGRAPHY

- Akazawa, M., and K. Kato, "Wear properties of Si_3N_4 in rolling-sliding contact," Wear, Vol.124, 1988, 123-132
- Ault, N.N., and R.L. Russell, "Silicon nitride," Minerals Rev., 72, No. 6, 1993, 117-118
- Bhagavatula, S.R., and R. Komanduri, "On Chemo-mechanical polishing of silicon nitride with chromium oxide abrasive," Philosophical Magazine A, Vol. 174, No. 4, 1996, 1003-1017
- Baron, J.M., "Technology of Abrasive machining in a magnetic field," Masino-strojenije, Leningrad, 1975, (in Russian)
- Childs, T.H.C., Jones, D.A., Mahmood, S., Kato, K., Zhang, B., and N. Umehara, "Magnetic fluid grinding mechanics," Wear, 175, 1994a, 189-198
- Childs, T.H.C., Mahmood, S., and H.J. Yoon, "The material removal mechanism in magnetic fluid grinding of ceramic ball bearings," Proc. Of I. Mech. E., 208, No. B1, 1994b, 47-59
- Coats, H.P., "Method and apparatus for polishing containers," US patent No. 2,196,058, (1940)
- Dock, M., "Electromagnetic float polishing of ceramic balls for bearing applications," Masters Thesis, Oklahoma State University, 1994
- Kato, K., Kim, S.S., Hokkirigawa, K., and H. Abe, "Wear mechanism of ceramic materials in dry rolling friction," Trans. Of The ASME, Vol. 108, 1986, 522-526
- Kato, K., "Tribology of ceramics," Wear, 136, 1990, 117-133
- Komanduri, R., Umehara, N., and M. Raghunandan, "On the possibility of chemomechanical action in the polishing of silicon nitride balls," Trans. Of The ASME, Vol.118, 1996, 1-7
- Komanduri, R., "On the mechanisms of material removal in fine grinding and polishing of advanced ceramics," Annals of CIRP, 44/1, 1996
- Makedonski, B.G., and A.D. Kotschmidov, "Schleifen im magnetfeld," Fertigungstechnik und Betrieb, 24, H.4, 1974, 230-235
- Raghunandan, M., "Magnetic float polishing of silicon nitride balls," Ph.D. Thesis, Oklahoma State University, 1996

- Raghuandan, M., Personal Communication, 1995
- Rosenweig, R.E., "Magnetic fluids," International Science and Technology, July 1966, 48-56
- Shinmura, T., Takazawa, K., Hatano, E., and T. Aizawa, "Study on magnetic-abrasive process, process principle and finishing possibility," Bull. Of JSME, 19/1, 1985, 54-55
- Shinmura, T., and T. Aizawa, "Study on internal finishing of a nonferromagnetic tubing by magnetic abrasive finishing process," Bull. Of Japan Soc. Of Prec. Engg., 23/1, 1989, 37-41
- Shinmura, T., Takazawa, K., and E. Hatano, "Study of magnetic abrasive finishing," Annals of CIRP, 39/1, 1990, 325-328
- Shinmura, T., Yamaguchi, H., and T. Aizawa, "A new internal finishing process for nonferromagnetic tubing by the application of a magnetic field - the development of a unit type finishing apparatus using permanent magnets," NAMRC, 1993
- Tani, Y., and K. Kawata, "Development of high-efficient fine finishing process using magnetic fluid," Annals. Of CIRP, 33/1, 1984, 217-220
- Umehara, N., and K. Kato, "Hydro-magnetic grinding properties of magnetic fluid containing grains at high speeds," Journal of Magnetism and Magnetic Materials, 65, 1987, 397-400
- Umehara, N., and K. Kato, "Principles of magnetic fluid grinding of ceramic balls," Applied Electromagnetics in Materials, 1, 1990, 37-43
- Umehara, N., "Magnetic fluid grinding -a new technique for finishing advanced ceramics," Annals of CIRP, 43/1, 1994, 185-188
- Umehara, N., Kobayashi, T., and K. Kato, "Internal polishing of tube with magnetic fluid grinding Part 1, fundamental polishing properties of tube with taper-type tools," Journal of Magnetism and Magnetic Materials, 149, 1995, 185-187
- Umehara, N., Kobayashi, T., and K. Kato, "Internal polishing of tube with magnetic fluid grinding Part 2. fundamental polishing properties with rotating balls and with oscillating balls," Journal of Magnetism and Magnetic Materials, 149, 1995, 185-187
- Yoshikawa, H., "Brittle-ductile behavior of crystal surface in finishing," Journal of JSPE, 35(10), 1967, 662-667 (in Japanese)

APPENDIX A

```

! Straight Field Geometry Script for ANSYS
/CLEAR
/filnam,str_fld
/prep7

/PNUM,AREA,ON
rectan,-.127,.2,-.019,.019
RECTAN,-.0457,.0457,.019+.1016,.019+.0203+.1016
RECTAN,-.0508,.0508,.019,.019+.1016
AADD,ALL

RECTAN,.0508,.12,.019,.019+.1016
RECTAN,-.0508,-.12,.019,.019+.1016
RECTAN,.2381,.2,-.019,.26
RECTAN,.2381,-.1,.26,.26+.0381
RECTAN,-.1,-.02,.23,.26
RECTAN,.02,.1,.23,.26
AADD,3,6,7,5,4

RECTAN,-.05,.05,.1409,.1409+.05
RECTAN,-.2,.3,-.05,.3
PTXY,-.0254,.1409,-.0152,.1282,.0152,.1282,.0254,.1409
POLY
!RECTAN,.0254,.0457,.1409,.1409+.03
AOVLAP,ALL
AGLUE,ALL
finish
!Base
!Lower Intensifer
!Core
!COIL RIGHT
!COIL LEFT
!RIGHT RISER
!UPPER YOKE
!upper intensifier
! " "
!FINE AIR POCKET
!EXTERNAL AIR
!CUTOUT

```

```

!      Straight Field Mesh Script for ANSYS
/prep7
/COM, **** MATERIAL PROPERTY DEFENITION ****
MP, MURX, 1, 1 ! MATL. 1 IS AIR

```

```

TB, BH, 2 ! MATL. 2 IS MILD STEEL

```

```

TBPT,,303, 0.8
TBPT,,333.3, 0.9
TBPT,,378.75, 1.0
TBPT,,492.4, 1.1
TBPT,,530.25, 1.2
TBPT,,621.15, 1.3
TBPT,,833.25, 1.33
TBPT,,1000, 1.4
TBPT,,1287.25, 1.45
TBPT,,1666.5, 1.5
TBPT,,2121, 1.55
TBPT,,3000, 1.6
TBPT,,4000, 1.63
TBPT,,5000, 1.645
TBPT,,6000, 1.669
TBPT,,7000, 1.685
TBPT,,8000, 1.7
TBPT,,9000, 1.73

```

```

ET,1,9      !INFINITY
ET,2,13     !FINITE

```

```

asel,all
aclear,all  ! Clear all nodes and elements
lclear,all

```

```

eshape,0
lselect,s,,31,32 ! select & mesh outer lines
lselect,a,,24,25
type,1
mat,1
esize,.025
lmesh,all

```

```

asel,s,area,,12 !select & mesh fine air
esla
type,2
mat,1

```

```
ESHAPE,2  
esize,0.001  
amesh,all  
ESHAPE,0
```

```
asel,s,area,,10 !select & mesh fine air  
esla  
type,2  
mat,1  
esize,0.005  
amesh,all  
/wait,10
```

```
asel,s,area,,9 !Select & mesh rough air  
asel,a,area,,6,7  
esla  
type,2  
mat,1  
esize,0.025  
amesh,all
```

```
asel,s,area,,11 !Select & mesh rough steel  
esla  
type,2  
mat,2  
esize,0.025  
amesh,all
```

```
allsel  
save  
finish
```

! Straight Field Solution Script for ANSYS

/solv

ntype,static

nropt,auto

asel,s,area,,9 !select and load left coil

esla

bfe,all,js,3,1.5e6

asel,s,area,,7 !select and load right coil

esla

bfe,all,js,3,-1.5e6

allsel

nsubst,5

kbc,0

neqit,1

lswrite,1

nsubst,1

neqit,20

save

lswrite,2

lssolve,1,2

finish

/post1

save

/show

plnsol,b,y

GEOMETRY SCRIPT FILE FOR THE RING POLE DESIGN

!NEW DESIGN FOR ELECTROMEGET

/CLEAR

/FILNAM,EM_1

/PREP7

/PNUM,AREA,ON

RECTAN,-0.2921,0.2921,0,0.0389 !ALUMINUM BASE

RECTAN,-0.2397,0.2397,0.0389,0.077 !STEEL BASE

RECTAN,-0.1911,-0.1531,0.077,0.2411 !LEFT SUPPORT

RECTAN,0.1531,0.1911,0.077,0.2411 !RIGTH SUPPORT

RECTAN,-0.1333,-0.0407,0.077,0.1951 !LEFT COIL

RECTAN,0.0407,0.1333,0.077,0.1951 !RIGTH COIL

RECTAN,-0.0407,0.0407,0.077,0.2411 !CORE

RECTAN,-0.1911,-0.0508,0.2411,0.2792 !TOP PLATE LEFT

RECTAN,0.0508,0.1911,0.2411,0.2792 !TOP PLATE RIGTH

RECTAN,-0.0508,0.0508,0.2411,0.2892 !MAGNETIC FLUID

RECTAN,-0.35,0.35,-0.15,0.4292 !EXTERNAL AIR

AOVLAP,ALL

MATERIAL SCRIPT FILE FOR THE RING POLE DESIGN

AGLUE,ALL/COM, ****MATERIAL PROPERTY DEFENITION ****

MP,MURX,1,1 !MATL.1 IS AIR

TB,BH,2 !MATL.2 IS MILD STEEL

TBPT,,303,0.8

TBPT,,333.3,0.9

TBPT,,378.75,1.0

TBPT,,492.4,1.1

TBPT,,530.25,1.2

TBPT,,621.15,1.3

TBPT,,833.25,1.33

TBPT,,1000,1.4

TBPT,,1287.25,1.45

TBPT,,1666.5,1.5

TBPT,,2121,1.55

TBPT,,3000,1.6

TBPT,,4000,1.63

TBPT,,5000,1.645

TBPT,,6000,1.669

TBPT,,7000,1.685

TBPT,,8000,1.7

TBPT,,9000,1.73

CONST = 12.6E-7

TB,BH,3 !MATL. 3 IS FERROFLUID

TBPT,,0,0

TBPT,,10000, CONST*16000

TBPT,,20000, CONST*31000

TBPT,,40000, CONST*57000

TBPT,,60000, CONST*80500

TBPT,,80000, CONST*102000

TBPT,,100000, CONST*123000

TBPT,,120000, CONST*143500

TBPT,,140000, CONST*164200

TBPT,,160000, CONST*184500

TBPT,,200000, CONST*225000

TBPT,,280000, CONST*305500

TBPT,,360000, CONST*386000

TBPT,,400000, CONST*426000

TBPT,,500000, CONST*526000

ET,1,9 !INFINITY

ET,2,13 !FINITE

MESHING SCRIPT FILE FOR THE RING POLE DESIGN

```
ESHAPE,0  
ASEL,S,,,3  
MAT,2  
TYPE,2  
ESIZE,0.01  
AMESH,ALL
```

```
ASEL,S,,,4  
MAT,2  
TYPE,2  
ESIZE,0.01  
AMESH,ALL
```

```
ASEL,S,,,13  
MAT,2  
TYPE,2  
ESIZE,0.01  
AMESH,ALL
```

```
ASEL,S,,,14  
MAT,2  
TYPE,2  
ESIZE,0.01  
AMESH,ALL
```

```
ASEL,S,,,15  
MAT,2  
TYPE,2  
ESIZE,0.01  
AMESH,ALL
```

```
ASEL,S,,,19  
MAT,2  
TYPE,2  
ESIZE,0.01  
AMESH,ALL
```

ASEL,S,,,5
MAT,1
TYPE,2
ESIZE,0.01
AMESH,ALL

ASEL,S,,,6
MAT,1
TYPE,2
ESIZE,0.01
AMESH,ALL

ASEL,S,,,12
MAT,1
TYPE,2
ESIZE,0.1
AMESH,ALL

ASEL,S,,,16
MAT,1
TYPE,2
ESIZE,0.01
AMESH,ALL

ASEL,S,,,17
MAT,1
TYPE,2
ESIZE,0.01
AMESH,ALL

ASEL,S,,,20
MAT,1
TYPE,2
ESIZE,0.1
AMESH,ALL

ASEL,S,,,18
MAT,3
TYPE,2
ESIZE,0.001
AMESH,ALL

```
LSEL,S,,41
LSEL,A,,,42
LSEL,A,,,43
LSEL,A,,,44
MAT,1
TYPE,1
ESIZE,0.1
LMESH,ALL
```

SOLUTION SCRIPT FILE FOR THE RING POLE DESIGN

```
ALLSEL,ALL
FINISH
!SOLUTION SCRIPT
/solv
ANTYPE,STATIC
NROPT,AUTO

ASEL,S,AREA,,5    !LEFT COIL
ESLA
BFE,ALL,JS,3,1.5E6

ASEL,S,AREA,,6    !RIGTH COIL
ESLA
BFE,ALL,JS,3,-1.5E6
ALLSEL

NSUBST,5
KBC,0
NEQIT,1
LSWRITE,1

NSUBST,1
NEQIT,20
SAVE
LSWRITE,2
LSSOLVE,1,2

FINISH
/POST1
/SHOW
PLNSOL,B,SUM/BATCH
```

AXI-SYMMETRIC SOLUTION SCRIPT FILE FOR THE MODIFIED RING POLE DESIGN

```
/COM,ANSYS RELEASE 5.3  UP071096      10:16:11  04/19/1997
/input,menust,tmp      ,,,,,,,,,,,,,,1
/TITLE,Deneme
!*
KEYW,PR_SET,1
KEYW,PR_STRUC,0
KEYW,PR_THERM,0
KEYW,PR_ELMAG,1
KEYW,PR_FLUID,0
KEYW,PR_MULTI,0
KEYW,PR_CFD,0
KEYW,LSDYNA,0
/PMETH,OFF
!*
/PREP7
!*
ET,1,PLANE13
!*
KEYOPT,1,1,0
KEYOPT,1,2,0
KEYOPT,1,3,1
KEYOPT,1,4,0
KEYOPT,1,5,0
KEYOPT,1,6,0
!*
!*
UIMP,1,EX, , , ,
UIMP,1,DENS, , , ,
UIMP,1,ALPX, , , ,
UIMP,1,REFT, , , ,
UIMP,1,NUXY, , , ,
UIMP,1,PRXY, , , ,
UIMP,1,GXY, , , ,
UIMP,1,MU, , , ,
UIMP,1,DAMP, , , ,
UIMP,1,KXX, , , ,
UIMP,1,C, , , ,
UIMP,1,ENTH, , , ,
UIMP,1,HF, , , ,
UIMP,1,EMIS, , , ,
UIMP,1,QRATE, , , ,
```

```

UIMP,1,MURX, , ,1,
UIMP,1,MGXX, , , ,
UIMP,1,RSVX, , , ,
UIMP,1,PERX, , , ,
UIMP,1,VISC, , , ,
UIMP,1,SONC, , , ,
!*
!*
UIMP,2,EX, , , ,
UIMP,2,DENS, , , ,
UIMP,2,ALPX, , , ,
UIMP,2,REFT, , , ,
UIMP,2,NUXY, , , ,
UIMP,2,PRXY, , , ,
UIMP,2,GXY, , , ,
UIMP,2,MU, , , ,
UIMP,2,DAMP, , , ,
UIMP,2,KXX, , , ,
UIMP,2,C, , , ,
UIMP,2,ENTH, , , ,
UIMP,2,HF, , , ,
UIMP,2,EMIS, , , ,
UIMP,2,QRATE, , , ,
UIMP,2,MURX, , ,1,
UIMP,2,MGXX, , , ,
UIMP,2,RSVX, , , ,
UIMP,2,PERX, , , ,
UIMP,2,VISC, , , ,
UIMP,2,SONC, , , ,
!*
TB,BH,3, , , ,
!*
TBMODIF,1,1,303
TBMODIF,1,2,0.8
TBMODIF,2,1,333.3
TBMODIF,2,2,0.9
TBMODIF,3,1,378.75
TBMODIF,3,2,1
TBMODIF,4,1,492.4
TBMODIF,4,2,1.1
TBMODIF,5,1,530.25
TBMODIF,5,2,1.2
TBMODIF,6,1,621.15
TBMODIF,6,2,1.3
TBMODIF,7,1,833.25

```

```

TBMODIF,7,2,1.33
TBMODIF,8,1,1000
TBMODIF,8,2,1.4
TBMODIF,9,1,1287.25
TBMODIF,9,2,1.45
TBMODIF,10,1,1666.5
TBMODIF,10,2,1.5
TBMODIF,11,1,2121
TBMODIF,11,2,1.55
TBMODIF,12,1,3000
TBMODIF,12,2,1.6
TBMODIF,13,1,4000
TBMODIF,13,2,1.63
TBMODIF,14,1,5000
TBMODIF,14,2,1.645
TBMODIF,15,1,6000
TBMODIF,15,2,1.669
TBMODIF,16,1,7000
TBMODIF,16,2,1.685
TBMODIF,17,1,8000
TBMODIF,17,2,1.7
TBMODIF,18,1,9000
TBMODIF,18,2,1.73
RECTNG,0,23.97,3.89,7.7,
/PNUM,KP,0
/PNUM,LINE,0
/PNUM,AREA,1
/PNUM,VOLU,0
/PNUM,NODE,0
/PNUM,SVAL,0
/NUM,0
!*
/PNUM,ELEM,0
/REPLOT
!*
RECTNG,15.31,19.11,7.7,24.11,
RECTNG,4.07,13.33,7.7,19.51,
RECTNG,0,4.07,7.7,24.11,
RECTNG,5.08,19.11,24.11,27.92,
RECTNG,0,31.11,-5,35.92,
FLST,2,6,5,ORDE,2
FITEM,2,1
FITEM,2,-6
AOVLAP,P51X
NUMCMP,AREA

```

```

/REPLOT
SAVE
CM,_Y,AREA
ASEL,, , 6
CM,_Y1,AREA
CMSEL,S,_Y
!*
CMSEL,S,_Y1
AATT,1,1,1,0,
CMSEL,S,_Y
CMDELE,_Y
CMDELE,_Y1
!*
CM,_Y,AREA
ASEL,, , 2
CM,_Y1,AREA
CMSEL,S,_Y
!*
CMSEL,S,_Y1
AATT,2,1,1,0,
CMSEL,S,_Y
CMDELE,_Y
CMDELE,_Y1
!*
FLST,5,4,5,ORDE,3
FITEM,5,1
FITEM,5,3
FITEM,5,-5
CM,_Y,AREA
ASEL,, , P51X
CM,_Y1,AREA
CMSEL,S,_Y
!*
CMSEL,S,_Y1
AATT,3,1,1,0,
CMSEL,S,_Y
CMDELE,_Y
CMDELE,_Y1
!*
SAVE
SMRTSIZE,5
FLST,5,6,5,ORDE,2
FITEM,5,1
FITEM,5,-6
CM,_Y,AREA

```

```

ASEL,,,P51X
CM,_Y1,AREA
CHKMSH,'AREA'
CMSEL,S,_Y
!*
AMESH,_Y1
!*
CMDEL,_Y
CMDEL,_Y1
CMDEL,_Y2
!*
/PNUM,KP,0
/PNUM,LINE,0
/PNUM,AREA,1
/PNUM,VOLU,0
/PNUM,NODE,0
/PNUM,SVAL,0
/NUM,0
!*
/PNUM,MAT,1
/REPLOT
!*
SAVE
ALLSEL,ALL
! THE FOLLOWING SELECT COMMANDS WERE GENERATED BY THE ALLSEL
COMMAND
VSEL,ALL
ASEL,ALL
LSEL,ALL
KSEL,ALL
ESEL,ALL
NSEL,ALL
FLST,2,6,5,ORDE,2
FITEM,2,1
FITEM,2,-6
ARSCAL,P51X,,.01,.01,1,,0,1
SAVE
EPLOT
/SOLU
FINISH
/SOLU
FLST,2,28,2,ORDE,2
FITEM,2,23
FITEM,2,-50
BFE,P51X,JS,1,,1500000,,

```

```

LPLOT
FLST,2,7,4
FITEM,2,33
FITEM,2,23
FITEM,2,22
FITEM,2,21
FITEM,2,32
FITEM,2,4
FITEM,2,26
DL,P51X,,ASYM
SAVE
/STAT,SOLU
SOLVE
/POST1
FINISH
/POST1
PLF2D,27,0,10,1
SAVE
!*
/VSCALE,1,1,0
!
!*
PLVECT,B,,,VECT,ELEM,ON
/GRAPHICS,POWER
!*
RSYS,0
AVRES,2
AVPRIN,0
!*
PLNSOL,B,SUM,0
PLNSOL,H,SUM,0
/TITLE,Modified Design of Electromagnetic Float Polishing Apparatus
PLNSOL,B,SUM,0
PLNSOL,H,SUM,0
PLNSOL,H,Z,0
PLNSOL,H,Y,0
PLNSOL,H,X,0
PLNSOL,H,SUM,0
PLNSOL,B,SUM,0
FINISH
! /EXIT,ALL
/BATCH
/COM,ANSYS RELEASE 5.3  UP071096      22:58:05  04/19/1997
/input,menust,tmp      ,,1
RESUME

```

```

/resume,emdeneme
/POST1
PLNSOL,B,SUM,0
PLF2D,27,0,10,1
PLNSOL,B,SUM,0
PLNSOL,H,SUM,0
PLNSOL,B,SUM,0
/SOLU
FINISH
/SOLU
EPLOT
/PNUM,KP,0
/PNUM,LINE,0
/PNUM,AREA,1
/PNUM,VOLU,0
/PNUM,NODE,0
/PNUM,SVAL,0
/NUM,0
!*
/PNUM,MAT,1
/REPLOT
!*
/PREP7
FINISH
/PREP7
/SOLU
FINISH
/SOLU
FLST,2,28,2,ORDE,2
FITEM,2,23
FITEM,2,-50
BFE,P51X,JS,1,, ,2302700, ,
LPLOT
FLST,2,7,4
FITEM,2,33
FITEM,2,23
FITEM,2,22
FITEM,2,21
FITEM,2,32
FITEM,2,4
FITEM,2,26
DL,P51X, ,ASYM
/STAT,SOLU
SOLVE
/POST1

```

```

FINISH
/POST1
PLF2D,27,0,10,1
PLNSOL,B,SUM,0
PLNSOL,H,SUM,0
/PREP7
FINISH
/PREP7
!*
TBMODIF,19,1,1000000
TBMODIF,19,2,2.85
!*
TBLIST,BH,ALL
EPlot
/PNUM,KP,0
/PNUM,LINE,0
/PNUM,AREA,1
/PNUM,VOLU,0
/PNUM,NODE,0
/PNUM,SVAL,0
/NUM,0
!*
/PNUM,MAT,1
/REPLOT
!*
/SOLU
FINISH
/SOLU
/STAT,SOLU
SOLVE
/POST1
FINISH
/POST1
PLNSOL,B,SUM,0
PLNSOL,H,SUM,0
PLF2D,27,0,10,1
SAVE
FINISH
! /EXIT,ALL
/BATCH
/COM,ANSYS RELEASE 5.3  UP071096      09:41:03  04/21/1997
/input,menust,tmp  ,,1
RESUME
/POST1
PLF2D,27,0,10,1

```

```

/show,halo,on
halo,print,on
! halo,print,on
PLF2D,27,0,10,1
PLNSOL,B,SUM,0
PLNSOL,B,SUM,0
/PREP7
FINISH
/PREP7
/POST1
FINISH
/POST1
PLNSOL,H,SUM,0
PLNSOL,B,SUM,0
FINISH
! /EXIT,NOSAV
/BATCH
/COM,ANSYS RELEASE 5.3   UP071096      09:57:19   04/21/1997
/input,menust,tmp      ,,,,,,,,,,,,,,1
RESUME,EMDeneme,db,..\",0
ERASE
/POST1
PLNSOL,B,SUM,0
PLNSOL,H,SUM,0
PLF2D,27,0,10,1
PLNSOL,B,SUM,0
/REPLOT,RESIZE
/REPLOT,RESIZE
PLNSOL,H,SUM,0
!*
/VSCALE,1,1,0
!
!*
PLVECT,B, , , ,VECT,ELEM,ON
!*
/VSCALE,1,1,0
!
!*
PLVECT,H, , , ,VECT,ELEM,ON
!*
/VSCALE,1,1,0
!
!*
PLVECT,D, , , ,VECT,ELEM,ON
!*

```

```

/VSCALE,1,1,0
!
!*
PLVECT,EF, , , ,VECT,ELEM,ON
!*
/VSCALE,1,1,0
!
!*
PLVECT,B, , , ,VECT,ELEM,ON
/REPLOT,RESIZE
PLF2D,27,0,10,1
/REPLOT,RESIZE
!*
/VSCALE,1,1,0
!
!*
PLVECT,H, , , ,VECT,ELEM,ON
APLOT
!*
/VSCALE,1,1,0
!
!*
PLVECT,H, , , ,VECT,ELEM,ON
/REPLOT,RESIZE
PLNSOL,H,SUM,0
/REPLOT,RESIZE
FINISH
! /EXIT,ALL

```

VITA

Murat Cetin

Candidate for the Degree of

Master of Science

Thesis: ELECTROMAGNETIC FIELD ASSISTED POLISHING (EMFP) OF
ADVANCED CERAMICS

Major Field: Mechanical Engineering

Biographical:

Personal Data: Born in Ankara, Turkey on April 12, 1971, the son of Arif Naci and Necla.

Education: Graduated from Ankara Atatürk High School, Ankara, Turkey in May 1989; received Bachelor of Science degree in Mechanical Engineering from Yildiz Technical University, Istanbul, Turkey in May 1993. Completed the requirements for the Master of Science degree with a major in Mechanical Engineering at Oklahoma State University in (July, 1997).

Experience: Employed by Berk Celik Co. as a manufacturing engineer; Berk Celik Co., Istanbul, Turkey 1993 to 1994; employed by Oklahoma State University, Department of Mechanical and Aerospace Engineering as a graduate research assistant; Oklahoma State University, Department of Mechanical and Aerospace Engineering, 1996 to present.

Professional Memberships: American Society of Mechanical Engineers, Professional Mechanical Engineers Society of Turkey.